The Molecular Mechanisms Underlying Fusion Events at the Lysosome Membrane

Mahmoud Abdul Karim

A

Thesis

in the Department

of

Biology

Presented in Partial Fulfillment of the Requirements

For the Degree of

Doctor of Philosophy (Biology) at

Concordia University

Montréal, Quebec, Canada

April 2017

CONCORDIA UNIVERSITY

SCHOOL OF GRADUATE STUDIES

This is to certify that the thesis prepared

By: Mahmoud Abdul Karim

Entitled: The Molecular Mechanisms Underlying Fusion Events at the Lysosome Membrane

and submitted in partial fulfillment of the requirements for the degree of

Doctor of Philosophy (Biology)

complies with the regulations of the University and meets the accepted standards with respect to originality and quality.

Signed by the final examining committee:

_____Chair
Dr. A. Chapman

_____External Examiner
Dr. C. Stroupe

_____External Examiner
Dr. P. Joyce

_____Examiner
Dr. V. Titorenko

_____Examiner
Dr. M. Sacher

_____Thesis Supervisor
Dr. C. Brett

Approved by:

_____
Dr. G. Brown, Graduate Program Director

April 5, 2017 _____
Dr. A. Roy, Dean, Faculty of Arts & Science

ABSTRACT

The Molecular Mechanisms Underlying Fusion Events at the Lysosome Membrane

Mahmoud Abdul Karim, Ph.D.
Concordia University, 2017

Lysosome membrane fusion represents the last step of the endocytic pathway. During endocytosis, internalized surface proteins are delivered to endosomes where they are packaged into intraluminal vesicles (ILVs). Multiple rounds of ILV formation produce mature multivesicular body (MVB) that fuses with lysosomes to expose protein-laden ILVs to lumenal acid hydrolases for catabolism. Lysosomes also undergo homotypic membrane fusion for remodeling in response to cellular stress, or aging, or for organelle inheritance. A unique feature of homotypic lysosome fusion is the formation of IntraLumenal Fragments (ILF), whereby portions of the membranes are internalized and degraded upon merging. Although critical for homeostasis and remodeling, it is not clear how ILFs are formed during the homotypic lipid bilayer fusion reaction, nor is it clear whether similar molecular mechanisms orchestrate MVB-lysosome fusion.

Using *Saccharomyces cerevisiae* and its vacuolar lysosome as a model, I show that coordinated interactions between the fusion protein machinery (Rab-GTPase Ypt7 and its effector Vps41), and the protein kinase Yck3, target hemifusion intermediates to control ILF formation upon vacuolar lysosome fusion. To do so, I introduced a point mutation in Ypt7 (D44N) that permits activation but impairs binding to Vps41 causing it to be phosphorylated by Yck3. Phosphorylated Vps41 causes the multisubunit tethering complex HOPS to dissociate from vacuolar lysosome membranes preventing efficient *trans*-SNARE pairing required for lipid bilayer pore formation. This stall in pore formation allows hemifusion diaphragms to expand across docked organelle interfaces causing fewer ILFs to form. Knocking out YCK3 stabilizes Vps41 and HOPS on membranes restoring fusion defects and ILF formation.

With a better understanding of homotypic vacuolar lysosome fusion and ILF formation, I next determined if MVB-vacuolar lysosome fusion relies on a similar mechanism. By developing a new luminal β-lactamase complementation assay to measure MVB-vacuolar lysosome fusion

in vitro, I show that both fusion events require Ypt7 and HOPS, but heterotypic fusion is distinct in that it uses a unique non-canonical Q-SNARE bundle composed of the endosomal Qa-SNARE Pep12, Qb-SNARE Vti1, and soluble Qc-SNARE Vam7, that complexes with the lysosomal R-SNARE Nyv1 to drive lipid bilayer merger. Loss-of-function mutations that impair MVB maturation-deleting the endosomal $Na^+(K^+)/H^+$ exchanger NHX1 or components of the ESCRT machinery that drive ILV formation blocks heterotypic membrane fusion. Correcting luminal pH rescues the fusion impairment caused by deleting NHX1, whereas activating the Rab-GTPase Ypt7 rescues fusion defects caused by ESCRT dysfunction.

Using new insights from these results, I present refined working models describing the molecular underpinnings of homotypic vacuolar lysosome and MVB-vacuolar lysosome fusion. Because all of the underlying machinery is conserved in all eukaryotic phyla, I anticipate that they will be used to help design strategies to treat human disorders linked to mutations in genes implicated in these pathways.

ACKNOWLEDGMENTS

First of all, and most importantly, I would like to thank my supervisor Dr. Christopher Brett. Chris, I want to thank you from the bottom of my heart for trusting my talent and for giving me the opportunity to perform my Masters and Ph.D. studies under your supervision. You are a rebel in our field, trying to revolutionize the way we do science! You have always been a great mentor, and a close friend, giving me guidance when needed, but also allowing me to be creative and develop my ideas and approaches to improve my research project.

I would also like to thank my committee members Dr. Vladimir Titorenko, and Dr. Michael Sacher for their support and valuable advice throughout my studies.

Also, special thanks to The Centre for Microscopy and Cellular Imaging (CMCI) at Concordia University and to its manager at the time Dr. Chloë van Oostende. Chloë I enjoyed every single second we shared in our little garden (our office) and for your patience and training.

Finally, I would like to thank my lab members Charlie, Erin, and Dieter for their help and scientific feedback and the fun time we spent together. I will always remember you guys.

DEDICATIONS

I would like to dedicate this work to my precious parents, Ahmad and Rabab, to my brother Yusuf and sister Souad, and to my aunt Sawsan who passed away before seeing me finish this degree. To them, whatever I do or say, I won't be thankful enough. I would also like to dedicate this work to my beautiful fiancée Mariam, who supported me on every single step of the way. Mariam, thank you for your patience and support, without which I surely could not have completed this degree.

CONTRIBUTION OF AUTHORS

Erin Kate McNally conducted experiments shown in Figure 6G, 6H, 6I, Figure 9A, Figure 16D and Figure 17D.

Sevan Mattie performed electron microscopy shown in Figure 6J and Figure 11G.

TABLE OF CONTENTS

LIST OF FIGURES

LIST OF TABLES

LIST OF ABBREVIATIONS

ALPS: Amphipathic Lipid Packing Sensor

ATP: Adenosine TriPhosphate

CBP: Calmodulin Binding Peptide

CCZ: Calcium Caffeine Zinc sensitivity

CORVET: Class C cOre Vacuole/Endosome Tethering complex

CPS: CarboxyPeptidase yscS

CPY: Vacuolar CarboxyPeptidase Y

DIC: differential interference contrast (microscopy)

EEA1: Early Endosome Antigen 1

ESCRT: Endosomal Sorting Complexes Required for Transport

FYVE: Fab1 YOTB Vac1 EEA1

GAP: GTPase Activating Protein

GDI: GDP-Dissociation Inhibitor

GDP: Guanosine DiPhosphate

GEF: Guanosine nucleotide Exchange Factor

GFP: Green Fluorescence Protein

GST: Glutathione S-Transferase

GTP: Guanosine TriPhosphate

GTPase: Guanosine TriPhosphatase

GTPγS: Guanosine 5'-o-[Gamma-thio] Triphosphate

HOPS: HOmotypic fusion and vacuole Protein Sorting

HVF: Homotypic Vacuolar lysosome Fusion

ILF: IntraLuminal Fragment

ILV: IntraLuminal Vesicle

LE: Late Endosome

MON: MONensin sensitivity

MTC: Multisubunit Tethering Complex

MVB: MultiVesicular Body

NHE/Nhx: Na^+/H^+ Exchanger

NSF: N-ethylmaleimide-Sensitive Factor

NYV: New Yeast V-SNARE

PEP: carboxyPEPtidase Y-deficient

Phox: Phospholipid-binding domain

PMSF: PhenylMethane Sulfonyl Fluoride

SDS-PAGE: Sodium Dodecyl Sulfate PolyAcrylamide Gel Electrophoresis

SEC: SECretory

SNAP: Soluble N-ethylmaleimide-sensitive factor Attachment Protein

SNARE: Soluable N-ethylmaleimide-sensitive factor Attachment Protein Receptor

TEM: Transmission Electron Microscopy

VAM: VAcuolar Morphogenesis;

VPS: Vacuolar Protein Sorting

VTI: Vps10 (Ten) Interacting

YCK: Yeast Casein Kinase

YPT: Yeast Protein Two

Chapter 1. Introduction

1.1 Lysosomes and their functions

Lysosomes are the recycling compartments within eukaryotic cells. Christian de Duve first discovered them in 1955 when studying the intracellular distribution of enzymes using centrifugal fractionation (de Duve, 2005). Three processes required for lysosomal function are membrane fusion, biomaterial catabolism, and nutrient recycling. Membrane fusion mediates the delivery of biomaterials to the lumen of the lysosome (Klionsky and Ohsumi, 1999; Teter and Klionsky, 2000). Received biomaterials are then broken down by acid hydrolases (proteases and lipases) into their constituents (amino acids, lipids, nucleotides; Klionsky et al., 1990). Transporter proteins embedded in the lysosome membrane move nutrients from the lumen to the cytoplasm where they are reused by the cell (Russnak et al., 2001).

1.2 Membrane trafficking pathways that feed biomaterials to lysosomes

The two major cellular pathways that deliver biomaterials to lysosomes (vacuolar lysosomes in *Saccharomyces cerevisiae*) are autophagy and endocytosis. Autophagy involves the encapsulation of intracellular biomaterials (cytoplasmic protein aggregates or damaged organelles) to form an autophagosome that fuses with the lysosome exposing their materials to hydrolases for recycling (Figure 1; Eskelinen and Saftig, 2009). The second pathway, endocytosis, encapsulates extracellular biomaterials or internalizes surface receptors and transporters by invagination of the plasma membrane to form early endosomes. Early endosomes undergo homotypic fusion to form a late endosome. Here internalized surface proteins are sorted and packaged into vesicles (ILVs) by the ESCRT (Endosomal Sorting Complexes Required for Transport) machinery. Multiple rounds of ILV formation produce a mature multivesicular body (MVB; Huotari and Helenius, 2011; Schmidt and Teis, 2012). The pathway culminates with MVB fusion with the lysosome to deliver biomaterials for recycling (Figure 1).

In addition to heterotypic (e.g. MVB-lysosome) membrane fusion, lysosomes also undergo homotypic (lysosome-lysosome) membrane fusion. Homotypic fusion is essential for lysosomes to control their shape, size, and copy number for organelle inheritance for example (Brett and Merz, 2008). Homotypic lysosome fusion also mediates the turnover of resident polytopic

proteins (Mattie et al., 2017; McNally et al., 2017). In response to substrates, TOR (target of rapamycin) signaling or misfolding, transporter proteins are labeled for degradation and sorted into an area of membrane called the boundary, encircled by fusogenic proteins and lipids that concentrate within a ring that forms at the vertex between adjacent docked lysosome membranes. Upon lipid bilayer merger at the vertex ring, the boundary membranes are internalized within the lumen of the fusion product as an intraluminal fragment (ILF; Figures 1 and 2). Inside the lumen, the ILF is exposed to acid hydrolases to recycle these lysosomal proteins and lipids (Wang et al., 2002). Thus, homotypic lysosome membrane fusion events are critical for organelle inheritance, homeostasis and remodeling.

Figure 1. *Saccharomyces cerevisiae* as a model organism to study membrane fusion

Cartoon model describing the pathways that rely on lysosome membrane fusion for biomaterial degradation and recycling in Baker's yeast (*S. cerevisiae*).

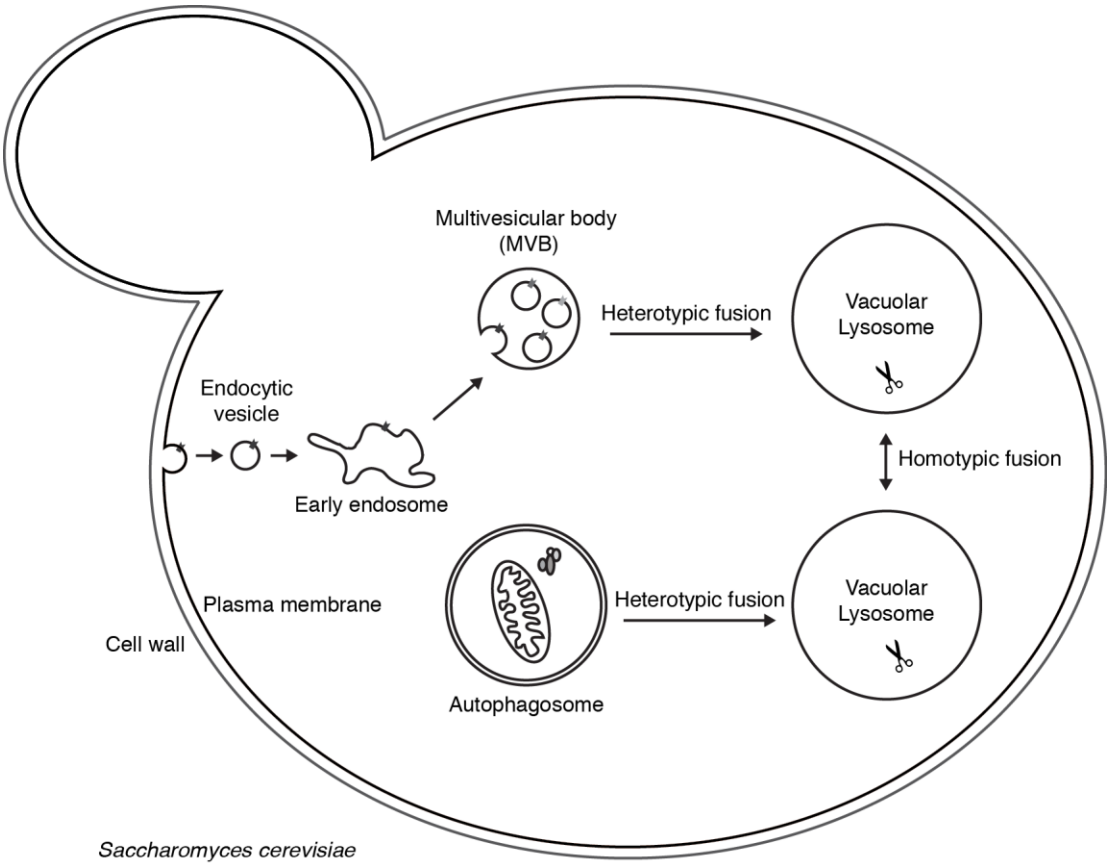

1.3 Homotypic vacuolar lysosome fusion as model for organelle membrane fusion

The mechanisms underlying lysosomal membrane fusion have been best characterized by studying the vacuolar lysosome of *Saccharomyces cerevisiae* as a model (Wickner and Haas, 2000; Wickner 2010). Yeast vacuolar lysosomes provide numerous advantages for studying membrane fusion including; the ease of genetic manipulations and organelle isolation, fluorescent microscopy techniques that allow visualization of vacuolar lysosome fusion events in live cells and *in vitro*, and well-established *in vitro* fusion assays to assess fusion kinetics. In brief, the homotypic vacuolar lysosome fusion (HVF) reaction is composed of four subreactions: priming, tethering, docking, and fusion (Figure 2). During priming, Sec18 a N-ethylmaleimide-sensitive factor (NSF) ortholog binds Sec17 (a SNARE chaperone) to disassemble cis-SNARE complexes composed of Vam3, Vti1, Vam7, and Nyv1 to reset the fusion machinery for a new round of fusion (Mayer et al., 1996). Tethering occurs when opposing vacuolar lysosome membranes make first contact. This event is governed by the activation of the Rab-GTPase Ypt7, and its effector Vps41 within the multisubunit tethering complex (MTC) called the HOPS (HOmotypic fusion and Protein Sorting) holocomplex (Brett et al., 2008). Docking involves recruitment of additional fusogenic proteins and lipids to the initial contact site, which concentrate at an expanding vertex ring between opposed membranes (Kato and Wickner, 2001). Also, SNAREs present on opposing membranes make contact and begin to form a tightly wound four-helical bundle called a *trans*-SNARE complex (Collins and Wickner, 2007). *Trans*-SNARE complex formation triggers the release of Ca^{2+} from the lumen, which then signals the SNAREs to fully zipper (Peters and Mayer, 1998; Merz and Wickner, 2004). Energy from SNARE zippering drives the merging of the lipid bilayers to complete fusion (Figure 2; Wiedelhold and Fasshauer, 2009; Jun and Wickner, 2007).

Figure 2. Homotypic vacuolar lysosome membrane fusion

Cartoon illustrating the subreactions (or stages) and proteins necessary for driving membrane fusion, and intraluminal fragment formation (ILF).

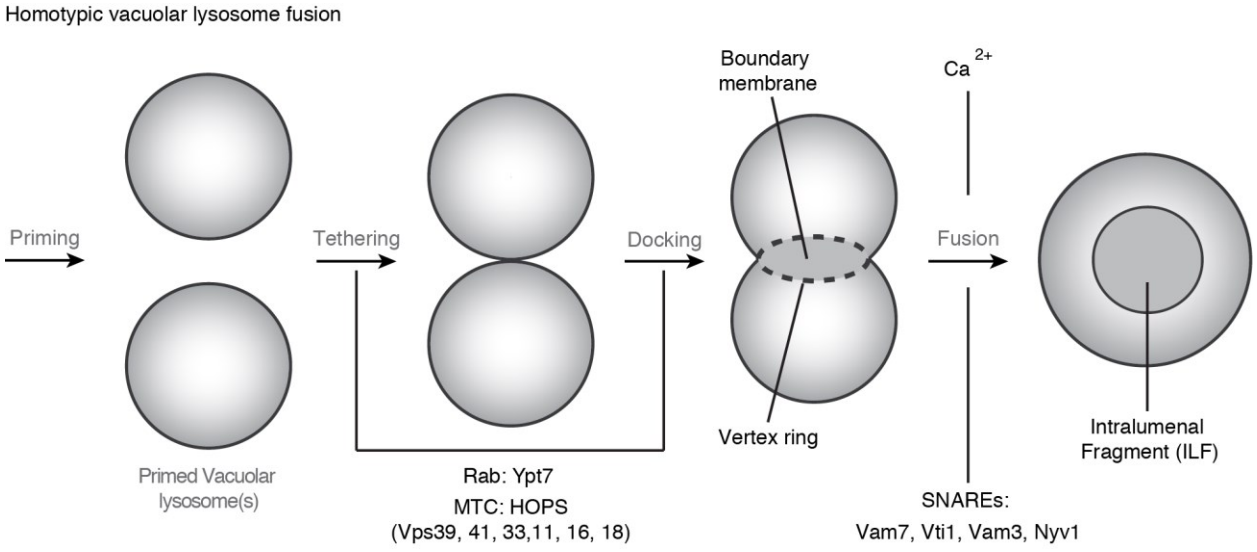

1. 4 The homotypic vacuolar lysosome fusion machinery

1.4.1 The Rab-GTPase Ypt7

Rab-GTPases are molecular timer switches that toggle from GDP (inactive) to GTP (active) bound states. They confer organelle identity and play important roles in protein trafficking and membrane fusion (Bourne et al., 1991; Grosshans et al., 2006). GDP-bound Rabs require Guanine nucleotide Exchange Factors (or GEFs) to convert them to their active GTP-bound state, which persists until a GTPase Activating Protein (GAP) initiates GTP hydrolysis and converts it back to the inactive GDP-bound state to complete the Rab cycle (Barr and Lambright, 2010). Rabs are anchored to membranes of organelles by two isoprenyl lipid (geranylgeranyl) moieties that decorate amino acids near their C-termini (Overmeyer and Maltese, 1992). Inactive Rabs are extracted from membranes by a GDP dissociation inhibitor (GDI), which masks their isoprenyl anchor and keeps them soluble in the cytoplasm (Goody et al., 2005). When active, Rab-GTPases interact with their effector proteins to mediate downstream events including signaling, transport, and fusion (Grosshans et al., 2006). During HVF, Ypt7 activity drives two stages of the reaction: tethering, and docking. It is thought that the roles of Ypt7 in both subreactions require binding and stabilizing its cognate effector within the multisubunit tethering complex HOPS (Figure 3).

1.4.2 The multisubunit tethering complex HOPS

The HOPS holocomplex contains six subunits: Vps39, which binds Ypt7 independent of its nucleotide bound state and facilitates activation by its cognate GEF protein complex Mon1-Ccz1 (Wang, 2003; Lawrence et al., 2014); Vps41, its cognate effector; and the Vps-C core complex composed of the remaining four subunits Vps16, Vps18, Vps11, and Vps33. Vps33 is an SM-protein that mediates *trans*-SNARE templating en route to bilayer fusion (Figure 3; Pieren et al., 2010). In the current model of HOPS driven membrane tethering, active Ypt7 is thought to bind Vps39 on one membrane and a second Ypt7-GTP binds Vps41, within the same complex, on the opposite membrane (Figures 2 and 3). Through these interactions, a single HOPS complex bridges opposed membranes to mediate tethering (Lürick et al., 2016). Vps33 then mediates interaction between the R-SNARE Nyv1 on one membrane and the Qa-SNARE Vam3 on the opposing membrane to drive *trans*-SNARE complex formation, a hallmark of the docking subreaction (Nichols et al., 1997; Price et al., 2000; Ostrowicz et al., 2010; Bröcker et al., 2012;

Pieren et al., 2010; Baker et al., 2015).

HOPS function is regulated by the action of the protein kinase Yck3, which phosphorylates the amphipathic lipid-packing sensor (ALPS) within Vps41 decreasing its affinity for membrane lipids causing it to dissociate from lysosomal membranes (LaGrassa and Ungermann, 2005; Brett et al., 2008; Cabrera et al., 2009). Thus when phosphorylated, HOPS is dependent on active Ypt7 for its association with the membrane (Hickey et al., 2009).

1.4.3 SNARE proteins

SNARE complex formation ultimately drives endomembrane fusion. Four SNARE proteins when assembled in trans mediate HVF (Nyv1, Vam3, Vti1, and Vam7; Collins and Wickner, 2007). With the exception of Vam7, these SNARE proteins consist of three domains: a C-terminal transmembrane domain, a SNARE domain, and an N-terminal domain. Depending on the amino acid residue at the 0 layer which is either a conserved arginine (R) or glutamine (Q) within the coiled-coil bundle that forms between their 4 SNARE domains, SNARE proteins are classified as R or Q-SNAREs. Each SNARE complex, including the one that drive vacuolar lysosome fusion, contain a single R-SNARE (Nyv1) donated by one membrane and three Q-SNAREs (Qa, Vam3; Qb, Vti1; and Qc, Vam7) that form a bundle donated by the opposing membrane (Fasshauer et al., 1998). Vam7, the only soluble SNARE without a transmembrane domain, is tethered to membranes by its PX (Phox) domain that binds phosphatidylinositol 3-phosphate [PI(3)P] (Boeddinghaus et al., 2002; Cheever et al., 2001). After assembly into partially wound *trans*-SNARE complexes during the docking stage of fusion, Ca^{2+} release from the lysosomal lumen into the cytoplasm is thought to promote full SNARE complex zippering that drives lipid bilayer mixing to complete the fusion reaction (Collins and Wickner, 2007; Schwartz and Merz, 2009; Lurick et al., 2015). Following lipid bilayer merging, the still-assembled four SNARE proteins complex is called a cis-SNARE complex. NSF (Sec18) and its chaperone α-SNAP (Sec17) disassemble the cis-SNARE complex for a new round of fusion to complete the SNARE cycle (Mayer et al., 1996).

Figure 3. Model depicting how the fusion machinery assembles at the vertex microdomain
Within the vertex microdomain, HOPS (Vps39, Vps41, Vps33, Vps18, Vps11) binds Ypt7-GDP with its Vps39 subunit to facilitate activation by its GEF Mon1/Ccz1. Active Ypt7 (GTP) then binds its cognate effector Vps41 to promote Vps33 mediated *trans-SNARE* templating between the R-SNARE Nyv1 and the Q-SNAREs Vam3, Vti1, and Vam7.

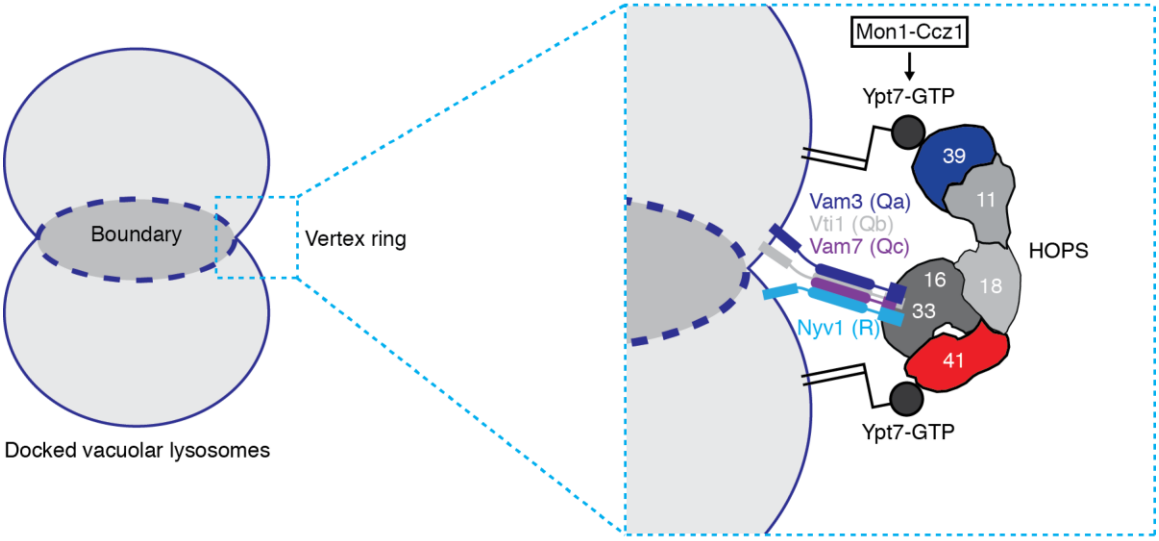

1.5 Heterotypic MVB-lysosome membrane fusion

Although critical for endocytosis, relatively little is known about the molecular mechanism that orchestrates MVB-lysosome fusion. But like other membrane fusion events within the endomembrane system (e.g. HVF), MVB-lysosome fusion is thought to require coordinated interactions between Rab-GTPases, multisubunit tethering complexes, and SNARE proteins. Based on results primarily acquired from genetic studies, the prevailing model of MVB-vacuolar lysosome fusion suggests that the same machinery orchestrating HVF is also responsible for driving MVB-vacuolar lysosome fusion in *S. cerevisiae*. For example, both the Rab-GTPase Ypt7 and its interacting tethering complex HOPS localize to the MVB and the vacuolar lysosome and are required for fusion (reviewed by Luzio et al., 2010; Markgraf et al., 2009; Balderhaar and Ungermann, 2013; Spang, 2016). In addition, the same SNARE proteins are implicated in this fusion event, as Vti1 also localizes to the MVB and Vam7 can also bind [PI(3)P] on the MVB membrane. The remaining two SNAREs required for fusion, Vam3 and Nyv1, are possibly donated by the vacuolar lysosome membrane. However, recent evidence suggests that SNARE complexes are initially formed through the activity of SM-proteins that promote interactions between an R-SNARE from one membrane with the cognate Qa-SNARE from the opposing membrane (Baker et al., 2015). As the Qa-SNARE Vam3 and R-SNARE Nyv1 are exclusively found on vacuolar lysosomes, it seems unlikely that they both contribute to MVB-vacuolar lysosome fusion, suggesting that another SNARE complex mediates this event (Figure 4; Von Mollard et al., 1997; Kweon et al., 2003; Furukawa and Mima, 2014). MVBs express their own Qa-SNARE (Pep12) and R-SNARE (Snc2) paralogs (Izawa et al., 2012; Furukawa and Mima, 2014), but neither has been implicated in MVB-vacuolar lysosome fusion.

Another distinguishing feature of MVB-vacuolar lysosome fusion is its possible dependence on MVB maturation: To ensure efficient degradation, it is assumed that internalized surface receptor and transporter proteins must be sorted and packed into ILVs at the MVB prior to fusion with vacuolar lysosomes. Although Rab activation has been implicated in sensing MVB maturation and triggering this fusion event (Russell et al., 2012), this hypothesis has not been formally tested. Thus, there are many open questions that must be answered for a comprehensive understanding of this process: which mechanisms are unique to MVB-vacuolar lysosome fusion? What triggers this event? Does the MVB need to be properly loaded with ILVs prior to fusion?

Figure 4. Cartoon model describing the fusion machineries at the MVB and the vacuolar lysosome

The Rab-GTPase Ypt7, its interacting MTC HOPS, and the Qb-SNARE Vti1 localize to both the MVB and the vacuole membranes. The Qa-SNARE Pep12 resides on MVBs, whereas its syntaxin ortholog Vam3, Vam7, and Nyv1 reside on the vacuole.

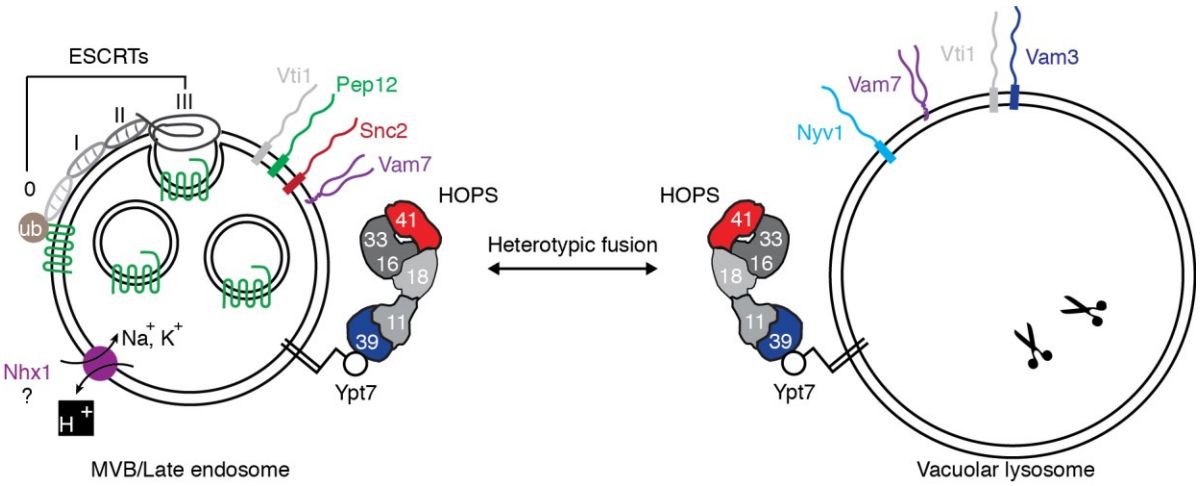

1.6 The MVB biogenesis machinery

1.6.1 The ESCRT pathway

The formation of MVBs is a crucial stage in the delivery of internalized surface transporter and receptor proteins destined for degradation by the lysosome. At the endosome, the ESCRT machinery which comprises five distinct complexes (ESCRT-0, I, II, III and Vps4) recognizes, binds, and sorts ubiquitylated cargos into ILVs giving rise to a mature MVB (Henne et al., 2011). Deleting any of the genes encoding the ESCRT machinery results in accumulation of internalized surface proteins in an abnormally enlarged pre-vacuolar compartment often containing aberrant stacks of flattened cisternae, which fail to fuse with the lysosome. This morphological characteristic is a hallmark of class E mutants, which represent a subset of genetic mutations identified in early screens that determined the molecular underpinnings of endocytosis and lysosome biogenesis (Rieder et al., 1996; Russell et al., 2012). ESCRTs mutants cause hyperactive Vps21 to accumulate on these aberrant compartments at the expense of inactivating Ypt7 by preventing recruitment of its cognate GEF complex Mon1-Ccz1 to membranes, breaking the Rab cascade that mediates progression of anterograde membrane trafficking to the lysosome (Russell et al., 2012). Because active Ypt7 recruits and stabilizes HOPS for SNARE-mediated fusion (Nordmann et al., 2010; Cabrera et al., 2014), it was proposed that ESCRT-mediated Vps21 to Ypt7 conversion may be an important trigger for mature MVB-lysosome fusion (Russell et al., 2012). However, the evidence supporting this hypothesis is scant, and it has not been formally tested using biochemical approaches due to lack of reliable, robust cell-free quantitative assays of MVB-vacuolar lysosome fusion.

1.6.2 The Sodium (Potassium)/Hydrogen exchanger Nhx1

Another important regulator of MVB biogenesis is the endosomal $Na^+(K^+)/H^+$ exchanger Nhx1 in yeast, which is orthologous to NHE6 and NHE9 in humans. Loss-of-function mutations in NHE6 and NHE9 have been linked to Autism Spectrum Disorders (ASDs; Gilfillan et al., 2008; Franke et al., 2009; Morrow et al., 2008). In *S. cerevisiae*, Nhx1 confers tolerance to osmotic and pH stress (Nass and Rao, 1998; Brett et al., 2005; Kallay et al., 2011), by presumably counteracting the activity of the V-type H^+-ATPase through luminal Na^+ or K^+ influx coupled to H^+ efflux (Nass and Rao, 1999; Kojima et al., 2012; Brett et al., 2005). Electroneutral ion exchange by Nhx1 regulates luminal pH and is required for delivery of

internalized surface proteins to the vacuolar lysosome (Bowers et al., 2000). Deleting NHX1 results in a vps class E phenotype including the appearance of an enlarged pre-vacuolar compartment where internalized proteins accumulate and the hyper acidification of the lumen (Bowers et al., 2000; Brett et al., 2005). Addition of the weak base chloroquine to *nhx1Δ* mutants alkalizes the compartmental lumen and permits delivery of internalized proteins to vacuolar lysosomes *in vivo* (Brett et al., 2005; Qiu and Fratti, 2010), leading to the hypothesis that the ion exchange activity of Nhx1 may regulate MVB-vacuolar lysosome fusion. This hypothesis has not been formally tested and would benefit from biochemical approaches (quantitative cell-free assays) to develop a comprehensive understanding of this process.

1.7 Summary

Membrane fusion is critical for lysosome function, biogenesis, homeostasis, remodeling and inheritance. Disruption of membrane trafficking pathways that culminate with lysosome fusion (e.g. autophagy) is thought to underlie many human neurological diseases and cancers (Levine and Kroemer, 2008; Kirkegaard and Jäättelä, 2009). Therefore, understanding the molecular mechanisms that orchestrate lysosomal fusion events is of great importance for understanding the etiology and designing new therapeutic strategies to treat lysosome-associated diseases.

Herein, I primarily use quantitative cell-free assays to study vacuolar lysosome fusion in the model organism *Saccharomyces cerevisiae* to elucidate the molecular mechanisms that drive membrane fusion. My work reveals the role of HOPS in synchronizing the interplay between Rab, kinase, and SNAREs cycles during membrane fusion. Specifically, I answer the following questions: (1) Is the Ypt7-Vps41 interaction required for vacuolar lysosome membrane tethering? (2) Does the protein kinase Yck3 phosphorylate Vps41 to regulate ILF formation during homotypic vacuolar lysosome fusion? (3) What are the unique mechanisms that distinguish MVB-vacuolar lysosome fusion from homotypic vacuolar lysosome fusion?

In Chapter 2, I characterize a point mutation in Ypt7 (D44N) that disrupts Vps41 binding without interfering with other Rab functions. By studying this mutation, I show that the Ypt7-Vps39 interaction alone is sufficient to drive vacuolar lysosome membrane tethering and docking, but *trans*-SNARE complex stabilization is impaired. Next, I show that Yck3 phosphorylates Vps41 within the HOPS complex to modulate the kinetics of SNARE-mediated pore formation, the rate-limiting step of the lipid bilayer fusion reaction, and control ILF

formation to regulate turnover of lysosomal membrane lipids and proteins.

In Chapter three, I developed and optimized a new cell-free content mixing assay to measure the kinetics of MVB-vacuolar lysosome fusion. Using this assay, I discovered that although Ypt7 and HOPS are shared, a non-cognate *trans*-SNARE complex distinguishes MVB-vacuole fusion from HVF. I also demonstrate that knocking out genes implicated in MVB biogenesis (NHX1 or ESCRTs) impairs heterotypic fusion, and reveal conditions that rescue fusion, uncovering possible therapeutic strategies to treat human diseases linked to loss-of-function mutations in orthologous genes.

Chapter 2. Rab-Effector-Kinase Interplay Regulates Intralumenal Fragment Formation During Lysosome Fusion

Mahmoud Abdul Karim, Erin Kate McNally, Sevan Mattie, Christopher Leonard Brett*

In preparation for resubmission to Developmental Cell

2.1 Abstract

Upon lysosome membrane fusion, a portion of the lipid bilayer is internalized within the lumen and degraded by acid hydrolases. Formation of this IntraLumenal Fragment (ILF) is important for protein and lipid degradation needed for organelle homeostasis and remodeling. But how ILF formation is regulated to optimize membrane turnover is not understood in detail. Here we show that interplay between the Rab-GTPase Ypt7, its cognate effector Vps41 (a component of the multisubunit tethering complex HOPS) and the casein kinase Yck3 controls ILF formation by targeting intermediates of the lipid bilayer fusion reaction. Fewer ILFs formed when the interaction between Ypt7 and Vps41 was interrupted. This was due to phosphorylation of HOPS by Yck3, preventing stabilization of *trans*-SNARE complexes needed for lipid bilayer pore formation. We propose that HOPS coordinates Rab, kinase and SNARE cycles to optimize lipid and protein turnover required for lysosome physiology.

2.2 Introduction

Biomaterials are recycled by lysosomes providing an important source of nutrients for eukaryotic cells (Perera and Zoncu, 2016). They require three fundamental processes to perform this function: Membrane fusion – to deliver membrane-encapsulated biomaterials (including internalized surface receptors, damaged organelles, toxic aggregates or invasive pathogens) to the lysosomal lumen (Huber and Teis, 2016); Biomaterial catabolism – within the lumen biomaterials encounter acid hydrolases that break them down into their constituents (e.g. lipids, amino acids, sugars); and Nutrient transport – nutrient transporter proteins return products of catabolism to the cytoplasm for reuse by the cell (Xu and Ren, 2015). Besides being critical for lysosome function, membrane fusion is also essential for organelle homeostasis, as it mediates delivery of biosynthetic cargoes (e.g. new hydrolase and transporter proteins; Odorizzi et al. 1998; Luzio et al. 2014), drives organelle inheritance (Weisman, 2003), and controls organelle morphology (Brett and Merz, 2008; Klumperman and Raposo, 2014). Thus the molecular underpinnings of lysosome membrane fusion have been under intense investigation since the discovery of the organelle by Christian de Duve and colleagues over 60 years ago (de Duve, 2005). The greatest insight into this process has been gleaned from the use of *Saccharomyces cerevisiae* and its vacuolar lysosome (or "vacuole") as models (Li and Kane, 2009; Nickerson et al., 2009; Wickner, 2010), whereby homotypic vacuole membrane fusion requires four biochemically distinct, sequential stages: Priming, tethering, docking and fusion.

Priming involves the ATP-dependent unraveling of cis-SNARE (Soluble NSF Attachment protein REceptor) complexes by the α-SNAP protein Sec17 and NSF ortholog Sec18 (Mayer et al., 1996). Tethering is when apposing organelle membranes make first contact. This requires the Rab-GTPase Ypt7, a Rab7 ortholog, and its cognate multisubunit tethering complex HOPS (HOmotypic vacuole fusion and protein sorting; Mayer and Wickner 1997; Hickey and Wickner 2010; Orr et al. 2015). HOPS contains six protein subunits, two of which have Ypt7-binding sites that mediate intermembrane attachment: Vps39 and Vps41 (Seals et al., 2000b; Brett et al., 2008; Nickerson et al., 2009; Bröcker et al., 2012). Vps39 binds Ypt7 independent of its nucleotide-bound state to accommodate activation by its GEF (Guanine nucleotide Exchange Factor) complex composed of Mon1 and Ccz1 (Nordmann et al., 2010). Whereas Vps41 is the cognate effector of Ypt7 and thus only binds the Rab when it is active (GTP-bound; Brett et al. 2008) to bridge opposed membranes during tethering. Vps41 may also associate with membranes through

its amphipathic lipid packing sensor (ALPS) domain (Cabrera et al., 2010), which is also thought to contribute to organelle membrane tethering (Ho and Stroupe, 2016).

Docking involves the recruitment and enrichment of fusogenic lipids and proteins in a ring formed at the vertex between apposed membranes (Wang et al., 2003; Fratti et al., 2004). Here Vps33, a SM-protein found within HOPS, mediates *trans*-SNARE complex formation between the R-SNARE Nyv1 on one membrane with the Qa-SNARE Vam3, Qb-SNARE Vti1 and soluble Qc-SNARE Vam7 on the opposing membrane (Seals et al., 2000; Lobingier and Merz, 2012; Baker et al., 2015). Partially zippered SNARE complexes are proofread when bound by HOPS (Starai et al., 2008), which also protects them from being disassembled by Sec18 (Xu et al., 2010; Lobingier et al., 2014). Orchestration of protein recruitment and assembly is further regulated by the casein kinase Yck3 that responds to Ypt7 inactivation to phosphorylate and inhibit activities of Vps41 and Vam3 (LaGrassa and Ungermann, 2005; Brett et al., 2008). Fusion is bilayer merger accomplished by full zippering of *trans*-SNARE-complexes to drive membranes together and form pores necessary for full lumenal content mixing (Nichols et al., 1997; Schwartz and Merz, 2009). As the lipid bilayer is severed at the vertex ring where the fusion machinery is located, the encircled area of membrane at the interface between apposing membranes (called the boundary) is entrapped within the lumen as a membrane fragment (Wang et al., 2002; Mattie et al., 2017). This IntraLumenal Fragment (ILF) is then degraded by lumenal hydrolases and recycled. Recently, we discovered that vacuolar nutrient transporter proteins are selectively sorted into the boundary, internalized and degraded in response to substrate levels, protein misfolding or TOR-signaling (McNally et al., 2017). Thus, ILF formation during fusion is important for vacuole lipid and protein turnover necessary for organelle homeostasis and remodeling.

Despite being critical for vacuolar lysosome biology, relatively little is known about how formation of ILFs is regulated. However, it is known that ILF formation relies on hemifusion intermediate formation during the organelle lipid bilayer fusion reaction (Wang et al., 2002; Jun and Wickner, 2007; Mattie et al., 2017). Termed ring fusion-by-hemifusion, vacuole lipid bilayer fusion is initiated by stalk formation, whereby lipids within the outer leaflets of opposing membranes within close proximity mix causing merger (Reese and Mayer, 2005; Jun and Wickner, 2007; Wickner, 2010). This lipid stalk then expands forming a hemifusion diaphragm, a lipid bilayer consisting of lumenal facing inner leaflets donated from each apposing membrane

(Mattie et al., 2017). Next *trans*-SNARE-pin zippering drives pore formation, the rate-limiting step of the lipid bilayer fusion reaction (Reese et al., 2005), whereby a small rupture is made within the hemifusion diaphragm allowing luminal contents to mix (Schwartz and Merz, 2009; D'Agostino et al., 2016). This pore then expands to complete full membrane merger resulting in a single organelle. The formation of ILFs during vacuole fusion relies on the delay between stalk and pore formation (Mattie et al., 2017): If pore formation is delayed, the stalk expands across the entire boundary membrane and when a pore forms, no membrane is entrapped during fusion. Thus, pore formation must occur rapidly after stalk expansion to form ILFs during vacuole fusion.

To better understand how these ILFs form (or not) during fusion, we showed that adding GTPγS, the non-hydrolyzable ortholog of GTP, to cell-free vacuole fusion reactions causes premature stalk formation preventing ILFs from forming (Mattie et al., 2017). Whereas addition of purified, recombinant Vam7 protein (the soluble Qc-SNARE) induces premature pore formation to enhance ILF formation upon fusion. Although it is apparent that altering the activities of GTPases or SNAREs regulates ILF formation during fusion, we were unable to demonstrate how the endogenous fusion machinery may perform this function. Because HOPS mediates the interplay between the Rab-GTPase Ypt7 and SNAREs (Wickner, 2010), we hypothesized that modulating interactions between these proteins may influence ILF formation during vacuolar lysosome fusion. Here we test this hypothesis and confirm that functional interactions between Ypt7, its effector Vps41 within HOPS and the kinase Yck3 regulate ILF formation during vacuolar lysosome fusion.

2.3 Results

2.3.1 Ypt7-D44N slows vacuole fusion and prevents ILF formation in live cells

To identify a Ypt7 mutation that may alter ILF formation during vacuole membrane fusion, we first examined the vacuole morphology within *S. cerevisiae* cells expressing different point mutations reported to either lock the Rab-GTPase in a GDP-bound (T22N; Liu et al. 2012; Lawrence et al. 2014) or GTP-bound state (Q68L and N126I; Brett et al. 2008; Rana et al. 2015), reduce its affinity for nucleotides (D129N; Kucharczyk et al. 2001), or disrupt (GTPase Activating Protein) GAP induced GTP hydrolysis and possibly effector binding (D44N; Vollmer et al., 1999). We expected that mutations of interest would not affect vacuolar morphology, as fusion itself should not be abolished, but should affect the production of ILFs (Mattie et al., 2017). We find that cells expressing Ypt7-T22N or Ypt7-D129N contain fragmented vacuoles that resemble those observed in *ypt7Δ* cells (Figure 5A and B), confirming that Ypt7 nucleotide binding and activation is required for homotypic vacuole fusion (Wichmann et al., 1992; Eitzen et al., 2000; Balderhaar et al., 2010). Nearly all cells expressing Ypt7-Q68L or Ypt7-N126I contained a single large vacuole, confirming that homotypic fusion was enhanced when Ypt7 is constitutively active (Rana et al., 2015). However, cells expressing Ypt7-D44N, a mutation that also prevents GAP-induced GTP hydrolysis but possibly interferes with effector binding, had similar vacuole morphologies as cells expressing wild type Ypt7 (Figure 5A and B). To further assess the Ypt7 mutants that permitted fusion, we recorded vacuole fusion events in live cells using video microscopy (Figure 5C, Video 1) and made two interesting observations: Vacuoles within cells harboring the Ypt7-D44N underwent fewer homotypic fusion events, as compared to cells expressing wild type Ypt7 or a GTP-locked mutant of Ypt7 (Q68L; Figure 5D). Furthermore, of the vacuole fusion events observed within Ypt7-D44N expressing cells, fewer produced visible intralumenal fragments whereas fusion events in Ypt7-Q68L cells produced more ILFs as compared to wild type cells (Figure 5E). Together, these preliminary findings suggest that introducing mutations that lock Ypt7 in a GTP-bound state (Q68L) or possibly disrupt Ypt7 effector binding (D44N) may affect the fusion-by-hemifusion reaction to alter ILF formation. We decided to focus our studies on the D44N mutation as it showed the strongest phenotype and we reasoned that characterizing a mutation that may disrupt Ypt7-HOPS interactions would provide new insights into how the underlying machinery orchestrates vacuole

fusion and ILF formation.

Figure 5. Ypt7-D44N impedes ILF formation during vacuole fusion *in vivo*

(A) Examples of fluorescence micrographs showing FM4-64 stained vacuoles within live yeast cells expressing different Ypt7 mutants. (B) Number of vacuoles per cell was calculated using micrographic data shown in A ($n \geq 300$). (C) Images from time-lapse videos (Video 1) showing examples of FM4-64 stained vacuoles undergoing homotypic fusion within live yeast cells expressing either wild type (WT) Ypt7, Ypt7-D44N or Ypt7-Q68L. Numbers represent time in seconds. Scale bars, 2 μm. From these videos, (D) percentage of cells that presented vacuole fusion events and (E) percentage of vacuole fusion events that failed to form visible ILFs were calculated. Mean ± S.E.M. are shown ($n \geq 200$). * indicates $P \leq 0.05$.

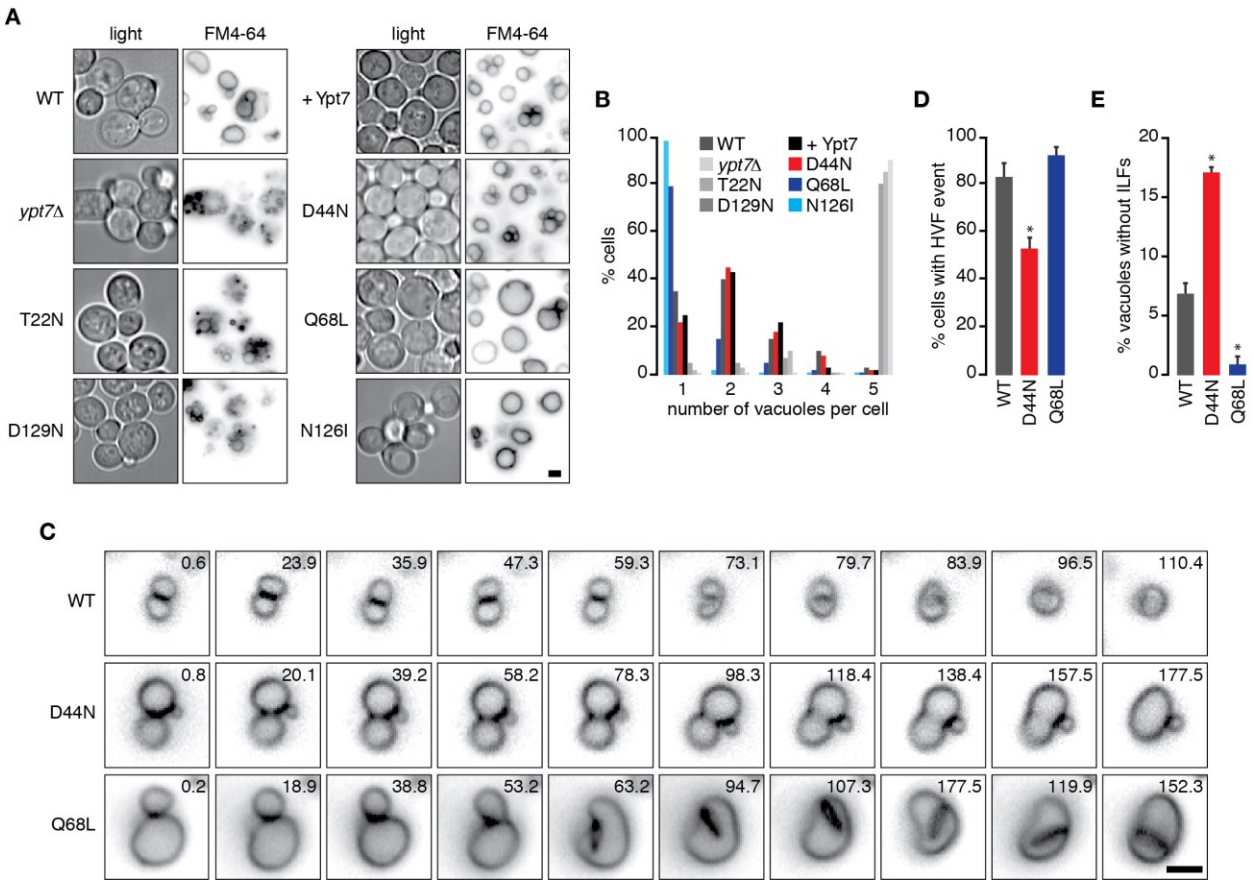
A
light
FM4-64
light
FM4-64
WT
ypt7Δ
T22N
D129N
+ Ypt7
D44N
Q68L
N126I
B
% cells
number of vacuoles per cell
WT
ypt7Δ
T22N
D129N
+ Ypt7
D44N
Q68L
N126I
D
% cells with HVF event
WT
D44N
Q68L
E
% vacuoles without ILFs
WT
D44N
Q68L
C
WT
D44N
Q68L
0.6
23.9
35.9
47.3
59.3
73.1
79.7
83.9
96.5
110.4
0.8
20.1
39.2
58.2
78.3
98.3
118.4
138.4
157.5
177.5
0.2
18.9
38.8
53.2
63.2
94.7
107.3
177.5
119.9
152.3

2.3.2 Ypt7-D44N impairs pore formation during vacuole fusion *in vitro*

To better understand how the D44N mutation in Ypt7 disrupts vacuole fusion, we studied the subreactions of the lipid bilayer fusion reaction *in vitro*. First, we isolated vacuoles from cells and measured the kinetics of membrane fusion using lipid or content mixing assays (Haas, 1995; Jun and Wickner, 2007). We found that the D44N mutation did not affect vacuole lipid mixing (Figure 6A) but severely impaired content mixing (Figure 6B) stimulated by ATP *in vitro*. To confirm that content mixing was indeed blocked, we imaged isolated vacuoles before and 60 minutes after fusion was stimulated with ATP *in vitro* (Figure 6C) and calculated vacuole surface area (Figure 6D) which increases upon vacuole content mixing. As expected, an increase in vacuole surface area was observed over time when vacuoles isolated from wild type cells were examined. This was blocked by the addition of the fusion inhibitor rGyp1-46, a purified, recombinant protein consisting of only the catalytic domain of the Rab-GAP Gyp1 (Eitzen et al., 2000; Brett et al., 2008), confirming that fusion (content mixing) was responsible for the observed increase in vacuole surface area. Importantly, the surface area of vacuoles isolated from cells expressing Ypt7-D44N did not increase over time, consistent with results from the content mixing assay. Thus, we are confident to report that the relative amount of lipid mixing to content mixing was much greater for the mutant as compared to wild type (Figure 6E) and the delay between these events was extended in the mutant (Figure 6F). We also noted that 60 minutes after ATP was added to induce fusion fewer ILFs were observed within vacuoles isolated from the mutant cells as compared to wild type (Figure 6G) consistent with observations made *in vivo* (Figure 6E). Together, these results indicated that only outer leaflets (not inner leaflets) of lipid bilayers have merged and hemifusion diaphragms may be accumulating between docked organelles.

To test this hypothesis, we first used a polytopic protein exclusion assay to study hemifusion diaphragm accumulation during vacuole fusion *in vitro* by fluorescence microscopy (Mattie et al., 2017). If a hemifusion diaphragm forms at the boundary membrane between apposing organelles, then polytopic proteins with large cytoplasmic domains such as GFP-tagged Vph1, the stalk domain of the V-type H^+-ATPase, will be excluded from this site because biophysical constraints prevent Vph1-GFP from entering a hybrid bilayer composed of lumenal facing leaflets on both sides (Nikolaus et al., 2010). Fusion reactions containing vacuoles isolated from wild type cells showed uniform distribution of Vph1-GFP on vacuole membranes,

i.e. it was present within nearly all boundary membranes observed (Figure 6H and 6I), as previously reported (Wang et al., 2002; Mattie et al., 2017; McNally et al., 2017). However, many boundary membranes between vacuoles isolated from cells expressing Ypt7-D44N did not contain Vph1-GFP, suggesting that hemifusion diaphragms had accumulated during fusion. We next imaged these fusion reactions using transmission electron microscopy at magnifications sufficient to identify hemifusion intermediates (Mattie et al., 2017). As expected, we found that more boundaries did not have a discernable intermembrane space separated apposing vacuole membranes when the D44N mutation was introduced into Ypt7 (Figures 6J and K). Although individual leaflets were not resolved, the membrane thickness at these boundaries was similar to the thickness of a single lipid bilayer, suggesting that these structures were hemifusion diaphragms. All things considered, the findings from *in vitro* experiments suggest that Ypt7-D44N stalls the bilayer fusion reaction immediately prior to pore formation causing hemifusion diaphragms to accumulate, which prevents formation of ILFs.

Figure 6. Ypt7-D44N impairs pore formation during vacuole fusion *in vitro*

Vacuole membrane (A) lipid mixing or (B) content mixing was measured *in vitro* in the presence or absence of ATP to stimulate fusion. Vacuoles were isolated from cells expressing wild type (WT) Ypt7 or Ypt7-D44N. Data shown represent mean ± S.E.M (n = 3). (C) Examples of fluorescence micrographs showing isolated vacuoles expressing WT Ypt7 or Ypt7-D44N stained with FM4-64 in the presence of ATP with or without 3.6 μM rGyp1-46 after incubation for 0 or 60 minutes. Scale bar, 2 μm. (D) Cumulative probability plot and median values showing surface area calculated from micrographic data shown in C. (E) Lipid to content mixing ratio, (F) times at half maximal lipid mixing (circles) and content mixing (squares) calculated using data shown in A and B. Numbers represent time intervals calculated between lipid and content mixing values. (G) Proportion of vacuoles containing visible ILFs calculated from data shown in H. Mean ± S.E.M. shown ($n \geq 284$). (H) Examples of fluorescence micrographs showing FM4-64 stained vacuoles isolated from wild type or Ypt7-D44N cells expressing Vph1-GFP acquired at 60 minutes after fusion was initiated. Interfaces containing (closed) or lacking (open arrowheads) GFP fluorescence are indicated. Scale bar, 2 μm. (I) Percentage of vacuolar lysosome boundaries that do not contain Vph1-GFP calculated from data shown in H. Mean ± S.E.M. shown ($n \geq 504$). (J) (top, left) Examples of transmission electron micrographs showing vacuoles isolated from WT or Ypt7-D44N cells observed under fusogenic conditions at 60 minutes. (bottom, left) Higher magnification images of membrane interfaces. Scale bars, 500 nm. (right) Linear density plots of areas shown at membrane interfaces. (K) Proportion of total vacuoles observed engaged in docking or hemifusion ($n \geq 78$). * indicates $P \leq 0.05$.

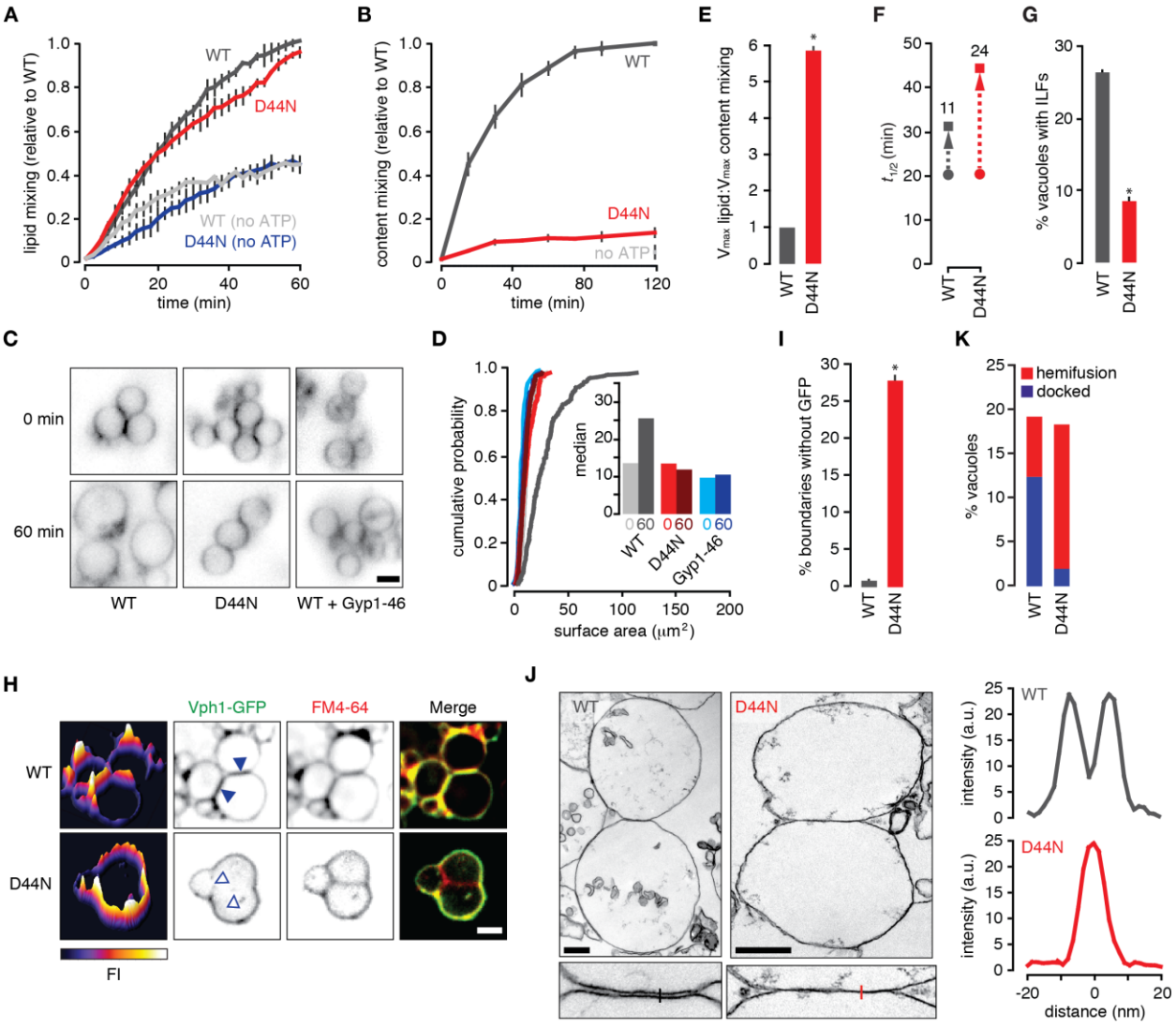
A
lipid mixing (relative to WT)
time (min)
WT
D44N
WT (no ATP)
D44N (no ATP)
B
content mixing (relative to WT)
time (min)
WT
D44N
no ATP
E
Vmax lipid:Vmax content mixing
WT
D44N
F
t1/2 (min)
11
24
WT
D44N
G
% vacuoles with ILFs
WT
D44N
C
0 min
60 min
WT
D44N
WT + Gyp1-46
D
cumulative probability
surface area (μm2)
median
WT
D44N
Gyp1-46
I
% boundaries without GFP
WT
D44N
K
hemifusion
docked
% vacuoles
WT
D44N
H
Vph1-GFP
FM4-64
Merge
WT
D44N
FI
J
WT
D44N
intensity (a.u.)
distance (nm)

2.3.3 Ypt7-D44N is active but does not bind and stabilize Vps41 on lysosome membranes

Residue D44 is found at the end of the switch I region (RabF1) within the Ypt7 protein that changes conformation upon Rab activation to mediate effector binding (Figure 7A; Constantinescu et al., 2002). As such, Gallowitz and colleagues originally hypothesized that changing this aspartate to an asparagine introduces chemical and electrostatic changes that may prevent switch I folding or directly interfere (as the residue is outward-facing) with effector binding without disrupting Rab activation (as it does not contribute to the nucleotide binding pocket; Vollmer et al., 1999). To test this hypothesis, we immobilized GST-tagged Ypt7 proteins on Sepharose beads decorated with glutathione and conducted pull-down assays using wild type cell lysate to determine if the D44N mutation disrupts Ypt7 binding to its cognate effector Vps41 (Seals et al., 2000b; Brett et al., 2008). As predicted, Ypt7-D44N does not bind Vps41 regardless of its nucleotide-bound state (Figure 7B). As controls, we confirmed that wild type Ypt7 only binds Vps41 when active (bound to GTP or GTPγS) but not inactive (bound to GDP), a hallmark of Rab-effector binding (Grosshans et al., 2006), and introducing a Q68L mutation that locks Ypt7 in an active state supports Vps41 binding even when the Rab is bound to GDP. Vps41 contains one of two Ypt7-binding sites in HOPS that orchestrates events downstream of Ypt7 required for vacuole fusion (Nickerson et al., 2009). The second site is present within Vps39, the subunit of HOPS that mediates Ypt7 activation by its GEF Mon1-Ccz1 (Nordmann et al., 2010). Unlike Vps41 binding that requires Ypt7 activation, Vps39 interacts with Ypt7 independent of its nucleotide-bound state and thus is not classified as an effector (Figure 7B; Brett et al. 2008). Importantly, we found that Ypt7-D44N robustly binds Vps39 in a nucleotide-independent manner, indicating that the mutant protein folds properly and that binding to its cognate effector Vps41 is exclusively impaired.

Although it is not implicated in homotypic vacuole fusion, the retromer complex is also thought to be an effector for Ypt7 (Liu et al. 2012). Thus, it is possible that the D44N mutation could also disrupt this interaction, impairing biosynthetic trafficking pathways that deliver the fusion machinery to the vacuole (Seaman et al., 1998) accounting for the observed defect in vacuole fusion. However, in our hands, Ypt7 binding to Vps35, a subunit of the retromer complex, was independent of its activation state (Figure 7B), suggesting that Vps35 is not a true effector of Ypt7. Furthermore, Ypt7-D44N continued to bind Vps35 in a nucleotide-independent manner, confirming that the mutation specifically disrupts Vps41 binding and does not affect its

interaction with the retromer protein complex.

To confirm that the D44N mutation does not interfere with Ypt7 activation, we next conducted a Rab-extraction assay using Gdi1, a Rab-chaperone protein that preferentially extracts inactive Rab proteins from membranes leaving only active Rab on membranes (Eitzen et al., 2000; Brett et al., 2008). Consistent with previous reports, we show that extraction of wild type Ypt7-GDP from membranes by purified, recombinant Gdi1 (rGdi1) increases when isolated vacuoles are pretreated with rGyp1-46 (a Rab-GAP) to inactivate Ypt7, and decreases when pretreated with GTPγS to activate Ypt7 (Figure 7C). However, in striking contrast, extraction of Ypt7-D44N by rGdi1 was not observed in the presence or absence of rGyp1-46 or GTPγS, suggesting that the entire pool of Ypt7-D44N on the vacuoles was active. This finding is consistent with this mutation causing reduced GTPase activity as observed previously by Gallowitz and colleagues (Vollmer et al., 1999). We also noted that less Ypt7-D44N co-purified with the organelles, which is consistent with reports suggesting that effector binding may stabilize Rab-GTPases on membranes by shielding them from Gdi1 (reviewed by Grosshans et al. 2006). However, these reports also suggest that interactions with effectors may be needed to recruit Rab proteins to the proper membrane locations within the cell (see Cabrera and Ungermann 2013). Although the presence of Ypt7-D44N in our organelle preparations implies proper localization, we also tagged Ypt7-D44N with GFP and imaged its cellular distribution by fluorescence microscopy to confirm that the mutation did not disrupt its cellular distribution (Figure 7D). Indeed, we found that GFP-Ypt7-D44N was present exclusively on vacuole membranes and intracellular puncta reminiscent of late endosomes, and this distribution was similar to wild type GFP-Ypt7 (also see Cabrera et al. 2009). Thus, it seems that Vps39-binding and activation of Ypt7-D44N is sufficient to target and stabilize a relatively small (Gdi1-resistant) pool of Rab on vacuole membranes.

Ypt7 activation is thought to be necessary for Vps41 (and HOPS) recruitment and stabilization on vacuole membranes (Hickey et al., 2009). Thus, we reasoned that fusion defects caused by D44N might be due to dissociation of Vps41 from membranes. To test this hypothesis, we sedimented vacuole membranes at different time points after stimulating vacuole fusion *in vitro* with ATP and conducted Western blot analysis to detect Vps41 in the membrane (pellet) and soluble (supernatant) fractions (Figure 7E). Consistent with previous reports (Brett et al., 2008), most Vps41 remains stabilized on membranes during fusion of vacuoles isolated from

wild type cells. In contrast, we found that nearly all Vps41 that co-purified with vacuoles isolated from cells expressing Ypt7-D44N dissociates from membranes over the course of the fusion reaction. The D44N mutation had no effect on Vps39 membrane association, consistent with the mutation only disrupting the interaction between Ypt7 and Vps41 but not Vps39. At first this result was somewhat perplexing as Vps41 and Vps39 are both subunits that comprise stable HOPS holocomplexes (Seals et al., 2000; Plemel et al., 2011; Bröcker et al., 2012). However, Vps41 and Vps39 each have moonlighting functions outside of HOPS (Angers and Merz, 2009; Hönscher et al., 2014) and HOPS has been proposed to be capable of remodeling itself on the fly (Ostrowicz et al., 2010). Thus, to better understand the impact of D44N on HOPS complex stabilization on membranes, we also studied Vps33, a SM-protein and subunit of the Vps-C core of HOPS, that like the effector Vps41, is thought to function downstream of Ypt7 activation to mediate *trans*-SNARE complex formation (Baker et al., 2015) and SNARE-mediated pore formation (Pieren et al., 2010; Lobingier and Merz, 2012). Similar to Vps41, we found that the D44N mutation caused more Vps33 to dissociate from membranes over the course of the vacuole fusion reaction *in vitro* (Figure 7E). Thus, introducing the D44N mutation into Ypt7 prevents stabilization of Vps41 and Vps33 on vacuole membranes during vacuole fusion.

In addition to binding active Ypt7, Vps41 is stabilized on membranes by its ALPS domain that incorporates itself into the outer leaflet of the vacuole membrane (Cabrera et al., 2010). The protein kinase Yck3 regulates Vps41 membrane association by phosphorylating residues S367, S368, S371 and S372 within the ALPS domain causing displacement from the outer leaflet (LaGrassa and Ungermann, 2005; Cabrera et al., 2010). When Ypt7 is inactivated, it renders Vps41 susceptible to phosphorylation by Yck3 causing it to dissociate from membranes (Brett et al., 2008; Zick and Wickner, 2012). As Vps41 easily dissociates from membranes harboring Ypt7-D44N, we hypothesized that Ypt7-D44N cannot bind and shield Vps41 from phosphorylation by Yck3. As Yck3 requires ATP to phosphorylate Vps41 *in vitro*, we first tested this hypothesis by examining Vps41 membrane association in the presence or absence of ATP. As previously reported, most Vps41 remains stabilized on membranes 45 minutes after adding ATP and this is dependent on the presence of wild type Ypt7, as extracting it from membranes with rGdi1 causes Vps41 also to dissociate (Figure 7F). However, nearly all Vps41 that co-purifies with vacuoles dissociates from membranes expressing Ypt7-D44N 45 minutes after adding ATP, in the absence or presence of rGdi1, demonstrating that Ypt7-D44N does not

prevent ATP-dependent dissociation of Vps41 from membranes. Importantly, these results correlate with Vps41 phosphorylation detected by Western blot (Figure 7G), whereby phosphorylated Vps41 migrates slower than the dephosphorylated form of the protein (see Brett et al. 2008). Phosphorylated Vps41 only appears in the presence of ATP and addition of GTPγS to activate wild type Ypt7 causes less to appear, consistent with active Ypt7 shielding Vps41 from Yck3. Introducing the D44N mutation into Ypt7 causes most Vps41 to be phosphorylated upon ATP addition and adding GTPγS had no effect. Together, these results support the hypothesis that Ypt7-D44N does not bind Vps41 making it susceptible to phosphorylation by Yck3 causing HOPS to dissociate from vacuole membranes.

Figure 7. D44N mutation in Ypt7 uncouples activation from effector binding and prevents stabilization of phosphorylated HOPS on membranes

(A) Structure of Ypt7 in its inactive GDP-bound (left) or active GppNHp-bound state (right; Constantinescu et al., 2002). Nucleotides (green), Switch I (blue), switch II (cyan) and D44 (red) are indicated. (B) Results of pull-down experiments performed using immobilized GST-Ypt7 (wild type, WT; D44N; or Q68L) preloaded with GDP (D), GTP (T) or GTPγS (γ) and cell lysates from Vps39-GFP cells. Amount of Vps35, Vps41 or Vps39-GFP bound to GST-Ypt7 resin or found in the lysate (load) were determined by immunoblotting. (C) (top) Cartoon illustrating the Rab-GTPase activity assay. (bottom) Vacuoles isolated from wild type (WT) or Ypt7-D44N (Δ) cells were incubated with ATP for 40 minutes in the presence or absence of 5 μM of rGdi1 during the last 10 minutes. Where indicated, reactions were pretreated with either 3.6 μM rGyp1-46 or 0.2 mM GTPγS. Organelle membranes (pellet, P) were separated from soluble factors (supernatant, S) by centrifugation and Ypt7 was detected by immunoblotting. (D) Fluorescence micrographs of live cells expressing wild type (WT) or mutant (D44N) GFP-Ypt7. Vacuole membranes were stained with FM4-64. Scale bars, 2 μm. (E) At times shown, vacuole fusion reactions containing organelles isolated from cells expressing wild type Ypt7 (WT) or Ypt-D44N (Δ) were sedimented and the presence of Vps41, Vps33 and Vps39 in membrane (pellet, P) and soluble (supernatant, S) fractions was assessed by immunoblotting. (F) As shown in C, vacuole fusion reactions containing organelles isolated from wild type (WT) or Ypt-D44N (Δ) cells were treated with rGdi1 in the presence or absence of ATP and the membrane association of Vps41 or Ypt7 was assessed by immunoblotting. (G) Vacuoles isolated from wild type (WT) or Ypt7-D44N cells were incubated in the absence or presence of ATP and/or 0.2 mM GTPγS for 60 minutes, and probed for Vps41 by immunoblotting. Slower (*) and faster (°) migrating bands representing phosphorylated and dephosphorylated forms of the protein, respectively (see Brett et al., 2008) are indicated. All experiments shown were repeated at least 2 times.

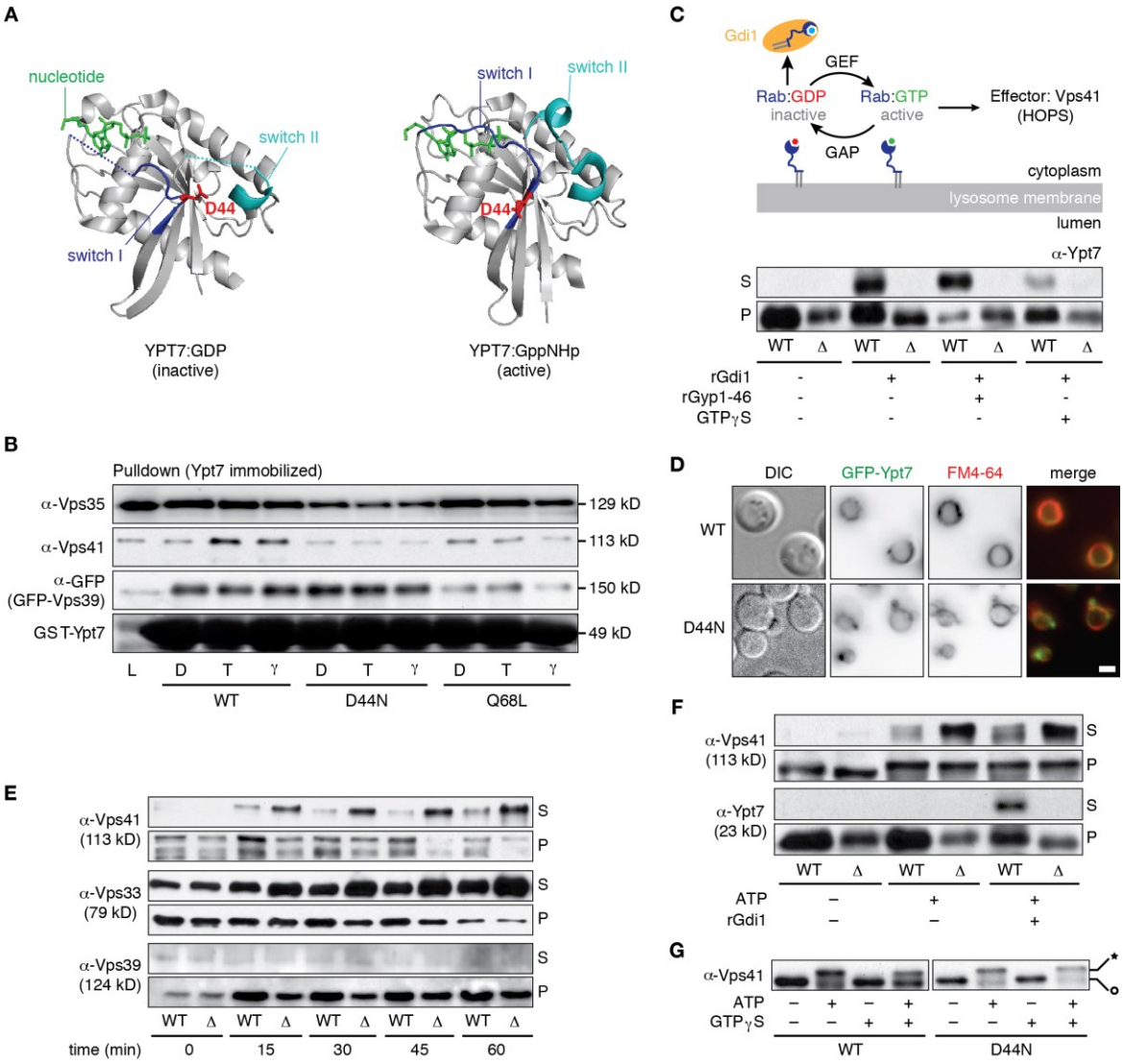
A
nucleotide
switch II
switch I
D44
YPT7:GDP
(inactive)
switch I
switch II
D44
YPT7:GppNHp
(active)
B
Pulldown (Ypt7 immobilized)
α-Vps35
α-Vps41
α-GFP
(GFP-Vps39)
GST-Ypt7
129 kD
113 kD
150 kD
49 kD
L D T γ D T γ D T γ
WT
D44N
Q68L
C
Gdi1
GEF
Rab:GDP
inactive
Rab:GTP
active
Effector: Vps41
(HOPS)
GAP
cytoplasm
lysosome membrane
lumen
α-Ypt7
S
P
WT Δ WT Δ WT Δ WT Δ
rGdi1 - + + +
rGyp1-46 - - + -
GTPγS - - - +
D
DIC
GFP-Ypt7
FM4-64
merge
WT
D44N
E
α-Vps41
(113 kD)
α-Vps33
(79 kD)
α-Vps39
(124 kD)
S
P
WT Δ WT Δ WT Δ WT Δ WT Δ
time (min) 0 15 30 45 60
F
α-Vps41
(113 kD)
α-Ypt7
(23 kD)
S
P
WT Δ WT Δ WT Δ
ATP – + +
rGdi1 – – +
G
α-Vps41
ATP – + – + – + – +
GTPγS – – + + – – + +
WT
D44N

2.3.4 Ypt7-D44N impairs *trans*-SNARE complex formation but not membrane tethering and docking

Ypt7 and HOPS mediate the tethering and docking stages of vacuole membrane fusion, leading to *trans*-SNARE complex zippering that drives pore formation. Specifically, the interactions between Ypt7 and its two binding partners within HOPS are thought to mediate membrane tethering, whereby HOPS bridges apposing membranes through the Ypt7-Vps41 interaction on one end of the complex and the Ypt7-Vps39 interaction on the opposing membrane at the other end (Bröcker et al., 2012; Lürick et al., 2016). However, disrupting the Ypt7-Vps41 interaction in our hands permits lipid mixing which would require tethering as a prerequisite. Thus, to confirm that isolated vacuoles expressing Ypt7-D44N continue to undergo tethering, we measured the number of vacuoles found in clusters after brief incubation with ATP using fluorescence microscopy – a conventional method to assess vacuole or vesicle membrane tethering (e.g. Mayer and Wickner 1997). We found that vacuoles expressing Ypt7-D44N undergo robust clustering and the extent of tethering was higher compared to vacuoles expressing wild type or the GTP-locked mutant (Q68L) Ypt7 (Figure 8A). This result was similar to the effect observed when GTPγS was added to wild type vacuoles to activate Ypt7 and stimulate tethering, which is consistent with the finding that the Gdi1-resistant pool of Ypt7-D44N on membranes is hyperactive. We also assessed vacuole membrane docking by measuring the boundary length between adjacent docked organelles (Figure 8B) and found that the D44N mutation increased boundary length as compared to wild type or Q68L Ypt7, which may be a byproduct of blocked content mixing. As a negative control, we also showed that Ypt7 activation was required for docking as adding the GAP peptide rGyp1-46 to inactivate wild type Ypt7 prevented boundary extension, a hallmark of the docking stage of vacuole fusion. Thus, these findings confirm that the Ypt7-Vps41 interaction is not required for the tethering and docking stages of vacuole membrane fusion.

During docking, HOPS plays a critical role in recruiting SNARE proteins to the vertex ring where it assembles *trans*-SNARE complexes and proofreads them prior to SNARE-pin zippering that drives pore formation for lipid bilayer merger (Starai et al., 2008; Zick and Wickner, 2013). Given that Ypt7-D44N blocks SNARE-mediated pore formation (Figure 6B), we hypothesized that perhaps *trans*-SNARE complex formation is impaired when Ypt7-HOPS binding is interrupted by this mutation. To test this hypothesis, we isolated these SNARE-complexes using

an approach that ensures that they are formed in *trans* during the vacuole fusion reaction *in vitro* (see Collins and Wickner 2007; Schwartz and Merz 2009): We isolated complexes from fusion reactions containing vacuoles isolated from cells lacking the R-SNARE Nyv1 and expressing the Qa-SNARE Vam3 fused to Calmodulin-Binding Protein (CBP-Vam3) mixed with vacuoles that express wild type Nyv1, ensuring that CBP-Vam3 can only pair with Nyv1 on opposing membranes (Figure 8C). In support of our model, we found that Ypt7-D44N impeded formation of stable *trans*-SNARE complexes under control conditions (ATP-stimulated fusion). Almost no Nyv1 co-precipitated with CBP-Vam3 when fusion was blocked on ice, confirming that all *trans*-SNARE complex formation observed occurred *in vitro*.

In response to *trans*-SNARE complex formation, Ca^{2+} is released from the vacuole lumen to promote downstream events required for lipid bilayer fusion (Merz and Wickner, 2004). Because Ypt7-D44N partially blocks formation of stable *trans*-SNARE complexes, we hypothesized that it also impairs downstream vacuole Ca^{2+} efflux. To test this hypothesis, we measured Ca^{2+} fluxes during vacuole fusion *in vitro* using a membrane-impermeant Ca^{2+}-sensing fluorophore whereby a decrease in fluorescence intensity indicates vacuole Ca^{2+} uptake and an increase indicates lumenal Ca^{2+} efflux. We found that Ypt7-D44N diminished the amplitude of Ca^{2+} efflux (Figure 8D), which correlated with the observed reduction in stable *trans*-SNARE complexes formed. Ca^{2+} influx was not affected by the mutation suggesting that all organelles were properly loaded with Ca^{2+}, and these Ca^{2+} fluxes were not observed in the absence of ATP, confirming that they only occur when vacuole fusion is stimulated. Together, these findings suggest that blocking the interaction between Ypt7 and Vps41 inhibits formation of stable *trans*-SNARE complexes.

If our interpretation of these data is correct then promoting formation of stable *trans*-SNARE complexes should rescue membrane fusion defects caused by Ypt7-D44N. Adding purified recombinant Vam7 (rVam7), a soluble Qc-SNARE protein, to isolated vacuoles drives *trans*-SNARE complex formation and membrane fusion without the requirement for Ypt7 or HOPS function (Thorngren et al., 2004). Thus, to test this hypothesis we added rVam7 to vacuole fusion reactions (Figure 8E) and found that it indeed rescued defects in vacuole content mixing caused by Ypt7-D44N. Fusion was rescued in the absence and presence of ATP, confirming that stabilization of Vps41 or HOPS on membranes was not required for rVam7-mediated fusion. Furthermore, we confirmed that rVam7 also rescued defects in *trans*-SNARE

complex formation caused by Ypt7-D44N (Figure 8C) in support of our hypothesis. Thus, we reason that the Ypt7-Vps41 interaction is required for *trans*-SNARE complex stabilization, a prerequisite for SNARE-pin zippering that drives pore formation, the final step of vacuole membrane fusion.

Figure 8. Ypt7-D44N allows tethering and docking but prevents stabilization of *trans*-SNARE complexes

(A) (top) Examples of fluorescence micrographs showing FM4-64 stained vacuoles isolated from cells expressing wild type (WT), D44N or Q68L Ypt7 observed after 10 minutes incubation with ATP to stimulate tethering. 0.5 mM GTPγS was added to WT vacuoles where indicated. (bottom) Number of vacuoles per cluster was calculated from micrographic data. Means ± S.E.M. are shown ($n \geq 177$) (B) (top) Examples of fluorescence micrographs showing FM4-64 stained vacuoles isolated from cells expressing wild type (WT), D44N or Q68L Ypt7 observed after 30 minutes incubation with ATP to stimulate docking. 3.6 μM rGyp1-46 was added to WT vacuoles where indicated. (bottom) Boundary length was calculated from micrographic data. Cumulative probability and mean values ± S.E.M. are plotted ($n \geq 150$). (C) (top) Cartoon illustrating method to assess *trans*-SNARE complex formation. (bottom) Example of results from *trans*-SNARE pairing experiments as evaluated by immunoblotting for Nyv1 associated with CBP-Vam3 in the presence of ATP (control conditions, CTL) or 100 nM rVam7. Reactions conducted under control conditions were placed on ice as a negative control. (middle) Band density was calculated from Western blots. Means ± S.E.M. are shown ($n = 3$). (D) Ca^{2+} fluxes during fusion of vacuoles isolated from wild type (WT) cells with or without ATP or Ypt7-D44N cells with ATP assessed by monitoring Oregon Green BAPTA-dextran fluorescence over time. Influx and efflux amplitudes calculated from these experiments are shown as means ± S.E.M. ($n = 6$). (E) Vacuole content mixing was measured at 90 minutes in the presence or absence of ATP or 100 nM rVam7. Vacuoles were isolated from either cells expressing wild type (WT) or D44N Ypt7. Means ± S.E.M. are shown ($n = 3$). * indicates $P \leq 0.05$. Scale bars, 2 μm.

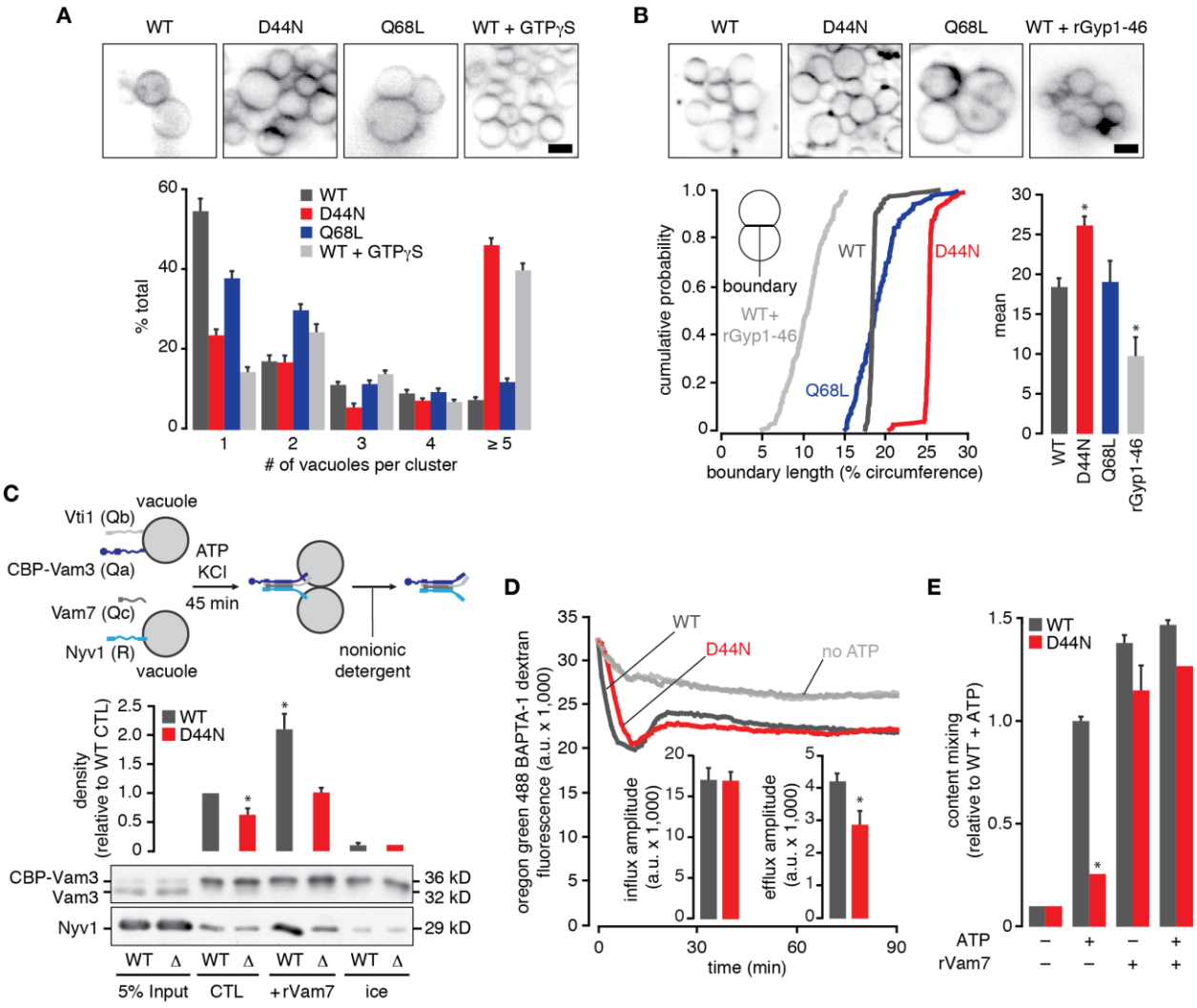
A
WT
D44N
Q68L
WT + GTPγS
% total
# of vacuoles per cluster
B
WT + rGyp1-46
boundary
WT+ rGyp1-46
cumulative probability
boundary length (% circumference)
mean
rGyp1-46
C
vacuole
Vti1 (Qb)
CBP-Vam3 (Qa)
Vam7 (Qc)
Nyv1 (R)
ATP
KCl
45 min
nonionic detergent
density (relative to WT CTL)
CBP-Vam3
Vam3
Nyv1
36 kD
32 kD
29 kD
5% Input
CTL
+rVam7
ice
D
oregon green 488 BAPTA-1 dextran fluorescence (a.u. x 1,000)
no ATP
influx amplitude (a.u. x 1,000)
efflux amplitude (a.u. x 1,000)
time (min)
E
content mixing (relative to WT + ATP)
ATP
rVam7

2.3.5 Stabilizing Vps41 on membranes by deleting YCK3 overcomes fusion defects caused by Ypt7-D44N

Based on the data presented, we developed a working model proposing that active Ypt7-D44N cannot bind Vps41 making its ALPS domain vulnerable to phosphorylation by Yck3, which in turn, causes it to dissociate from vacuole membranes. This then prevents HOPS from forming stable *trans*-SNARE complexes required for membrane pore formation to complete vacuole fusion. If true then blocking Yck3 activity should prevent Vps41 dissociation from membranes and rescue fusion defects caused by Ypt7-D44N. To test this hypothesis, we first deleted YCK3 in cells harboring wild type or mutant Ypt7 and assessed vacuole morphology in living cells by fluorescence microscopy (Figure 9A). Under standard isotonic conditions, we found that deleting YCK3 causes fewer cells to have multilobed vacuoles, an indication that vacuole fusion was enhanced, consistent with previous reports (LaGrassa and Ungermann, 2005; Brett et al., 2008). Importantly, knocking out YCK3 rescued the vacuole morphology defect observed in cells expressing Ypt7-D44N, as the number of cells with multilobed vacuoles was similar to wild type cells. Deleting YCK3 also prevents vacuoles from remaining fragmented after hypertonic stress (LaGrassa and Ungermann, 2005), presumably because an inhibitory circuit that prevents assembly of the fusion machinery is disrupted (Brett et al., 2008). We repeated this experiment and found that vacuoles did not remain fragmented after hypertonic shock in absence of YCK3 even in cells harboring Ypt7-D44N (Figure 9A), confirming that YCK3 contributed to fusion defects caused by this mutation. We next studied vacuole fusion events in live cells using video microscopy (Figure 9B, Video 2) and observed a similar number of fusion events (Figure 9C) and visible ILFs (Figure 9D) in wild type cells and *yck3Δ* cells expressing Ypt7-D44N. Together, these results suggest that deleting YCK3 rescues fusion defects caused by Ypt7-D44N *in vivo* in support of our model.

To confirm that the hypothesized mechanisms underlying this rescue were correct, we next measured vacuole content mixing *in vitro*. As predicted, deleting YCK3 completely rescued the defect in content mixing caused by Ypt7-D44N (Figure 9E). This correlated with the stabilization of Vps41 and HOPS (Vps33) on membranes over the course of the fusion reaction *in vitro* (Figure 9F). ATP-dependent dissociation of these proteins was no longer observed and the slower migrating form of Vps41 did not appear in samples lacking YCK3 (Figure 9G), confirming that Vps41 was not phosphorylated and thus was stabilized on membranes, even

when binding to active Ypt7 was disrupted by the D44N mutation. As previously reported (Brett et al., 2008), extracting wild type Ypt7 did not cause dissociation of Vps41 from membranes either, confirming that active Ypt7 is no longer required to stabilize Vps41 on membranes when YCK3 is absent. Finally, it is possible that deleting YCK3 may alter the post-translational modification profile of Vps41 allowing it to bind Ypt7-D44N, accounting for observed alleviation of fusion defects. To eliminate this possibility, we repeated Ypt7 protein pull-down experiments presented in Figure 7B with lysate from cells lacking YCK3 (Figure 9H). We found that deleting YCK3 was not able to recover the interaction defect, whereby Vps41 did not bind to Ypt7-D44N in the absence or presence of YCK3. All together, these findings support our working model, which describes how Yck3, Ypt7 and Vps41 work in concert to accommodate SNARE-mediated pore formation during homotypic vacuole fusion. Importantly, by exclusively targeting this last step of the lipid bilayer fusion reaction, interplay between these proteins regulates formation of ILFs during vacuole fusion.

Figure 9. Deleting YCK3 suppresses effects of Ypt7-D44N on vacuole fusion

(A) (left) Examples of fluorescence micrographs showing FM4-64 stained vacuoles within live wild type (WT), Ypt7-D44N, *yck3Δ*, or Ypt7-D44N::*yck3Δ* cells before (0 min) and 2 min or 30 min after treatment with 0.4 M NaCl. Dotted lines outline each cell as observed by DIC. (right) Proportion of cells with multi-lobed vacuoles calculated using the micrographic dataset ($n \geq 255$). (B) Images from time-lapse videos (Video 2) showing examples of FM4-64 stained vacuoles undergoing homotypic fusion within live wild type (WT) Ypt7, Ypt7-D44N, *yck3Δ* or Ypt7-D44N::*yck3Δ* cells. Numbers represent time in seconds. From these videos, (C) percentage of cells that presented vacuole fusion events and (D) percentage of vacuole fusion events that failed to form visible ILFs were calculated. Mean ± S.E.M. are shown ($n \geq 200$). (E) Vacuoles were isolated from wild type (WT), Ypt7-D44N, *yck3Δ* or Ypt7-D44N::*yck3Δ* cells and vacuole content mixing in the presence of ATP was measured over time. Mean ± S.E.M. are shown ($n = 4$). (F) Results from Rab activity assays (see Figure 7C) conducted using vacuoles isolated from wild type (WT), Ypt7-D44N, *yck3Δ* or Ypt7-D44N::*yck3Δ* cells in the presence or absence of ATP. Membrane association of Vps41, Vps33 or Ypt7 was assessed by immunoblotting. Membrane (pellet, P) and soluble (supernatant, S) fractions are shown ($n = 2$). (G) Vacuoles isolated from wild type (WT), Ypt7-D44N, *yck3Δ*, or Ypt7-D44N::*yck3Δ* cells were incubated with ATP for 0 or 30 minutes and membrane association of Vps41 and Vps33 was assessed by immunoblot. Membrane (pellet, P) and soluble (supernatant, S) fractions are shown ($n = 2$). (H) Results of pull-down experiments performed using immobilized GST-Ypt7 (WT or D44N) preloaded with GDP (D), GTP (T) or GTPγS (γ) and cell lysates from WT or *yck3Δ* cells. Amount of Vps41 bound to GST-Rab resin or found in the lysate (load) was determined by immunoblotting ($n = 2$). * indicates $P \leq 0.05$. Scale bars, 2 μm.

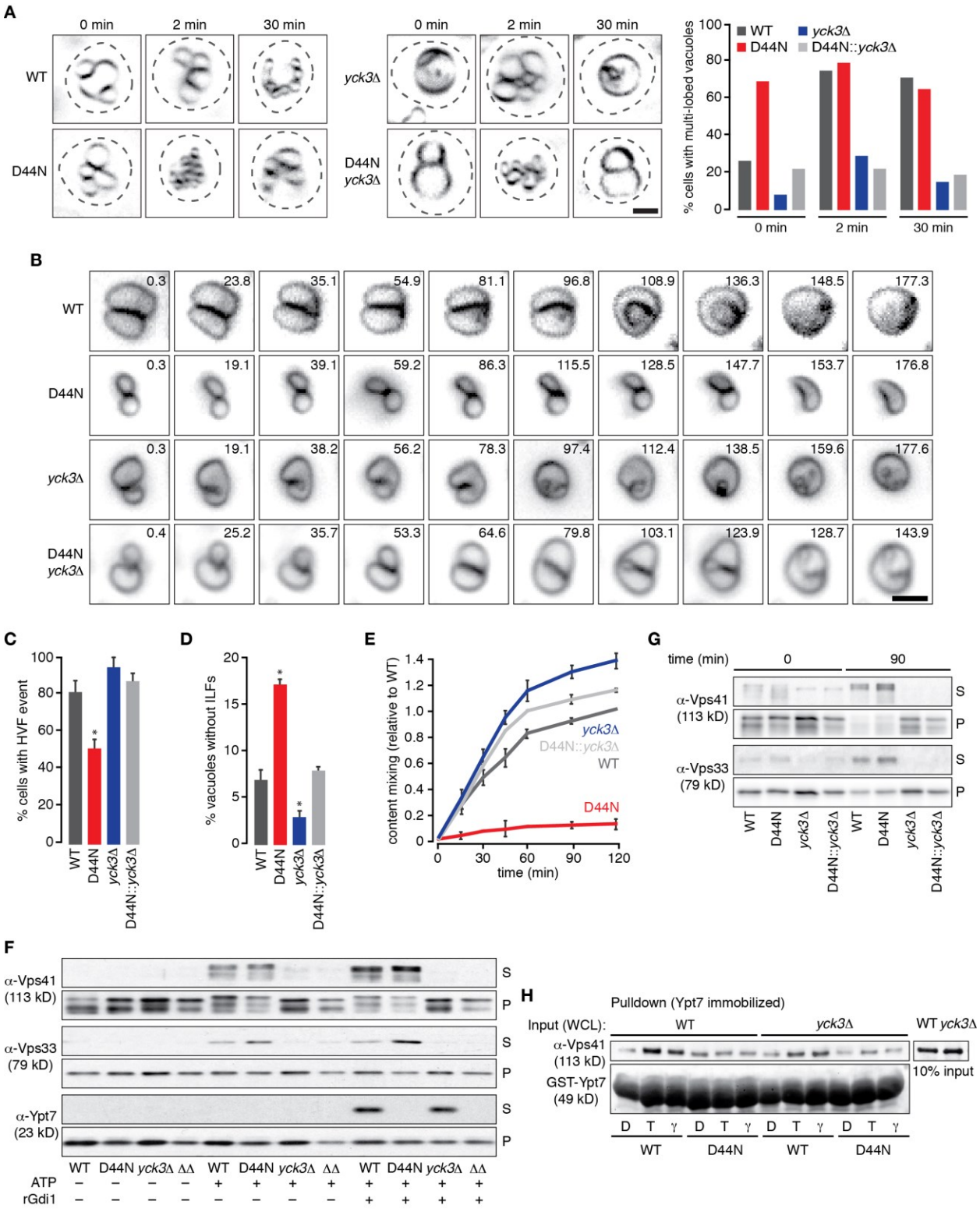
A
0 min
2 min
30 min
WT
D44N
yck3Δ
D44N yck3Δ
% cells with multi-lobed vacuoles
WT
yck3Δ
D44N
D44N::yck3Δ
B
WT
D44N
yck3Δ
D44N yck3Δ
C
% cells with HVF event
D
% vacuoles without ILFs
E
content mixing (relative to WT)
time (min)
yck3Δ
D44N::yck3Δ
WT
D44N
G
time (min)
α-Vps41 (113 kD)
α-Vps33 (79 kD)
S
P
F
α-Vps41 (113 kD)
α-Vps33 (79 kD)
α-Ypt7 (23 kD)
ATP
rGdi1
H
Pulldown (Ypt7 immobilized)
Input (WCL):
α-Vps41 (113 kD)
GST-Ypt7 (49 kD)
10% input

2.4 Discussion

2.4.1 ILF formation is regulated by the Ypt7-Vps41 interaction and HOPS phosphorylation

Here we show that uncoupling Ypt7 activation from Vps41 binding (Figure 7B and C) interferes with pore formation (Figure 6B) required for vacuole membrane merger. This is because Ypt7-GTP no longer shields Vps41 from Yck3 causing its phosphorylation (Figures 7G and 9G) and subsequent dissociation of HOPS from membranes (Figures 7E and F, 9F and G). Vps33 within HOPS then releases and exposes *trans*-SNARE complexes to Sec18, which unravels them. Thus, because *trans*-SNARE complexes are not stabilized (Figure 8C), SNARE-pins cannot efficiently zipper to drive pore formation. Importantly, although pore formation is stalled, stalk formation persists in the presence of Ypt7-D44N (Figure 6A) causing a delay between stalk and pore formation (Figure 6G) allowing hemifusion diaphragms to expand across boundary membranes (Figure 6H-K). So, when fusion events do occur, fewer intralumenal membrane fragments are formed (Figures 5F and 6F). Thus, the interplay between Rab-GTPase, effector and kinase regulates ILF formation during vacuolar lysosome fusion.

Previously we showed that lysosomal polytopic proteins are selectively sorted into the boundary and packaged within ILFs for degradation (McNally et al., 2017). Whereas, here we show that ILF formation can be regulated to control the amount of membrane lipids and proteins internalized. It has been proposed that sorting and packaging of internalized surface transporter and receptor proteins into intralumenal vesicles by ESCRTs at the endosome triggers Ypt7 activation to stimulate multivesicular body fusion with lysosomes (Shideler et al., 2015). As Ypt7 has been implicated in sorting and packaging of lysosomal transporter proteins into ILFs (McNally et al., 2017), we speculate that a similar signaling mechanism may exist to sense lysosomal polytopic protein entry into the boundary and adjust the amount of membrane internalized for efficient degradation. Our interpretation of these results also offers an alternative function for SNARE complex proofreading by HOPS (Starai et al., 2008), whereby this activity seems to be important for adjusting the kinetics of pore formation, the rate limiting step of the bilayer fusion reaction (Reese and Mayer, 2005), to regulate production of ILFs during fusion. Furthermore, Yck3 is a member of the type I casein kinase family of protein kinases that have diverse roles in cell physiology, and are highly integrated into cellular signaling cascades (Knippschild et al., 2005), suggesting that it may represent a hub for signal integration to control ILF formation and coordinate vacuolar lysosome remodeling as part of global cellular changes

induced by aging or replication programs. Thus, it seems that the interplay between Ypt7, Vps41 and Yck3 does not simply encode an analog switch to control fusion as originally implied (Brett et al., 2008). Rather, we propose that it represents a digital modulator that fine-tunes intermediate formation during ring fusion-by-hemifusion to adjust ILF formation in response to cellular signaling for vacuolar lysosome homeostasis and remodeling.

2.4.2 Contribution of the Ypt7-Vps41 interaction to lysosome fusion

In addition to describing a mechanism that regulates ILF formation, these results provide missing evidence needed to advance our understanding of how the protein machinery mediates organelle membrane fusion. Recently, multiple groups have published conflicting reports concerning the role of the interactions between Ypt7, HOPS and Yck3 in tethering, docking and fusion by primarily studying reconstituted, synthetic proteoliposomes (e.g. Hickey et al. 2009; Ho and Stroupe 2016; Lürick et al. 2016; Zick and Wickner 2016). Here we took the unique approach of modifying Ypt7 to block Vps41 binding and find that tethering (Figure 8A) and docking (Figure 8B) of native organelle membranes persists. We are confident that proper docking occurs because Ypt7-D44N allows polytopic protein sorting to occur at boundary membranes (Figure 6G), the mutation did not affect the prevalence of interactions observed between apposing vacuole membranes as visualized by TEM (Figure 6K), and the mutation permits *trans*-SNARE complex formation (Figure 8C) and Ca^{2+}-efflux (Figure 8D). Thus, our results suggest that the Ypt7-Vps41 interaction is dispensable for membrane tethering and docking of organelles. Moreover, we find that blocking the Rab-effector interaction specifically abolishes vacuole content mixing (Figure 6B) but permits lipid mixing (Figure 6A). This maps the interaction to SNARE-mediated pore formation. Importantly, deleting YCK3 rescues all fusion defects caused by this mutation by preventing Vps41 dissociation from membranes (Figure 9). Thus, to account for all observations, we propose a new working model of HOPS-mediated vacuolar lysosome fusion that describes how Rab, kinase and SNAREs cycles may be synchronized to regulate ILF formation and to reset the machinery immediately after pore formation (Figure 10).

Assuming the fusion machinery is reset (inactive and dispersed) after a previous fusion event, we propose that most Ypt7 is GDP-bound on the vacuole membrane during the priming stage of fusion. Thus, Ypt7 likely stabilizes HOPS on vacuole membranes by exclusively binding Vps39 on one end of the complex (Bröcker et al., 2012). To accommodate tethering, we

propose that the ALPS domain within Vps41 on the other end of HOPS interacts with acidic lipids within the opposing vacuole membrane to initiate contact (Ho and Stroupe, 2016). This requires dephosphorylated Vps41, which may be promoted by the protein phosphatase 1 ortholog Glc7, as it may contribute to many stages of homotypic vacuole fusion (Peters et al., 1999). Once contact is made, we propose that Vps39 within one HOPS complex interacts with the GEF Mon1-Ccz1 to activate Ypt7 (Nordmann et al., 2010), which in turn binds Vps41 located nearby within a second flipped HOPS complex donated from the opposing membrane (Zick and Wickner, 2016). By closing a positive feedback loop (Brett et al., 2008), Rab signaling in trans would drive recruitment and stabilization of the fusion protein machinery at the vertex ring only between two membranes, preventing abortive assembly on single membranes. As docking occurs, membranes are drawn close enough together (~8 nm; Mattie et al. 2017) to encourage *trans*-SNARE templating and partial complex assembly by Vps33 within HOPS (Baker et al., 2015). *Trans*-SNARE complex formation correlates with Ca^{2+} efflux (Merz and Wickner, 2004) and is sufficient for stalk formation (Reese and Mayer, 2005; Schwartz and Merz, 2009; Pieren et al., 2010). This is when *trans*-SNARE complex proofreading by HOPS occurs (Starai et al., 2008), which shields complexes from Sec18 to prevent unraveling (Xu et al., 2010; Lobingier et al., 2014), while promoting complete SNARE-pin zippering to drive pore formation (Pieren et al., 2010). Pore expansion then completes the fusion reaction, and seems to occur concomitantly with dispersal of the vertex ring suggesting that fusion protein machinery is inactivated and disassembled (see Videos1 and 2; Wang et al. 2002; Mattie et al. 2017; McNally et al. 2017).

Consistent with previous reports (Zick and Wickner 2012; Orr et al. 2015; Ho and Stroupe 2015; Ho and Stroupe 2016; Lürick et al. 2016; Zick and Wickner 2016), we find that Vps41 association with the membrane either through binding Ypt7-GTP or insertion of its dephosphorylated ALPS domain is sufficient to drive all stages of fusion. However, our findings from studying Ypt7-D44N reveal that Yck3 activation may occur after *trans*-SNARE pairing. This introduces a protein kinase cycle during the fusion reaction that defines distinct roles for each mechanism: When dephosphorylated, the ALPS-domain of Vps41 stabilizes HOPS on membranes to support tethering and docking (Ho and Stroupe, 2016; Zick and Wickner, 2016). However, when this domain is phosphorylated after *trans*-SNARE pairing, the Ypt7-Vps41 interaction stabilizes HOPS on membranes (Zick and Wickner, 2012; Orr et al., 2015; Ho and Stroupe, 2015; Lürick et al., 2016) to ensure *trans*-SNARE complex proofreading and

subsequent zippering to complete fusion. But why would Yck3, an inhibitory kinase, be activated during the vacuole fusion reaction?

Although we argue that it may control pore formation (the rate-limiting step of the fusion-by hemifusion reaction) to regulate ILF formation, it may also coordinate completion of Rab and SNARE cycles needed to reset the system: Another target of Yck3 is the Qa-SNARE Vam3, which is phosphorylated when fusion is blocked, suggesting that this may inhibit its function (Brett et al., 2008). Yck3 also phosphorylates Mon1 (a component of the Ypt7 GEF complex) causing it to dissociate from the membrane (Lawrence et al., 2014). In *Dictyostelium discoideum*, Ca^{2+} release during vacuole fusion stimulates GAP activity and inactivates Rab to complete vacuole membrane fusion (Parkinson et al., 2014). Thus, we speculate that coordination of Yck3 activation and Ca^{2+} efflux upon *trans*-SNARE pairing may promote Ypt7 inactivation by its cognate GAP Gyp7 (Brett et al., 2008), which together with Vam3-phosphorylation, may release SNAREs from HOPS and synchronize disassembly of the fusion machinery (e.g. cis-SNARE pin unraveling by Sec18; Alpadi et al. 2012) immediately upon SNARE-pin zippering to perhaps accommodate pore expansion and prevent future rounds of fusion (LaGrassa and Ungermann, 2005). We speculate that this molecular circuitry acts analogously to a Rab-cascade mechanism (Hutagalung and Novick, 2011) to reset the fusion machinery after homotypic fusion, where both membranes share identical components.

Our findings also provide insight into the potential role for Ca^{2+} in ring-fusion-by hemifusion: During docking, negatively charged, fusogenic lipids concentrate at the vertex ring, the site of highest membrane curvature and where membranes are closely apposed (~8 nm apart, Figure 2J; Fratti et al. 2004; Wickner 2010; Mattie et al. 2017). Thus, it has been proposed that divalent calcium cations released into the intermembrane space may directly drive lipid mixing by forming anhydrous trans complexes between negatively charged phospholipids within apposing outer leaflets (Wilschut et al., 1980). However, we argue that this is unlikely because introducing Ypt7-D44N reduces the amplitude of Ca^{2+} efflux (Figure 8D) but does not affect lipid mixing (Figure 6A). Furthermore, adding GTPγS to fusion reactions does not change Ca^{2+} efflux (data not shown) but enhances lipid mixing (Mattie et al., 2017). Others have reported similar findings that show no correlation between Ca^{2+} efflux and lipid mixing (e.g. Ca^{2+} signaling is delayed but kinetics of lipid mixing are unaffected by knocking out YBT1; Sasser et al. 2012), suggesting that stalk formation is Ca^{2+}-independent. Rather, *trans*-SNARE pairing

alone may be sufficient for lipid mixing (Reese and Mayer, 2005; Schwartz and Merz, 2009; Pieren et al., 2010) and Ca^{2+} may exclusively mediate downstream SNARE-pin zippering for pore formation (Hofmann et al., 2006; D'Agostino et al., 2016). This is analogous to its role in synaptic vesicle fusion to synchronize rapid neurotransmitter release, whereby synaptotagmin and complexin mediate Ca^{2+}-dependent stalk-to-pore transition at the synapse (Krishnakumar et al., 2011). But the contributions of orthologous proteins to vacuolar lysosome fusion are not understood in detail and orthologs are not present on vacuolar lysosomes within *S. cerevisiae*. Now that the physiological relevance of ring fusion-by-hemifusion is apparent, we hypothesize that Ca^{2+}-mediated pore formation may be repurposed to control ILF formation during vacuolar lysosome fusion for organelle homeostasis and remodeling, warranting further investigation in the near future.

2.4.3 Physiological relevance of regulating ILF formation by ring fusion-by-hemifusion

An intriguing question arises from our findings: Can ILFs form during other membrane fusion events within cells? Although we are unaware of any published studies that directly address this question, we hypothesis that ILF formation during fusion may be an underappreciated and widespread mechanism for cellular membrane remodeling based on the following: First, orthologous fusion machinery (Rabs, MTCs, SNAREs) is found on most membranes in cells (Nickerson et al., 2009; Kuhlee et al., 2015; Dubuke and Munson, 2016) where it mediates fusion events required for exocytosis and endocytosis for example, and this machinery is evolutionarily conserved in all eukaryotes (Balderhaar and Ungermann, 2013; Spang, 2016). Second, intralumenal membrane vesicles are present within endosomes when ESCRTs are impaired (Stuffers et al., 2009; Edgar et al., 2014), suggesting that organelle fusion events may instead be responsible for their formation. Finally, reports that imply ILF formation during fusion at other membranes are beginning to emerge, e.g. extracellular membrane fragments appear during large astrocytic vesicle exocytosis (Peng et al., 2013) and during non-selective intracellular compartment exocytosis for plasma membrane wound healing (Davenport et al., 2016). But why form fragments during these fusion events? We speculate that selective protein (and possibly lipid) sorting into these fragments during exocytosis offers the opportunity to ensure that newly added membrane from intracellular compartments is devoid of molecules that would interfere with plasma membrane identity or function, or to remodel the plasma membrane.

However, currently ILF formation has only been convincingly documented during homotypic vacuolar lysosome fusion. We argue that this reflects current limitations in light microscopy, whereby vacuolar lysosomes and boundaries formed between them during fusion are relatively large (~2 μm diameter) facilitating the visualization of protein sorting and membrane internalization by HiLo fluorescence microscopy (Tokunaga et al., 2008). But visualizing boundary and ILF formation during fusion of smaller organelles (e.g. endosomes, ~500 nm diameter; mammalian lysosomes, as small as 200 nm; (Klumperman and Raposo, 2014) are impossible using most optical methods due to the limited diffraction of light that prevents resolving two adjacent fluorophores closer than ~250 nm apart. However, new methods in super-resolution fluorescence microscopy (e.g. lattice light-sheet microscopy; Chen et al., 2014) that overcome these technical barriers are beginning to emerge. Thus, we believe that the answer to this important question will be revealed soon and predict that regulated ILF formation during membrane fusion will have a broad impact on organelle biogenesis, homeostasis and remodeling in all eukaryotic cells.

Figure 10. Working model of regulated ILF formation during vacuolar lysosome fusion

Cartoon showing how Rab-GTPase, protein kinase and SNARE –cycles are coordinated by HOPS to regulate intermediates of the ring-fusion-by-hemifusion reaction to control ILF formation during homotypic vacuolar lysosome fusion. Disrupting the Ypt7-Vps41 interaction by introducing the D44N mutation maps to a late stage of docking when active Ypt7 is required to stabilize phosphorylated HOPS on membranes to promote SNARE-mediated pore formation.

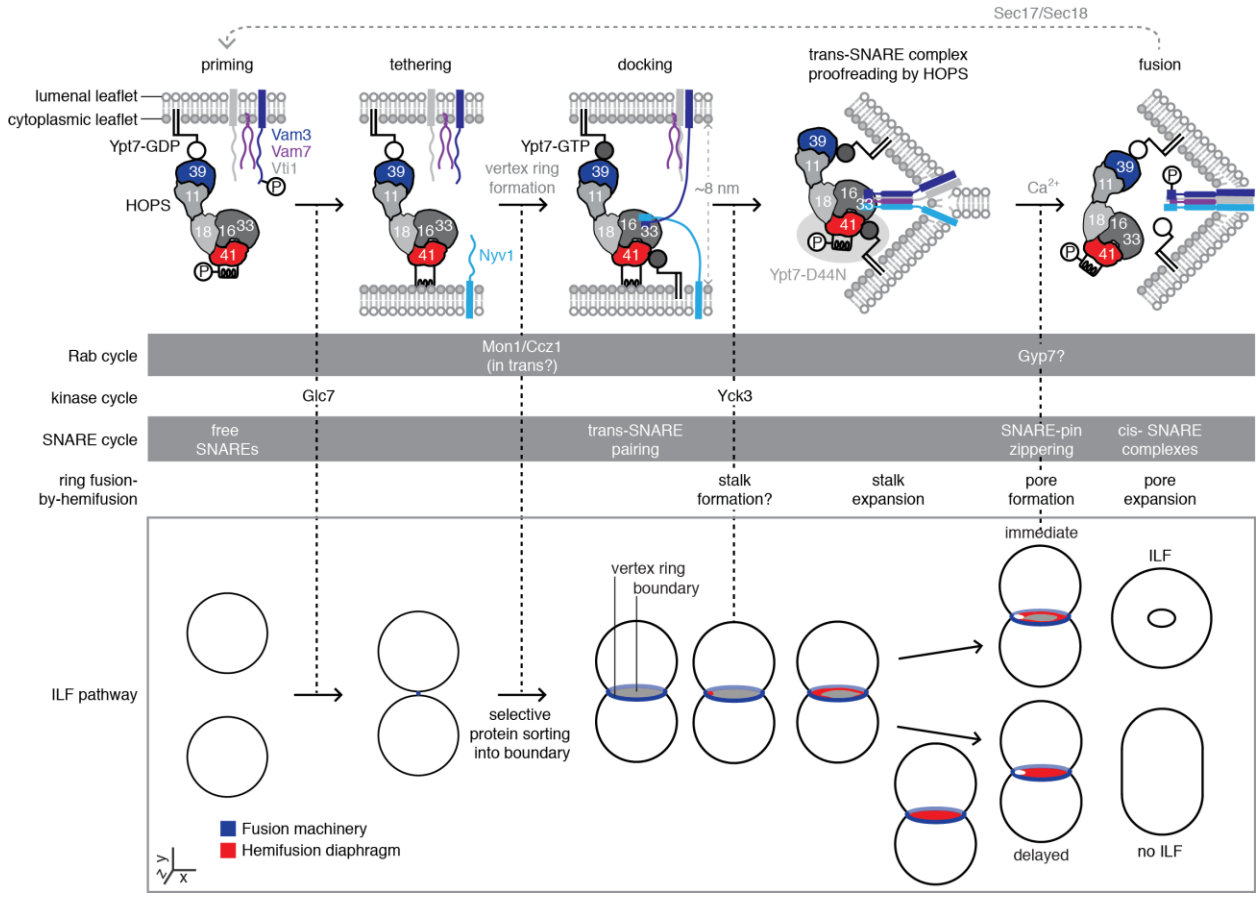
Sec17/Sec18
priming
tethering
docking
trans-SNARE complex proofreading by HOPS
fusion
lumenal leaflet
cytoplasmic leaflet
Ypt7-GDP
Vam3
Vam7
Vti1
HOPS
Nyv1
Ypt7-GTP
vertex ring formation
~8 nm
Ypt7-D44N
Ca2+
Rab cycle
Mon1/Ccz1 (in trans?)
Gyp7?
kinase cycle
Glc7
Yck3
SNARE cycle
free SNAREs
trans-SNARE pairing
SNARE-pin zippering
cis- SNARE complexes
ring fusion-by-hemifusion
stalk formation?
stalk expansion
pore formation
pore expansion
ILF pathway
vertex ring boundary
selective protein sorting into boundary
immediate
ILF
delayed
no ILF
Fusion machinery
Hemifusion diaphragm

2.5 Materials and Methods

2.5.1 Yeast strains and reagents

All strains and plasmids used in this study are listed in Table 1. For cell-free organelle fusion assays (content or lipid mixing), we used the complimentary *Saccharomyces cerevisiae* strains BJ3505 [*MATα pep4::HIS3 prbΔ1-1.6R his3–Δ200 lys2–801 trp1-Δ101 (gal3) ura3–52 gal2 can1*] and DKY6281 [*MATα leu2-3 leu2-112 ura3-52 his3- Δ200 trpl-Δ901 lys2-801 suc2-Δ9 pho8::TRP1*]. SEY6210 (Vph1-GFP) [*MATα, leu1-3, 112 ura3-52 his3-200, trp1-901 lys2-801 suc2-Δ9, VPH1-GFP::TRP1*] was used to assess hemifusion interphases (Mattie et al., 2017). DKY6281-CBP::Vam3 *nyv1Δ* was used to evaluate *trans*-SNARE complex association (Collins and Wickner, 2007). SEY6210 (GFP-Vps39) [*MATα, leu1-3, 112 ura3-52 his3-200, trp1-901 lys2-801 suc2-Δ9, Vam6::His3, pGFP-Vps39*] was used to prepare whole cell lysate for protein pull-down assays. YPT7 knock out in SEY6210 (Vph1-GFP) or DKY6281-CBP::Vam3 *nyv1Δ* and YCK3 knock out in BJ3505 or DKY6281 cells were performed using the Longtine method (Longtine et al., 1998). Plasmids encoding Ypt7-D44N or GFP-Ypt7-D44N under the control of the ADH1-promoter were generated by cycle PCR site-directed mutagenesis from pRS405-Ypt7 or pRS405-GFP-Ypt7 respectively, and inserted into the genome of the strains lacking YPT7. All biochemical and yeast growth reagents were purchased from Sigma-Aldrich, Invitrogen or BioShop Canada Inc. All restriction enzymes, Ni-Sepharose 6FF, and glutathione Sepharose 4B, polymerases, and ligases were purchased from New England Biolabs (County Rd, Ipswich, MA, USA). Purified rabbit polyclonal antibody against Ypt7, Vps33, Vps41, and Vps39 were gifts from Alexey Merz (University of Washington, Seattle, WA, USA). Recombinant rabbit IgG against GFP was purchased from Abcam (Toronto, ON). Proteins used include recombinant Gdi1 purified from bacterial cells using a calmodulin-binding peptide intein fusion system (Brett et al., 2008), recombinant Gyp1-46 (the catalytic domain of the Rab-GTPase activating protein Gyp1) purified as previously described (Eitzen et al., 2000), and recombinant soluble Qc-SNARE Vam7 purified as previously described (Schwartz and Merz, 2009). Reagents used in fusion reactions were prepared in 10 mM Pipes-KOH, pH 6.8, and 200 mM sorbitol (Pipes-Sorbitol buffer, PS).

2.5.2 Vacuole isolation and cell-free fusion assays

Organelles were isolated from yeast cells by the Ficoll floatation method as previously

described (Haas et al., 1994). Lipid mixing assays were assessed according to Jun and Wickner (2007) with slight modifications. Vacuoles (300 µg) isolated from BJ3505 or BJ3505 (Ypt7-D44N) were incubated with 150 µM octadecyl rhodamine B (R18) in a total volume of 400 µl PS buffer for 10 minutes at 4°C. Stained vacuoles were then mixed gently with 600 µl 15% (wt/vol) Ficoll and transferred to a thin wall polypropylene tube (13 x 51 mm, Beckman), overlaid with 1 ml 8% (wt/vol) Ficoll, 1 ml 4% (wt/vol) Ficoll, and 1 ml of PS buffer without ficoll, and centrifuged for 30 minutes (105000 g, 4°C) in an SW 55 Ti rotor (Beckman). To evaluate vacuole lipid bilayer mixing, 6X reactions (180 µl) containing 4 µg of R18-labeled vacuoles and 32 µg of unlabeled vacuoles from DKY6281 or DKY6281 (Ypt7-D44N) were mixed under fusion conditions (125 mM KCl, 5 mM $MgCl_2$, 1 mM ATP, 40 mM creatine phosphate, 0.5 mg/ml creatine kinase, 10 µM CoA) in PS buffer. Reactions were transferred to a black, half-volume 96-well flat-bottom microtiter plates and rhodamine fluorescence (λ_{ex}= 544 nm; λ_{em}= 590 nm) was measured using a BioTek Synergy H1 plate reading fluorometer. Readings were taken every two minutes for 60 minutes at 27°C. Data shown were normalized to values obtained at 60 minutes under standard fusion conditions. Content mixing assays were conducted as described previously (Haas et al., 1994). Briefly, 30 µl reactions containing 3 µg of vacuoles lacking the protease Pep4 (BJ3505), and 3 µg of vacuoles from cells without Pho8 (DKY6281) in fusion reaction buffer were incubated at 27°C for 120 minutes, and then assayed for ALP maturation. Data shown were normalized to values obtained at 120 minutes under standard fusion conditions.

2.5.3 Ypt7 extraction assay

The Rab-GTPase extraction assay was performed as previously described (Brett et al., 2008). Briefly, 5X reactions (150 µl) containing 30 µg organelles from DKY6281 (wild type or Ypt7-D44N) cells were incubated under fusion condition for 30 minutes at 27°C. rGdi1 (5 µM) was added, and the reactions were further incubated for 10 more minutes. Samples were placed on ice for 2 minutes and protease inhibitors were added (0.46 µg/ml leupeptin, 3.5 µg/ml pepstatin, 2.4 µg/ml pefabloc, 1 mM PMSF). Samples were immediately centrifuged (5000 g, 5 minutes, 4°C) to separate membrane-bound proteins from those in the supernatant. The supernatant (100 µl) was transferred into fresh tubes and mixed with 25 µl 5X Laemmli SDS sample buffer while the pellets were resuspended in 100 µl 1X of the same sample buffer and boiled at 95°C for 10 minutes. One tenth of the total isolated supernatant or pellet was analyzed

by Western blot.

2.5.4 Rab-GTPase pull-down assay

pGST-Ypt7 (D44N) was generated from pGST-Parallel-1 Ypt7 (Brett et al., 2008) by cycle PCR site directed mutagenesis. The resulting plasmid was expressed in *E. coli* BL21-pRIL cells. GST-tagged proteins (Ypt7-WT, D44N, or Q68L) were bound to glutathione–Sepharose 4B resin (GE Healthcare) as described previously (Brett et al., 2008). Rab proteins were loaded with GDP, GTP, or GTPγS by incubating Rab-bound resin in nucleotide loading buffer (50 mM Tris-Cl, pH 8.5, 100 mM NaCl, 0.01% 2-mercaptoethanol, 5 mM $MgCl_2$, and 500 µM guanine nucleotide) for 1 hour. The resin was washed 3 times with 500 µl pull-down buffer (50 mM Hepes-KOH, pH 7.8, 100 mM NaCl, 5 mM $MgCl_2$, and 5 mM 2-mercaptoethanol). Nucleotide-loaded GST-Rab resin (50 µl) was then incubated with 150 µg of whole cell lysates for two hours at 4°C. The resin was then washed 3 times with 500 µl lysis buffer (20 mM Hepes-KOH, pH 7.4, 50 mM potassium acetate, 200 mM sorbitol, 0.01% 2-mercaptoethanol, 5 mM $MgCl_2$, 0.7 µg/ml leupeptin, 0.5 µg/ml pepstatin, and 1 mM PMSF). GST-Rabs and their bound proteins were eluted by boiling samples in 1X Laemmli SB (95°C, 10 minutes). To prepare whole cell lysates, 1 L of cells expressing Vps39-GFP or cells from DKY6281 missing the YCK3 gene were grown to an OD_{600}= 1. The cell wall was digested with zymolyase (30°C, 30 minutes) and the resulting spheroplasts were resuspended in lysis buffer and Dounce homogenized (30 strokes) on ice. The lysate was solubilized with 1% Triton X-100 and clarified by centrifugation (20000 g, 15 min).

2.5.5 Tethering and docking assays

To evaluate vacuole clustering, 1X reactions (30 µl) containing 6 µg of vacuoles from DKY6281-WT, Ypt7-D44N, or Ypt7-Q68L were incubated in fusion reaction buffer (10 mM Pipes/KOH, pH 6.8, 200 mM sorbitol, 125 mM KCl, 5 mM $MgCl_2$, 1 mM ATP, 40 mM creatine phosphate, 0.5 mg/ml creatine kinase, 10 µM CoA) and supplemented with 3 µM FM4-64 for 10 minutes at 27°C. Samples were then chilled on ice, and 10 µl aliquots were transferred to pre-chilled slides and imaged by fluorescence microscopy. The docking assay was as described (Wang et al., 2002) with minor modifications. Vacuoles (6 µg) from DKY6281-WT, Ypt7-D44N, or Ypt7-Q68L were preincubated with 3 µM FM4-64 for 10 minutes. Stained vacuoles were brought to 30 µl total volume with fusion reaction buffer, incubated for 30 minutes at 27°C, and then placed immediately on ice. Aliquots (10 µl) were transferred to pre-chilled slides and

imaged by fluorescence microscopy.

2.5.6 *Trans*-SNARE paring assay

Analysis of *trans*-SNARE complex formation was assayed as described (Jun and Wickner, 2007), whereby the levels of Nyv1 that co-immunoprecipitate with CBP::Vam3 was determined. Briefly, 45 µg of vacuoles each from DKY6281-CBP::Vam3 *nyv1Δ* and BJ3505 or DKY6281 (Ypt7-D44N, CBP::Vam3 *nyv1Δ*) and BJ3505 (Ypt7-D44N) were incubated under fusion conditions for 45 minutes. Reactions were then placed on ice for 5 minutes, and samples were centrifuged (11000 g, 15 minutes, 4°C). Supernatants were decanted, and membrane fractions were resuspended in 180 µl solubilization buffer (20 mM Tris-Cl pH 7.5, 150 mM NaCl, 1 mM $MgCl_2$, 0.5% Nonidet P alternative, 10% glycerol) with protease inhibitors (0.46 µg/ml leupeptin, 3.5 µg/ml pepstatin, 2.4 µg/ml pefabloc, 1 mM PMSF). Reactions were topped up to a final volume of 560 µl and nutated for 20 minutes at 4°C. Reactions were centrifuged again (16,000 g, 20 minutes, 4°C) and supernatants collected. Ten percent of the extracts were collected as input samples, and the remaining extracts were brought to 2 mM $CaCl_2$. The CBP::Vam3/Nyv1 complexes were recovered with calmodulin Sepharose beads 4B (GE Healthcare) by nutating overnight at 4°C, collected by brief centrifugation (4,000 g, 2 minutes, 4°C), washed five times with sample buffer, and followed by bead sedimentation. Bound proteins were eluted by boiling beads (95°C, 10 minutes) in SDS sample buffer containing 5 mM EGTA for SDS-PAGE analysis and immunoblotting.

2.5.7 HiLo Fluorescence microscopy

Live yeast cells stained with FM4-64 to label vacuole membranes were prepared for imaging using a pulse-chase method as previously described (Brett et al., 2008). For *in vitro* imaging, vacuolar lysosomes isolated from DKY6281-WT, Ypt7-D44N, Ypt7-Q68L or strains expressing Vph1-GFP (WT or Ypt7-D44N) were stained with FM4-64 by treating organelles with 3 µM FM4-64 for 10 minutes at 27°C before addition to fusion reaction buffer. Reactions were then incubated at 27°C for 60 minutes and placed on ice prior to visualization using a Nikon Eclipse TiE inverted microscope equipped with a motorized laser TIRF illumination unit, Photometrics Evolve 512 EM-CCD camera, an ApoTIRF 1.49 NA 100x objective lens, and bright (50 mW) blue and green solid-state lasers operated with Nikon Elements software (housed in the Centre for Microscopy and Cellular Imaging at Concordia University). Micrographs were processed

using ImageJ software (National Institutes of Health) and Adobe Photoshop CC. Images shown were adjusted for brightness and contrast, inverted and sharpened with an unsharp masking filter.

2.5.8 Transmission electron microscopy

As previously described (Mattie et al., 2017), fusion reactions were incubated at 27°C for 30 minutes, vacuoles were gently pelleted (5000 g for 5 minutes) at 4°C and immediately fixed with 2.5% glutaraldehyde in 0.1 M cacodylate buffer (pH 7.4) overnight at 4°C. Vacuole pellets were washed with 0.1 M sodium cacodylate (3 times, 10 minutes) and then fixed with 1% osmium tetroxide for two hours at 4°C. Pellets were washed with water (3 times, 5 minutes) followed by gradual dehydration in ethanol (30-100%) and 100% propylene oxide. Pellets were infiltrated with epon:propylene oxide for 1 hour and then embedded in pure epon by polymerization (48 hour at 57°C). Samples were cut into 100 nm thick sections using an ultra-diamond knife and Reichert Ultracut II microtome, loaded onto 200-mesh copper grids, and stained with uranyl acetate (8 minutes) and Reynold's lead (5 minutes). Sections were imaged at 120 kV using a FEI Tecnai TEM outfitted with a Gatan Bioscan digital camera (1k × 1k pixels) housed in the Facility for Electron Microscopy Research (FEMR) at McGill University. For each condition, images were obtained from at least three separate vacuole fusion reactions. Micrographs shown were adjusted for brightness and contrast and sharpened with an unsharp masking filter using Adobe Photoshop CC software.

2.5.9 Western blot analysis

Sodium dodecyl sulfate-polyacrylamide gel electrophoresis (SDS-PAGE) was performed using a Bio-Rad mini protein system (Bio-Rad Laboratories, Hercules, CA, USA). After separation, proteins were transferred onto a nitrocellulose membrane by wet transfer method at 12 V for 8 hours using a Royal Genie Blotter apparatus (Idea Scientific, Minneapolis, MN, USA). Membranes were blocked with 3% BSA in PBST buffer (137 mM NaCl, 2.7 mM KCl, 10 mM Na_2HPO_4, 2 mM KH_2PO_4, 0.1% Tween-20) and then washed twice with PBST and incubated with primary antibody diluted to 1:1000 in PBST for 1 hour at room temperature. Membranes were washed with PBST five times, and then incubated with HRP-labeled goat anti-rabbit IgG diluted 1:10000 in PBST for 1 hour at room temperature. After an additional 5 washes with PBST, the membranes were probed to detect bound secondary antibody using GE Amersham Imager 600 (GE Healthcare, Piscataway, NJ, USA).

2.5.10 Data analysis and presentation

To calculate vacuoles surface area, we took two measurements for the diameter across from each other (assuming that vacuoles were spherical) and averaged them. Boundary lengths of vacuole interfaces were calculated as a percentage of the vacuole circumference (calculated using diameter measurements) represented by the interface between two vacuole membranes (measured as the distance along apposed flattened membranes). All quantitative data were processed using Microsoft Excel v.14.0.2 software (Microsoft Cooperation, Redmond, WA, USA), including calculation of mean and S.E.M. Comparisons were calculated using Student two-tailed t-test, P values < 0.05 indicate significant differences. Data were plotted using Kaleida Graph v.4.0 software (Synergy Software, Reading, PA, USA). All figures were prepared using Adobe Illustrator CC software (Adobe Systems, San Jose, CA, USA).

Table 1: Yeast strains and plasmids used in this study.

Strain	Genotype	Source
BJ3505	*MATα pep4::HIS3 prb1-Δ1.6R his3–200 lys2–801 trp1Δ101 (gal3) ura3–52 gal2 can1*	Jones et al., 1982
DKY6281	*MATα leu2-3 leu2-112 ura3-52 his3- Δ200 trpl-Δ901 lys2-801 suc2-Δ9 pho8::TRP1*	Hass et al., 1994
BJ3505, Ypt7-D44N	*MATα pep4::HIS3 prb1-Δ1.6R his3–200 lys2–801 trp1Δ101 (gal3) ura3–52 gal2 can1 ypt7Δ::YPT7(D44N)*	Vollmer et al., 1999
DKY6281, Ypt7-D44N	*MATα leu2-3 leu2-112 ura3-52 his3- Δ200 trpl-Δ901 lys2-801 suc2-Δ9 pho8::TRP1 ypt7Δ::YPT7(D44N)*	Vollmer et al., 1999
SEY6210, GFP-Vps39	*MATα, leu1-3, 112 ura3-52 his3-200, trp1-901 lys2-801 suc2-Δ9, Vam6::His3, pGFP-Vps39*	Wang et al., 2002
SEY6210, Vph1-GFP	*MATα, leu1-3, 112 ura3-52 his3-200, trp1-901 lys2-801 suc2-Δ9, VPH1-GFP::TRP1*	Wang et al., 2002
DKY6281, CBP-Vam3	DKY6281; *CBP-VAM3::KANMX nyv1Δ::NATMX*	Collins and Wickner 2007
DKY6281, Ypt7-Q68L	*MATα leu2-3 leu2-112 ura3-52 his3- Δ200 trpl-Δ901 lys2-801 suc2-Δ9 pho8::TRP1 ypt7Δ::YPT7(Q68L)*	Eitzen et al., 2000
DKY6281, Ypt7-T22N	*MATα leu2-3 leu2-112 ura3-52 his3- Δ200 trpl-Δ901 lys2-801 suc2-Δ9 pho8::TRP1 ypt7Δ::YPT7(T22N)*	Eitzen et al., 2000
DKY6281, Ypt7-N126I	*MATα leu2-3 leu2-112 ura3-52 his3- Δ200 trpl-Δ901 lys2-801 suc2-Δ9 pho8::TRP1 ypt7Δ::YPT7(N126I)*	Brett et al., 2008
DKY6281, Ypt7-D129N	*MATα leu2-3 leu2-112 ura3-52 his3- Δ200 trpl-Δ901 lys2-801 suc2-Δ9 pho8::TRP1 ypt7Δ::YPT7(D129N)*	Kucharczyk et al., 2001
CBY063	DKY6281; *ypt7Δ::KANMX*	This study
CBY069	DKY6281; *CBP-VAM3::KANMX nyv1Δ::NATMX ypt7Δ::HIS3 pCB038.ADHIpr-YPT7(D44N)*	This study
CBY074	BJ3505; *yck3Δ::KANMX*	This study
CBY075	DKY6281; *yck3Δ::KANMX*	This study
CBY076	BJ3505; *YPT7(D44N)::NATMX yck3Δ::KANMX*	This study
CBY077	DKY6281; *YPT7(D44N)::NATMX yck3Δ::KANMX*	This study
CBY115	SEY6210,Vph1-GFP; *ypt7Δ::KanMX pCB038.ADHIpr-YPT7(D44N)*	This study
CBY192	DKY6281; *ypt7Δ::KANMX pCB042.ADHIpr-GFP-YPT7*	This study
CBY193	DKY6281; *ypt7Δ::KANMX pCB043.ADHIpr-GFP-YPT7(D44N)*	This study
Plasmid	**Description**	**Source**
pGST-Ypt7	pEX-GST *AMP*; *LacOpr-Ypt7*	Brett et al., 2008
pGST-Ypt7 (Q68L)	pEX-GST *AMP*; *LacOpr-Ypt7(Q68L)*	Brett et al., 2008
pCB033	pEX-GST *AMP*; *LacOpr-Ypt7(D44N)*	This study
pCB037	pRS405 *LEU*; *ADHIpr-YPT7*	This study

pCB038	pRS405 *LEU*; *ADHIpr-YPT7(D44N)*	This study
pCB042	pRS405 *LEU*; *ADHIpr-GFP-YPT7*	This study
pCB043	pRS405 *LEU*; *ADHIpr-GFP-YPT7(D44N)*	This study

Chapter 3. Characteristics of Multivesicular Body-Lysosome Membrane Fusion Revealed by A New Cell-Free Assay

Mahmoud A Karim, Erin K McNally, Sevan Mattie and Christopher L Brett*

In preparation

3.1 Abstract

Endocytosis controls expression of surface polytopic proteins for cellular housekeeping, signaling and survival. Internalized proteins marked for degradation are delivered to endosomes and packaged into intraluminal vesicles by the ESCRT machinery to form a multivesicular body (MVB). When mature, the MVB fuses with lysosomes exposing proteins to lumenal hydrolases for catabolism. To better understand this last step of endocytosis, we developed a luminal β-lactamase complementation assay to measure membrane fusion between MVBs and vacuolar lysosomes isolated from *Saccharomyces cerevisiae*. We show that MVB- vacuolar lysosome fusion is driven by the Rab-GTPase Ypt7, multisubunit tethering complex HOPS, and the endosomal syntaxin ortholog Pep12 in complex with the lysosomal SNAREs Nyv1, Vti1 and Vam7, but does not require Ca^{2+}. Deleting the endosomal $Na^{+}(K^{+})/H^{+}$ exchanger NHX1 or the ESCRT machinery impairs MVB-vacuolar lysosome fusion. These defects are overcome by chloroquine or Ypt7 activation, respectively; offering strategies to treat human disorders linked to mutations in orthologous genes.

3.2 Introduction

Endocytosis is critical for regulating surface expression levels of polytopic proteins such as transporters and receptors for cellular signaling and survival in all eukaryotic organisms. Proteins destined for degradation are labeled with ubiquitin and cleared from the surface by invagination of the plasma membrane to form early endosomes. Through membrane fusion events, early endosomes deliver cargo proteins to an endosomal compartment where they encounter the ESCRT (Endosomal Sorting Complexes Required for Transport) machinery that sorts them into intraluminal vesicles (ILVs). Many rounds of ILV formation produce a multivesicular body (MVB; Huotari and Helenius 2011; Schmidt and Teis 2012), that when mature, fuses with the vacuolar lysosome to expose the ILVs to lumenal hydrolases for catabolism (Luzio et al., 2003; Piper and Katzmann, 2007). Although critical for surface protein degradation, we still do not understand many aspects of this terminal step of the endocytic pathway in molecular detail.

However, based on results primarily acquired using genetic approaches and microscopy, a model has emerged describing the mechanisms underlying MVB-vacuolar lysosome fusion that are thought to be conserved in all eukaryotic species (reviewed by Luzio et al. 2010; Markgraf et al. 2009; Balderhaar and Ungermann 2013; Spang 2016). Most evidence supporting this model comes from studies employing the genetically tractable model organism *Saccharomyces cerevisiae* (see Balderhaar and Ungermann 2013; Spang 2016). From these studies, it is apparent that MVBs contain two paralogs of almost every component of the fusion machinery (Lachmann et al., 2011; Furukawa and Mima, 2014). Presumably, one set is required for endosome membrane fusion events responsible for anterograde membrane trafficking to the MVB (for surface protein delivery and organelle biogenesis), and the other set is proposed to mediate MVB-vacuolar lysosome fusion. Most reports suggest that the machinery underlying the latter fusion event is redundant with mechanisms that drive homotypic vacuolar lysosome fusion, as components of this machinery are found on MVB and vacuolar lysosome membranes (Numrich and Ungermann, 2014; Spang, 2016). As such, inferences have been drawn from detailed knowledge of the homotypic vacuolar lysosome membrane fusion reaction generated from the use of cell-free membrane fusion assays (Balch et al., 1984; Conradt et al., 1994; Jun and Wickner, 2007). This powerful biochemical approach has permitted dissection of this process in

molecular detail revealing four distinct subreactions required for organelle membrane fusion and the critical players for each that presumably mediate MVB-vacuolar lysosome fusion as well (see Figure 12A):

"Priming", the first subreaction, requires Sec17, an α-SNAP [soluble NSF (N-ethylmalemide-sensitive factor) attachment protein] ortholog and SNARE chaperone, and Sec18, an NSF ortholog and homohexameric ATPase, to unravel cis-SNARE complexes from previous fusion events to free up individual SNARE proteins for future rounds of membrane fusion (Mayer et al., 1996; Ungermann et al., 1998). As the only α-SNAP and NSF orthologs in *S. cerevisiae* Sec17 and Sec18 are thought to mediate all SNARE-mediated membrane fusion events in the cell, but their roles in MVB-vacuolar lysosome fusion have not been investigated. Afterwards (or possibly concomitantly), organelle membranes undergo "tethering", the second subreaction, whereby apposing membranes make first contact. This requires activation of the Rab-GTPase Ypt7 and interaction with its cognate multisubunit tethering complex (MTC) called HOPS (homotypic fusion and vacuole protein sorting complex; Seals et al. 2000; Wurmser et al. 2000; Hickey and Wickner 2010). Next, fusogenic proteins (e.g. Ypt7, HOPS and SNAREs) and lipids are recruited to the initial contact site where they assemble into an expanding ring at the vertex between adjacent organelles (Wang et al., 2003; Fratti et al., 2004). Called "docking", this subreaction also includes the formation of *trans*-SNARE protein complexes mediated by HOPS (Collins and Wickner, 2007; Starai et al., 2008; Baker et al., 2015). Like homotypic vacuolar lysosome fusion, Ypt7 and HOPS are also implicated in MVB-vacuolar lysosome fusion where they presumably contribute to tethering and docking (Balderhaar et al., 2010; Peterson and Emr, 2001; Bugnicourt et al., 2004). During the last subreaction called "fusion", *trans*-SNARE complexes fully zipper driving lipid bilayer merger (Schwartz and Merz, 2009). Only one of four SNAREs (Vam3, Vti1, Vam7 and Nyv1) within the complex that mediates homotypic vacuolar lysosome fusion is also found on MVB membranes (Vti1; Gossing et al. 2013; Jun et al. 2007) and the SNAREs donated by each organelle to the complex that drives MVB-vacuolar lysosome fusion are unknown.

Recognizing the impact of this approach on our understanding of homotypic vacuolar lysosome fusion, we developed a similar cell-free assay to measure MVB-vacuolar lysosome membrane fusion and use it to study the mechanisms underlying this heterotypic fusion event. We also sought to understand how specificity is conferred in this system by identifying features

of this process that differ from homotypic vacuolar lysosome fusion. In addition to the fusion protein machinery, we examine other factors that contribute to the membrane fusion process, including Ca^{2+} signaling (Merz and Wickner, 2004), pH (although this is contentious; Coonrod et al., 2013; Desfougères et al., 2016) and monovalent cations (e.g. K^+; Starai et al., 2005; Cang et al., 2015). The latter two factors are controlled by the activity of Nhx1, a $Na^+(K^+)/H^+$ exchanger that resides on MVB membranes (Nass and Rao, 1998). Deleting NHX1 causes endocytic defects that implicate a role in MVB-vacuolar lysosome fusion (Bowers et al., 2000; Brett et al., 2005; Kallay et al., 2011). Herein we use this assay to test this hypothesis and understand how Nhx1 activity may regulate the fusion machinery. We also use it to address how MVBs delay fusion with vacuolar lysosomes until they fill with ILVs by testing the hypothesis that, after ILV formation, the ESCRT machinery stimulates a Rab-cascade mechanism to activate Ypt7, which in turn stimulates MVB-vacuolar lysosome fusion (Russell et al., 2012; Shideler et al., 2015). From these results, we propose a refined model describing the mechanisms that mediate or regulate MVB-vacuolar lysosome membrane fusion, and use it to identify strategies to overcome fusion defects caused by deleting components of the ESCRT machinery or NHX1, as analogous mutations in orthologous genes are linked to human neurological diseases and cancers (Saksena and Emr, 2009; Ouyang et al., 2013).

3.3 Results

3.3.1 A new cell-free assay to measure MVB-vacuole membrane fusion

The prevailing model of MVB-vacuolar lysosome fusion is almost exclusively supported by evidence derived from genetic approaches that often inadvertently prevent delivery of fusogenic proteins to vacuolar lysosome membranes. Thus, to better understand the molecular underpinnings of this event, we took an alternative biochemical approach by developing a new cell-free MVB-vacuole membrane fusion assay based on a strategy used by Jun and Wickner (2007) that relies on the reconstitution of β-lactamase upon luminal content mixing (Figure 11A): To target the first fusion probe to the MVB lumen, we fused the C-terminus of the endosomal Qa-SNARE Pep12 to the proto-oncogene product c-Fos followed by the ω-subunit of β-lactamase (Pep12-Fos-Gs-ω). To target our second fusion probe to the vacuolar lysosome lumen, we fused the targeting sequence of lysosomal protease carboxypeptidase Y (CPY; first 50 amino acids) to Jun, a cognate binding partner of c-Fos, followed by the α-subunit of β-lactamase (CPY50-Jun-Gs-α). Upon MVB-vacuole lipid bilayer merger, organellar lumenal contents containing the probes mix allowing Jun and c-Fos to interact driving the complementary halves of β-lactamase together to reconstitute enzyme activity. Reconstituted β-lactamase activity is then measured by monitoring nitrocefin hydrolysis (by recording absorbance at 492 nm over time) to quantify MVB-vacuolar lysosome fusion.

To confirm that the fusion probes were properly localized within cells, we created yeast strains expressing versions of the probes tagged with GFP at their C-termini, stained them with FM4-64 to label vacuole membranes and imaged them using fluorescence confocal microscopy (Figure 11B). The Pep12-GFP fusion protein appeared on puncta consistent with MVB localization as reported previously (Becherer et al., 1996), whereas the CPY50-GFP fusion protein was found within the vacuole lumen. Next, we fractionated cellular membranes by sucrose gradient (Figure 11C) and used Western blot analysis to confirm that Pep12-Fos-Gs-ω is found in similar fractions (9-12) as Vps10, a resident protein on MVBs (Marcusson et al., 1994), as well as endogenous Pep12. CPY50-Jun-Gs-α is not found in fractions containing the MVB fusion probe, but rather in fractions (3-4) containing Nyv1, a R-SNARE that is exclusively found on vacuolar lysosome membranes (Wen et al., 2006), and endogenous CPY a vacuole resident protein. Notably, the two Rab-GTPases thought to mediate MVB fusion, the endosomal Rab Vps21 and the vacuolar Rab Ypt7, as well as components of the HOPS complex (Vps41 and

Vps33) and the Qa-SNARE Vam3 were found in the same fractions as both fusion probes. We then collected the fractions containing MVB membranes (9-12) from Pep12-Fos-Gs-ω expressing cells or vacuole membranes (3-4) from CPY50-Jun-Gs-α expressing cells and mixed them together under conditions that promote the homotypic vacuole membrane fusion reaction *in vitro* (see Jun and Wickner 2007). Unfortunately, these preparations were fusion incompetent, as we did not observe β-lactamase activity in reactions containing either MVB and vacuole membranes or vacuole membranes alone containing vacuole localized fusion probes (i.e. CPY50-Fos-Gs-ω and CPY50-Jun-Gs-α; Figure 11D). Thus, we sought an alternative method to isolate the organelles to optimize our cell-free fusion assay.

Based on a method to isolate intact, fusogenic vacuolar lysosomes from yeast cells (see Conradt et al. 1992), we decided to use a 4-step Ficoll gradient to isolate both MVBs and vacuoles in the same preparations. Although vacuoles are known to accumulate at the 0-4% Ficoll interface, it is not clear whether MVBs also migrate to this layer during centrifugation. Thus, we performed Ficoll based fractionation experiments using cells expressing GFP-tagged versions of the fusion probes, collected organelles that accumulated at the 0-4% Ficoll interface, stained their membranes with FM4-64 and imaged them by confocal fluorescence microscopy (Figure 11E). Pep12-GFP is present in the preparation and localizes to small puncta adjacent to vacuole membranes reminiscent of MVB structures, whereas CPY50-GFP is found within the lumen of isolated vacuolar lysosomes, consistent with our observations of living cells shown in Figure 11B. We also observed the presence of our fusion probes (Pep12-Fos-Gs-ω or CPY50-Jun-Gs-α) in this fraction by Western blot analysis (Figure 11F). Other markers of both MVBs (Vps10, endogenous Pep12) and vacuolar lysosomes (Nyv1, endogenous CPY) were also present confirming that both organelles can be found in this preparation. The presence of MVBs and vacuoles was also confirmed by visualization of the samples by transmission electron microscopy (Figure 11G). We observed structures reminiscent of MVBs based on size and morphology (e.g. a round organelle of 500 nm diameter containing numerous circular ILVs of 20-80 nm diameter; (Friend, 1969; Russell et al., 2012) immediately adjacent to larger (> 1 μm radius) single membrane encased organelles containing lipophilic materials characteristic of vacuolar lysosomes (Mattie et al., 2017). We next mixed equal proportions of organelles isolated from cells only expressing the MVB fusion probe and organelles isolated from cells exclusively expressing the vacuole fusion probe with 125 mM KCl, 5 mM $MgCl_2$ and 1 mM ATP and

incubated the reactions at 27°C for up to 90 minutes to promote MVB-vacuolar lysosome fusion *in vitro*. Upon measuring reconstituted β-lactamase activity (Figure 11H), we observed robust heterotypic fusion showing a signal up to 10 times greater than background (i.e., reactions run without ATP or left on ice during the duration of the reaction). Although the extent of fusion was less, rates of heterotypic fusion were comparable to those observed for homotypic vacuole fusion suggesting that the kinetics of the membrane fusion subreactions may be similar. This new assay offers us a method to study MVB-vacuolar lysosome fusion using similar biochemical approaches that have been applied to successfully characterize homotypic vacuole fusion with molecular precision (see Wickner 2010). Herein, we use it to better understand the molecular underpinnings of this organelle fusion event, and to determine how MVB maturation triggers fusion to permit efficient delivery of surface proteins to vacuolar lysosomes for degradation.

Figure 11. A cell-free assay to measure MVB-lysosome membrane fusion

(A) Cartoon illustrating the approach used to develop a new cell-free assay to quantify MVB-vacuole fusion. One fusion probe contains c-Fos and the ω-fragment of β-lactamase fused to the C-terminus of Pep12 to target it to the MVB lumen. The complementary fusion probe contains Jun and the α-fragment of β-lactamase fused to the C-terminus of a peptide encoding the first 50 amino acid of CPY to target it to the vacuolar lysosome lumen. Fluorescence micrographs of (B) live cells or (E) isolated organelles (using the Ficoll method) expressing Pep12-GFP or CPY50-GFP. Vacuole membranes were stained with FM4-64. Dotted lines outline the yeast cell as observed by DIC. Scale bars, 2 μm. (C) Western blots of yeast membranes fractionated by sucrose gradient. (D) Membrane fusion values obtained from reactions containing organelles isolated by the sucrose fractionation method. (F) Western blot analysis of organelles isolated using the Ficoll floatation method. (G) Transmission electron micrographs of a fusion reaction containing MVBs and vacuolar lysosomes imaged at 30 minutes in the presence of ATP. Panels below show higher magnification images of boxed regions illustrating docking sites between apposing organelles. V, vacuolar lysosomes. Scale bar, 500 nm. (H) Membrane fusion values obtained from reactions containing organelles isolated using the Ficoll floatation method. Reactions were conducted in the presence or absence of ATP for 90 minutes at 27°C. Mean ± S.E.M. values are plotted and at least 3 experiments were performed for each condition shown. (Note that panel H also appeared in the M.Sc. thesis of Mahmoud Karim, 2013)

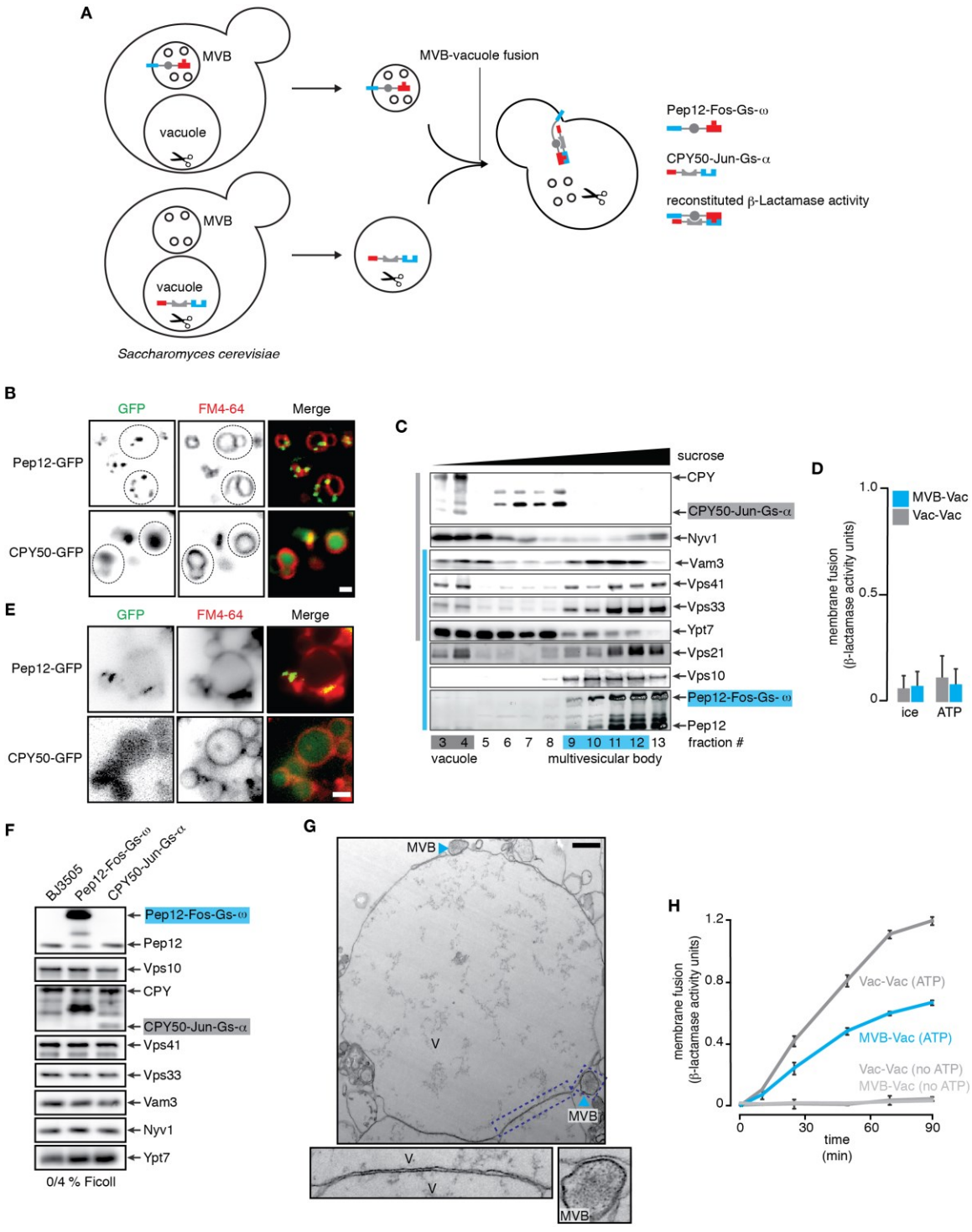
A
MVB
vacuole
MVB-vacuole fusion
Pep12-Fos-Gs-ω
CPY50-Jun-Gs-α
reconstituted β-Lactamase activity
Saccharomyces cerevisiae
B
GFP
FM4-64
Merge
Pep12-GFP
CPY50-GFP
E
C
sucrose
CPY
CPY50-Jun-Gs-α
Nyv1
Vam3
Vps41
Vps33
Ypt7
Vps21
Vps10
Pep12-Fos-Gs- ω
Pep12
3 4 5 6 7 8 9 10 11 12 13
fraction #
vacuole
multivesicular body
D
MVB-Vac
Vac-Vac
membrane fusion
(β-lactamase activity units)
1.0
0.5
0
ice
ATP
F
BJ3505
Pep12-Fos-Gs-ω
CPY50-Jun-Gs-α
Pep12-Fos-Gs-ω
Pep12
Vps10
CPY
CPY50-Jun-Gs-α
Vps41
Vps33
Vam3
Nyv1
Ypt7
0/4 % Ficoll
G
MVB
V
V
V
MVB
MVB
H
membrane fusion
(β-lactamase activity units)
1.2
0.8
0.4
0
Vac-Vac (ATP)
MVB-Vac (ATP)
Vac-Vac (no ATP)
MVB-Vac (no ATP)
0
30
60
90
time
(min)

3.3.2 Protein machinery required for MVB-vacuole membrane fusion

Homotypic vacuole membrane fusion requires the coordination of fusogenic proteins and lipids with ion fluxes to orchestrate four progressive subreactions (priming, tethering, docking and fusion) culminating with lipid bilayer merger (Wickner, 2010). Based on genetic studies and the analysis of endocytic trafficking *in vivo*, it is thought that many of these mechanisms also mediate MVB-vacuolar lysosome fusion, as both events involve the lysosomal membrane (Balderhaar et al., 2010; Bröcker et al., 2012; Balderhaar and Ungermann, 2013), lending to the prevailing model of MVB-vacuolar lysosome fusion shown in Figure 12A. To test this model, we first studied the proteins required for the priming subreaction by targeting Sec17, an α-SNAP ortholog that functions as a SNARE chaperone required for unraveling vacuolar cis-SNARE complexes from previous fusion events to permit future ones (Figure 12B). Consistent with Sec17 being the only α-SNAP ortholog encoded in the *S. cerevisiae* genome that contributes to membrane fusion at many sites within the cell (Griff et al., 1992; Mayer et al., 1996), we found that addition of anti-Sec17 antibody to block Sec17 activity impairs heterotypic fusion, like homotypic fusion, suggesting that it also mediates the priming subreaction of MVB-vacuolar lysosome fusion.

The subsequent stage of the organelle membrane fusion reaction is tethering, which is operationally defined as when apposing membranes make first contact. Afterwards, fusogenic proteins and lipids are recruited to and assemble at this site to stabilize the interaction between membranes in preparation for lipid bilayer merger, a hallmark of the docking subreaction (Wang et al., 2003; Fratti et al., 2004). Both tethering and docking are thought to be driven by activation of Rab-GTPases (Eitzen et al., 2000; Ostrowicz et al., 2010; Balderhaar et al., 2010, 2013). Thus, we predict that the addition of Rab inhibitors such as recombinant Gdi1 protein (rGdi1), a Rab-GTPase chaperone that extracts inactive Rab proteins from membranes (Garrett et al., 1994), or purified Gyp1-46, the active domain of the Rab-GAP protein Gyp1 that inactivates Rabs (Will and Gallwitz, 2001), will block heterotypic fusion. As predicted, heterotypic fusion, like homotypic fusion, is blocked by Rab inhibitors suggesting a role for Rab-GTPase activation in MVB-vacuolar lysosome fusion (Figure 12B). Two Rab proteins are present on these organelles, the endosomal Rab Vps21 and the vacuolar Rab Ypt7. To determine which Rab contributes to MVB-vacuolar lysosome fusion, we added purified antibodies raised against either Rab protein to fusion reactions to impair Rab activity and examined the effects on fusion (Figure 12B). Like

homotypic vacuole fusion (Eitzen et al., 2000), we find that heterotypic fusion requires Ypt7 and not Vps21, confirming reports by other groups (Balderhaar et al., 2010).

To mediate tethering and docking, active Rab-GTPases must interact with cognate effector proteins found within a multisubunit tethering complex (Price et al., 2000). Two MTCs could mediate the MVB-vacuolar lysosome fusion reaction: CORVET (class C core vacuole/endosome tethering complex) found on MVBs or HOPS found on vacuoles and MVBs (Peplowska et al., 2007; Nickerson et al., 2009; Balderhaar and Ungermann, 2013). Both complexes are composed of 6 subunits, but share 4 of them including Vps33, a SM-protein ortholog important for *trans*-SNARE complex assembly (Subramanian, 2004; Brett et al., 2008; Baker et al., 2015). Thus, to first determine if either MTC contributes to MVB-vacuolar lysosome fusion, we added affinity-purified anti-Vps33 antibody to fusion reactions to block Vps33 activity within the CORVET and HOPS complexes (Figure 12B). As predicted, anti-Vps33 antibody blocks both heterotypic and homotypic fusion confirming the involvement of MTCs in this process. To determine which MTC is involved in MVB-vacuolar lysosome fusion, we targeted unique subunits found in each complex: Vps41, an effector protein that binds to active Ypt7, that is only found in HOPS and its ortholog Vps8, a Vps21 effector protein, that is exclusively found in CORVET (Peplowska et al., 2007; Markgraf et al., 2009; Price et al., 2000; Ostrowicz et al., 2010). First, we added a purified antibody raised against Vps41 to fusion reactions to block Vps41 activity. Like homotypic fusion which requires Vps41 function, heterotypic fusion was impaired suggesting that Vps41 and HOPS mediate this event. Next, because we did not have access to a reliable antibody raised against Vps8, we took a genetic approach to block Vps8 activity by knocking out the VPS8 gene in yeast strains harboring the fusion probes. After determining that the probes were properly localized in the *vps8Δ* mutant cells (Figure 12C), we found that knocking out VPS8 had no effect on homotypic vacuole fusion (Figure 12D), which was expected given that Vps8 is not found on vacuole membranes and CORVET does not mediate this fusion event. However, we find that the deleting the VPS8 gene enhances MVB-vacuolar lysosome fusion (Figure 12D). Although unexpected, this result confirms our hypothesis that VPS8 is not required for MVB-vacuolar lysosome fusion and offers insight into how Vps-C complex numbers are balanced on MVB membranes, whereby loss of one complex (CORVET) may free up shared subunits needed to increase the abundance of the other complex (HOPS). In any case, together these results support the prevailing model of MVB-vacuolar lysosome fusion by confirming the involvement of Ypt7

and HOPS in the tethering and docking stages of the reaction.

The final stage of the organelle fusion reaction is lipid bilayer merger driven by SNARE-pin formation (Nichols et al., 1997). For homotypic vacuole fusion, *trans*-SNARE complexes are minimally composed of the three Q-SNAREs – the syntaxin ortholog Vam3 (Qa), Vti1 (Qb) and the SNAP25 ortholog Vam7 (Qc) and the R-SNARE Nyv1, a synaptobrevin ortholog (Ungermann and Wickner, 1998; Ungermann et al., 1998) whereby Vam7, a soluble protein, complexes with Vam3 and Vti1 on one membrane and Nyv1 on the opposing membrane (Schwartz and Merz, 2009; Baker et al., 2015). Of these 4 SNAREs, only the Qb-SNARE Vti1 is expressed on MVBs (Furukawa and Mima, 2014). Otherwise MVBs express orthologous Qa- (Pep12), Qc- (Tlg1) and R- (Snc2) SNAREs (Becherer et al., 1996; Von Mollard et al., 1997), but it is not clear which ortholog contributes to the *trans*-SNARE complex that drives MVB-vacuolar lysosome fusion. Elegant work by Joji Mima's group revealed that reconstituted Pep12 protein is capable of forming stable, fusogenic complexes with the vacuolar SNARE proteins in place of Vam3 (Furukawa and Mima, 2014). Thus, we hypothesized that a *trans*-SNARE complex composed of Pep12, Vti1, Vam7 and Nyv1 may drive MVB-vacuole membrane fusion. To test this hypothesis, we added purified antibodies against Pep12 or Vam3 to fusion reactions to specifically block the activity of each Qa-SNARE protein (Figure 12B). As predicted, anti-Vam3 antibody blocked homotypic, but had a lesser effect on heterotypic fusion, whereas anti-Pep12 antibody completely blocked heterotypic but had no effect on homotypic fusion, suggesting that Pep12 is the Qa-SNARE necessary for MVB-vacuolar lysosome fusion. To demonstrate that Vam7 is also in the SNARE complex that drives MVB-vacuolar lysosome membrane fusion, we added recombinant Vam7 protein (rVam7) to isolated organelles in the absence of ATP. Because it is sufficient to drive homotypic vacuole fusion *in vitro* (Thorngren et al., 2004), we reasoned that it could also stimulate MVB-vacuolar lysosome fusion if our model is accurate. As expected, rVam7 is sufficient to drive heterotypic fusion (Figure 12E), and like homotypic fusion, it further stimulates fusion when organelles are pretreated with anti-Sec17 antibody to prevent unraveling of newly formed SNARE complexes (see Stroupe et al. 2006). To demonstrate that the R-SNARE Nyv1 mediates MVB-vacuolar lysosome membrane fusion, we deleted the NYV1 gene from yeast strains containing fusion probes. After confirming the probes were properly localized (Figure 12C), we measured organelle fusion and found that neither heterotypic or homotypic fusion occurred when NYV1 was absent (Figure 12D), suggesting that

Nyv1 is necessary for MVB-vacuolar lysosome fusion.

Having shown that SNARE complexes containing Pep12, Vam7 and Nyv1 are necessary and sufficient for MVB-vacuolar lysosome fusion, we next sought to isolate these complexes using an approach that ensures that they are formed in *trans* during the membrane fusion reaction *in vitro* (see Collins and Wickner 2007; Schwartz and Merz 2009): We isolated organelles from cells that are missing the NVY1 gene and expressing Pep12 fused to Calmodulin-Binding Protein (CBP::Pep12) and mixed them with organelles isolated from cells missing the gene encoding Pep12 (Figure 12F). We then incubated the organelle fusion reactions for 60 minutes, sufficient time to allow *trans*-SNARE pairing, melted membranes using a non-ionic detergent, performed a pull-down assay for CBP::Pep12 using calmodulin Sepharose resin and used Western blotting to detect co-precipitation of Nyv1 with CBP::Pep12. In support of our model, we found that Nyv1 and Vti1 co-purify with CBP::Pep12 but only under fusion conditions (Figure 12G). Addition of rVam7 was sufficient to drive complex formation, consistent with it driving MVB-vacuolar lysosome fusion. We used CBP::Vam3 in place of CBP::Pep12 as a positive control, and demonstrated that *trans*-SNARE complexes required for homotypic fusion formed *in vitro*, as reported previously (Figure 12H; Schwartz and Merz 2009). Importantly, Pep12 does not co-purify with CBP::Vam3 and Vam3 does not co-purify with CBP::Pep12 confirming that these proteins act as the Qa-SNARE in separate complexes that mediate different fusion events.

Figure 12. Characterization of the protein machinery underlying MVB-vacuole fusion

(A) Cartoon illustrating the subreactions and proteins proposed to mediate MVB-vacuolar lysosome fusion. (B) Homotypic and heterotypic membrane fusion measured in the presence or absence of affinity purified antibodies against Sec17 (1.8 μM), Ypt7 (1.8 μM), Vps21 (1.2 μM), Vps33 (1.8 μM), Vps41 (1.8 μM), Pep12 (1.2 μM), Vam3 (2.6 μM), or purified recombinant Gdi1 (4 μM) or Gyp1-46 (5 μM) proteins. (C) Micrographs of live wild type (WT), *vps8Δ* or *nyv1Δ* cells expressing Pep12-GFP or CPY50-GFP. Vacuole membranes were stained with FM4-64. Scale bars, 2 μm. (D) Membrane fusion values from reactions containing organelles isolated from cells with or without VPS8 or NYV1. (E) Membrane fusion values from reactions conducted with or without ATP or rVam7 (100 nM) to stimulate fusion. Fusion reactions were also pre-treated with 1.8 μM anti-Sec17 for 10 minutes to reveal more SNARE proteins (Thorngren et al., 2004). (F) Cartoon illustrating method used to isolate *trans*-SNARE complexes from *in vitro* organelle fusion reactions. (G, H) Western blots showing results from pull-down experiments used to study *trans*-SNARE complexes containing CBP::Pep12 (G) or CBP::Vam3 (H) that form *in vitro* 60 minutes after addition of ATP (Std) or 100 nM rVam7 to stimulate organelle fusion. Reactions were kept on ice to prevent fusion as negative control. Mean ± S.E.M. values are plotted and $n \geq 2$ for all conditions shown. (Note that panels B and E also appeared in the M.Sc. thesis of Mahmoud Karim, 2013).

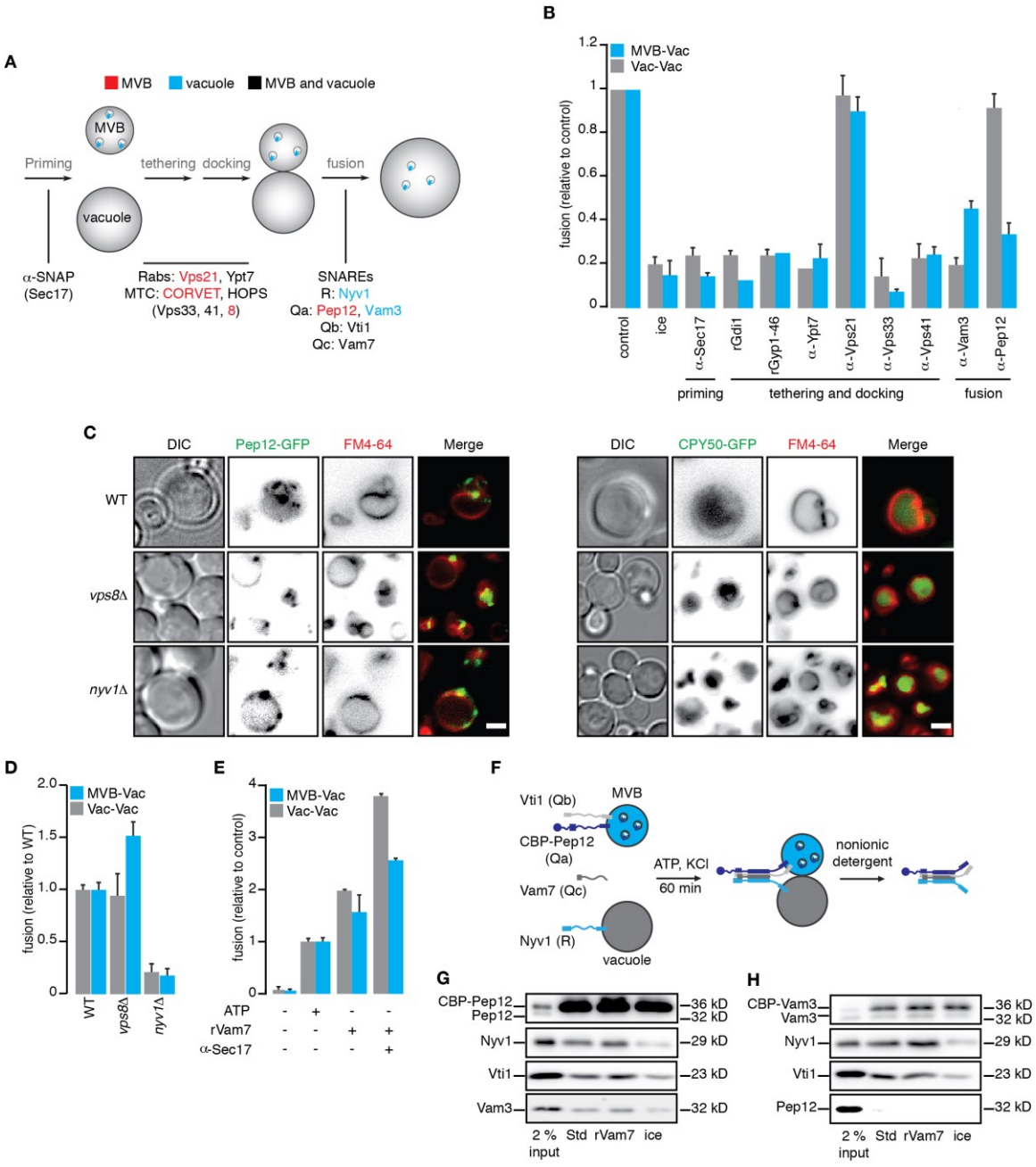
A
MVB
vacuole
MVB and vacuole
Priming
tethering
docking
fusion
α-SNAP
(Sec17)
Rabs: Vps21, Ypt7
MTC: CORVET, HOPS
(Vps33, 41, 8)
SNAREs
R: Nyv1
Qa: Pep12, Vam3
Qb: Vti1
Qc: Vam7
B
MVB-Vac
Vac-Vac
fusion (relative to control)
control
ice
α-Sec17
rGdi1
rGyp1-46
α-Ypt7
α-Vps21
α-Vps33
α-Vps41
α-Vam3
α-Pep12
priming
tethering and docking
fusion
C
DIC
Pep12-GFP
FM4-64
Merge
WT
vps8Δ
nyv1Δ
DIC
CPY50-GFP
FM4-64
Merge
D
MVB-Vac
Vac-Vac
fusion (relative to WT)
WT
vps8Δ
nyv1Δ
E
MVB-Vac
Vac-Vac
fusion (relative to control)
ATP
rVam7
α-Sec17
F
Vti1 (Qb)
MVB
CBP-Pep12
(Qa)
Vam7 (Qc)
Nyv1 (R)
vacuole
ATP, KCl
60 min
nonionic
detergent
G
CBP-Pep12
Pep12
Nyv1
Vti1
Vam3
36 kD
32 kD
29 kD
23 kD
32 kD
2 % input
Std
rVam7
ice
H
CBP-Vam3
Vam3
Nyv1
Vti1
Pep12
36 kD
32 kD
29 kD
23 kD
32 kD
2 % input
Std
rVam7
ice

3.3.3 Elevated Ca^{2+} levels block MVB-lysosome fusion

Lumenal calcium efflux is required for homotypic vacuolar lysosome fusion: *trans*-SNARE complex formation drives Ca^{2+} release, which in turn promotes full SNARE zippering for lipid bilayer merger (Merz and Wickner, 2004). As such, adding Ca^{2+} chelators to *in vitro* reactions blocks membrane fusion (Peters and Mayer, 1998; Starai et al., 2005). On the other hand, adding $CaCl_2$ to mimic release has no effect, as the amount of Ca^{2+} normally released is sufficient for fusion and the earlier stages of fusion are Ca^{2+}-independent (Figure 13A). However, in contrast, we found that adding $CaCl_2$ blocked heterotypic fusion (Figure 13A). In accord, we found that adding low concentrations (< 0.5 mM) of the rapid divalent cation chelator BAPTA (Figure 13B; Ricci et al. 1998) stimulated MVB-vacuolar lysosome fusion. Higher concentrations of BAPTA block both homotypic and heterotypic fusion, consistent with previous reports that suggest that it alters ionic strength causing the Q-SNARE Vam7 and the HOPS complex to dissociate from vacuole membranes (Starai et al., 2005; Pryor et al., 2000). Regardless, these observations suggest that although heterotypic and homotypic fusion events share underlying machinery, Ca^{2+}-dependence is a distinct feature of homotypic fusion. Furthermore, heterotypic fusion seems to be inhibited by cytoplasmic Ca^{2+}, suggesting that luminal Ca^{2+} release may act as a switch mechanism to direct membrane trafficking by stalling MVB-vacuolar lysosome fusion when homotypic vacuolar lysosome fusion occurs.

Figure 13. Effect of Ca^{2+} on MVB-vacuole fusion

Organelle membrane fusion was measured in the absence or presence of increasing concentrations of $CaCl_2$ (A) or the rapid divalent metal chelator BAPTA (B). All fusion reactions were incubated for 90 minutes at 27°C in the presence of ATP. Mean ± S.E.M. values are plotted and $n \geq 3$ for all conditions shown.

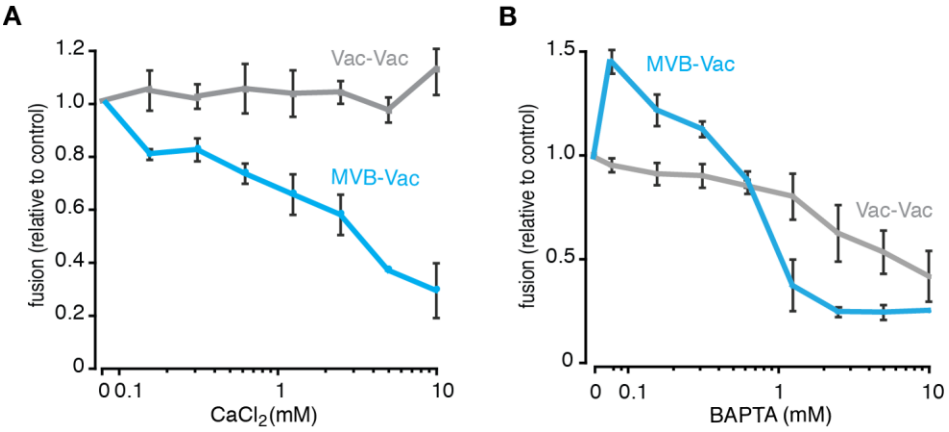

3.3.4 Ionic requirements for MVB-vacuole fusion

Ionic and osmotic gradients regulate endocytosis and membrane fusion (Heuser, 1989; Starai et al., 2005). MVBs and vacuoles have distinct luminal environments controlled by unique sets of resident transporters. For example, MVBs are more alkaline than vacuoles due to the activity of the $Na^+(K^+)/H^+$ exchanger Nhx1 that opposes the activity of the V-ATPase (Nass and Rao, 1998, 1999; Huotari and Helenius, 2011), and they are thought to lack channels and transporters responsible for Ca^{2+} signaling. On the other hand, vacuolar lysosomes are important contributors to cellular pH and Ca^{2+} homeostasis and signaling (Denis and Cyert, 2002), and act as cellular stores for ions, metals, polyphosphates and other biomolecules, which are sequestered and released by unique resident transporters (Luzio et al., 2003) that may contribute to homotypic membrane fusion (Sasser and Fratti, 2014). Thus, we hypothesized that homotypic and heterotypic fusion have different ionic requirements. To test this hypothesis, we first changed the pH of the reaction buffer to mimic changes in cytoplasmic $[H^+]$ and examined the effect on organelle fusion *in vitro* (Figure 14A).

Compared to homotypic fusion, heterotypic fusion was less tolerant to changes in pH although the peak fusion signal was near resting cytoplasmic pH (6.80) for both events. In mammalian cells, alkalinization of the MVB lumen promotes fusion with lysosomes (Cao et al., 2015). Thus, to determine if changing lumenal pH also affects MVB-vacuolar lysosome fusion in our system, we treated isolated organelles with chloroquine, a weak base that accumulates within MVBs and vacuoles and raises lumenal pH (Pearce et al. 1999; Qiu and Fratti 2010; Figure 14B). We found that both homotypic and heterotypic fusion were enhanced by chloroquine, however it had a greater effect on MVB-vacuolar lysosome fusion. Together, these results confirm that MVB-vacuolar lysosome fusion responds to changes in cytoplasmic and lumenal pH, and reveals that this response is different than homotypic lysosome fusion, suggesting that these events may be differentially regulated by cellular signaling events mediated by pH transients, e.g., budding (Henderson et al., 2014), or that involve changes in MVB function in response to changes in environmental pH, e.g. Rim20-Rim101 pathway (Xu et al., 2004; Boysen and Mitchell, 2006). Specific monovalent cations and osmotic balance are required for homotypic lysosome fusion (Starai et al., 2005; Brett and Merz, 2008). Thus, we next studied the effect of increasing [KCl], an important cytoplasmic osmolyte, on MVB-lysosome fusion (Figure 14C). Heterotypic fusion is less tolerant to shifts of [KCl] than homotypic fusion, which may reflect how the organelles

regulate their volume using different mechanisms. We then tested the dependence of fusion on K^+ by replacing it with different monovalent cations in the reaction buffer (Figure 14D). Replacing K^+ with Na^+ had no effect on either fusion event, whereas replacing it with NH_4^+ diminished both fusion events. However, one distinguishing feature of MVB-vacuolar lysosome fusion was tolerance to replacing K^+ with Rb^+. Nhx1, which is exclusively found on MVBs, can transport Rb^+ in place of K^+ or Na^+ (Brett et al., 2005) and is needed to deliver surface proteins to vacuolar lysosomes for degradation (Bowers et al., 2000; Brett et al., 2005). Thus, this unique monovalent cationic profile may reflect a function for Nhx1 in MVB-vacuolar lysosome fusion, possibly explaining how loss-of-function mutations in endosomal NHEs disrupt endocytosis.

Figure 14. Ionic requirements for MVB-vacuole fusion

Organelle membrane fusion was measured in the presence of increasing pH (A), [chloroquine] (B) or [KCl] (C), or when KCl was replaced with other salts (125 mM; D). All fusion reactions were incubated for 90 minutes at 27°C in the presence of ATP. Mean ± S.E.M. values are plotted and n ≥ 3 for all conditions shown. Note that panels A, C, and D also appeared in the M.Sc. thesis of Mahmoud Karim, 2013.

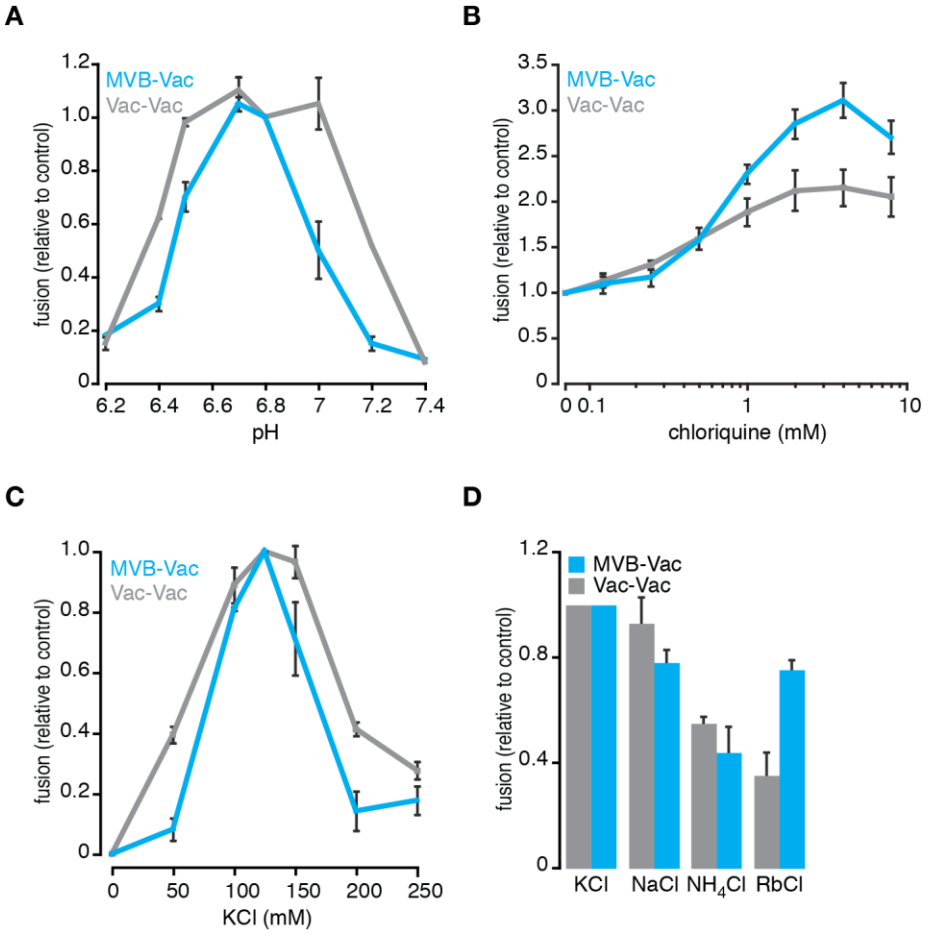

3.3.5 Nhx1 activity contributes to MVB-lysosome fusion

Deleting NHX1 causes aberrant accumulation of internalized surface proteins within enlarged MVBs (Bowers et al., 2000; Brett et al., 2005). Similar phenotypes are observed when knocking out genes encoding the ESCRT machinery responsible for protein sorting and intralumenal vesicle formation, two processes required for MVB maturation (Henne et al., 2011). However, a unique feature of abnormal MVBs within *nhx1Δ* cells is the presence of intralumenal vesicles (Kallay et al., 2011), suggesting that deleting NHX1 blocks delivery of proteins to vacuolar lysosomes after ESCRT function. The only known requirement for protein delivery to the vacuolar lysosome for degradation after ESCRT function is MVB-vacuolar lysosome fusion. Thus, to test the hypothesis that Nhx1 contributes to MVB-vacuole fusion, we knocked out NHX1 in yeast strains harboring fusion probes, isolated their organelles, and confirmed that the fusion probes properly localized to the MVB and vacuolar lysosome lumen (Figure 15A and B). We also isolated organelles from cells expressing Nhx1 tagged with GFP and examined them by fluorescence microscopy to demonstrate that Nhx1-positive MVBs were found in our isolated organelle preparations (Figure 15C). Examination of these preparations under conditions that promote fusion revealed the accumulation of Nhx1-GFP on vacuole membranes over time (Figure 15C), suggesting that Nhx1-GFP positive MVBs were fusing with vacuolar lysosomes *in vitro*. Next, we measured fusion between MVBs and vacuolar lysosomes isolated from either wild type or *nhx1Δ* cells and found that knocking out NHX1 impaired heterotypic fusion (Figure 15D). Deleting NHX1 has been shown to block delivery of some biosynthetic cargo to the vacuolar lysosome (Bowers et al., 2000; Brett et al., 2005). Thus, it is possible that impaired fusion may be a consequence of improper delivery of the fusion machinery to vacuolar lysosomes in *nhx1Δ* cells. To eliminate this possibility, we mixed organelles isolated from either wild type or *nhx1Δ* cells expressing complementary fusion probes and measured membrane fusion *in vitro* (Figure 15E). Reactions containing *nhx1Δ* vacuolar lysosomes and wild type MVBs showed similar fusion values as reactions containing wild type organelles, confirming that the fusion machinery was properly delivered to vacuolar lysosomes in *nhx1Δ* cells. Furthermore, fusion between wild type vacuolar lysosomes and *nhx1Δ* MVBs showed impairment similar to fusion between only *nhx1Δ* organelles, confirming that underlying defect is inherent to MVB, not vacuolar lysosome, dysfunction.

It has been proposed that cation-proton exchange by Nhx1 underlies its function in

endocytosis, as deleting NHX1 hyper-acidifies the lumen of the vacuole and treating live cells with a weak base that accumulates in acidic compartments rescues associated endocytic defects in the absence of the transporter (Ali et al., 2004; Brett et al., 2005; Kojima et al., 2012). However Nhx1 is predominantly found on MVBs (Nass and Rao 1998; Bowers et al. 2000; Brett et al. 2005; Figure 15C). Thus, we reasoned that lumenal pH of the MVB would also be abnormally acidic when NHX1 is deleted if it acts as a proton leak mechanism as proposed (Nass and Rao, 1998; Brett et al., 2005). To test this hypothesis, we measured lumenal MVB pH using a ratiometric fluorescence method that includes tagging the lumenal face of Pep12 with a pH-sensitive variant of GFP, called pHluorin, fused to mCherry, a relatively pH-insensitive fluorescent protein with different spectral properties. After demonstrating that the probe was properly localized to MVBs (Figure 15F) and responsive to pH in our preparations (Figure 15G), we determined that enlarged MVBs isolated from *nhx1Δ* cells were indeed hyperacidic as compared to those isolated from wild type cells (Figure 15H). Adding a weak base to correct pH defects overcomes endocytic impairments caused by knocking out NHX1 in living cells (Brett et al., 2005). To determine if restoration of MVB-vacuolar lysosome fusion underlies this observation, we next added the weak base chloroquine to fusion reactions and found that it rescued MVB-vacuolar lysosome fusion defects caused by knocking out NHX1 (Figure 15I). Together, these results suggest that proton transport by Nhx1 is important for the MVB-vacuolar lysosome fusion stage of endocytosis.

As lumenal proton export by Nhx1 is coupled to monovalent cation import (Nass and Rao, 1998; Brett et al., 2005), we next examined if monovalent cation transport by Nhx1 is also critical for MVB-vacuolar lysosome fusion. When characterizing the ionic requirements for MVB-vacuolar lysosome fusion, we found that this fusion event tolerates replacement of K^+ with Rb^+ (Figure 14D) and hypothesized that perhaps Nhx1 activity accounts for this observation, as it is the only known mechanism on MVBs that transports Rb^+ in place of Na^+ or K^+ (Brett et al., 2005). To test this hypothesis, we measured MVB-vacuolar lysosome fusion in the presence of RbCl and found that it is entirely abolished when NHX1 is deleted (Figure 15J), suggesting that Rb^+ transport by Nhx1 is required for MVB-vacuolar lysosome fusion under these conditions. This effect is specific for Rb^+, as deleting NHX1 continued to impair fusion by 50% if K^+ was replaced with Na^+ or NH_4^+. Together, these findings confirm that cation-proton exchange by Nhx1 mediates its role in MVB-vacuolar lysosome fusion.

Figure 15. Loss of Nhx1 activity impairs MVB-vacuole fusion

Fluorescence micrographs of live cells (A) or isolated organelles (B) with (WT) or without (*nhx1Δ*) NHX1 expressing Pep12-GFP or CPY50-GFP. (C) Fluorescence micrographs of fusion reactions containing organelles isolated from WT cells expressing Nhx1-GFP acquired at time points after addition of ATP to stimulate fusion. Vacuole membranes were stained with FM4-64. (D) MVB-vacuolar lysosome fusion values acquired over time after adding ATP to reactions containing organelles isolated from WT or *nhx1Δ* cells. (E) MVB-vacuolar lysosome fusion values acquired 90 minutes after addition of ATP to reactions containing organelles mixed from WT and *nhx1Δ* cells. (F) Fluorescence micrographs of live WT or *nhx1Δ* cells expressing the MVB lumenal pH probe Pep12-pHluorin-mCherry. (G) Lumenal pH calibration curves for MVBs isolated from WT and *nhx1Δ* cells expressing Pep12-pHluorin-mCherry. (H) Lumenal MVB pH values for organelles isolated from WT or *nhx1Δ* cells expressing Pep12-pHluorin-mCherry in the absence or presence of ATP. (I, J) MVB-vacuole fusion values acquired 90 minutes after addition of ATP to reactions containing organelles mixed from WT and *nhx1Δ* strains in the presence or absence of 4 mM chloroquine (I), or when KCl was replaced with different salts (125 mM; J). All fusion values shown are means ± S.E.M. normalized to standard fusion conditions (wild type organelles, 90 minutes after adding ATP). $n \geq 3$ for all conditions shown. All scale bars, 2 μm. Note that panels D and J also appeared in the M.Sc. thesis of Mahmoud Karim, 2013.

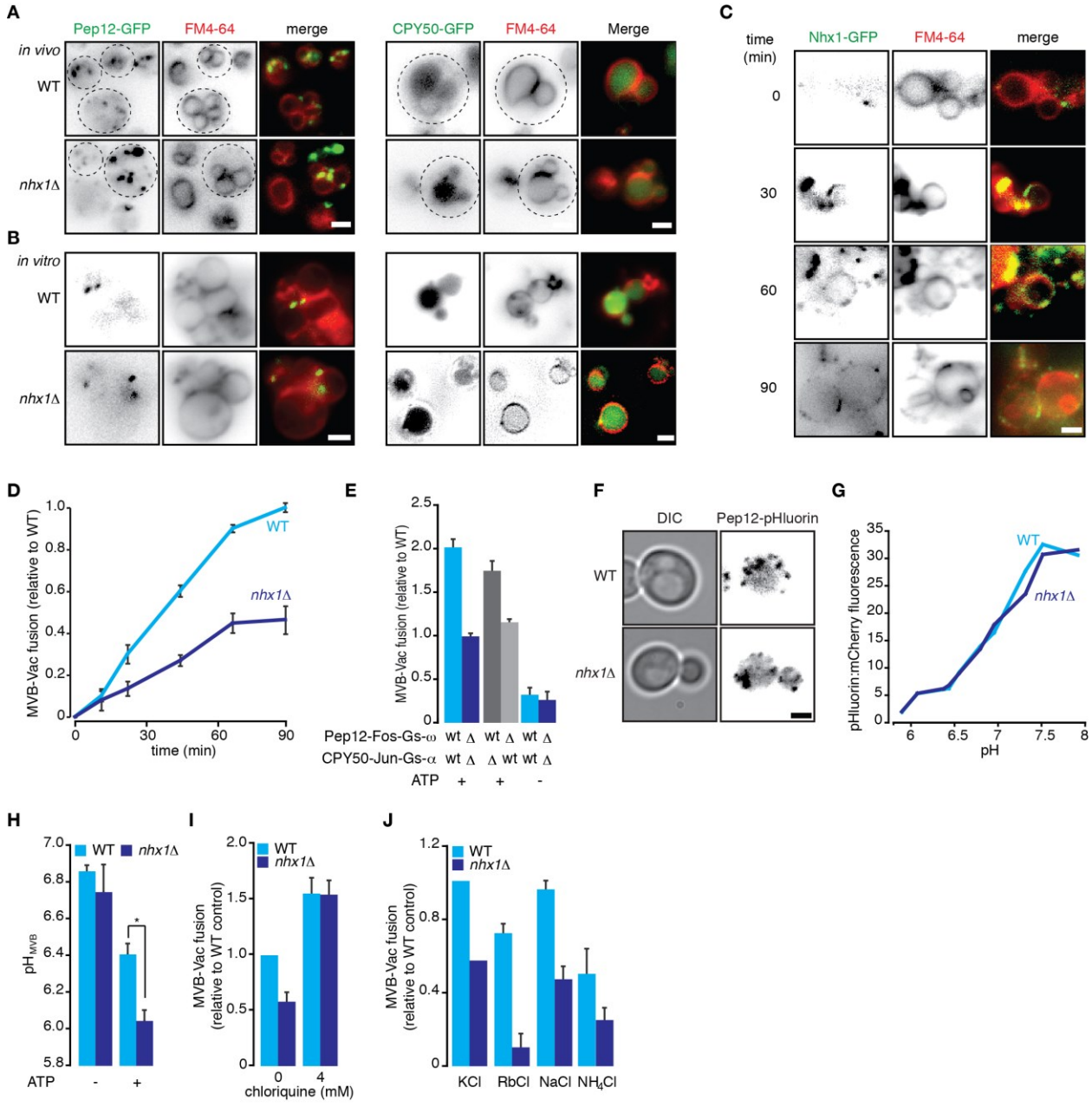
A
Pep12-GFP
FM4-64
merge
CPY50-GFP
FM4-64
Merge
in vivo
WT
nhx1Δ
B
in vitro
WT
nhx1Δ
C
time (min)
Nhx1-GFP
FM4-64
merge
0
30
60
90
D
MVB-Vac fusion (relative to WT)
WT
nhx1Δ
time (min)
E
MVB-Vac fusion (relative to WT)
Pep12-Fos-Gs-ω wt Δ wt Δ wt Δ
CPY50-Jun-Gs-α wt Δ Δ wt wt Δ
ATP + + -
F
DIC
Pep12-pHluorin
WT
nhx1Δ
G
pHluorin:mCherry fluorescence
WT
nhx1Δ
pH
H
WT
nhx1Δ
pH_MVB
ATP - +
I
WT
nhx1Δ
MVB-Vac fusion (relative to WT control)
chloriquine (mM)
J
WT
nhx1Δ
MVB-Vac fusion (relative to WT control)
KCl
RbCl
NaCl
NH4Cl

3.3.6 Nhx1 targets SNAREs, not Ypt7 activity to regulate organelle fusion

How does ion transport by Nhx1 affect the machinery underlying the membrane fusion reaction? It was previously shown that Nhx1 binds Gyp6, a Rab GTPase Activating Protein (Rab-GAP) that inactivates the Rab-GTPase Ypt6, and to a lesser extent Ypt7, which are implicated in MVB fusion with the *trans*-Golgi network and vacuolar lysosome, respectively (Ali et al., 2004; Brett et al., 2008; Vollmer et al., 1999; Will and Gallwitz, 2001), and knocking out GYP6 partially suppresses endocytic defects observed in *nhx1Δ* cells (Ali et al., 2004). Given that Rab conversion at the MVB is required to activate Ypt7, and Ypt7 activation is needed for MVB-vacuolar lysosome fusion, we hypothesized that Nhx1 may target Rab activity to regulate MVB-vacuolar lysosome fusion, whereby loss of NHX1 may cause inactivation of Ypt7 which accounts for the observed impairment in organelle fusion. To test this hypothesis, we employed an assay to assess the proportion of active Ypt7 protein present on isolated organelles: We added rGdi1, a Rab-chaperone protein, that selectively binds and extracts inactive Rab from isolated membranes and separated the pool of soluble rGdi1-bound inactive Ypt7 (supernatant) from membrane bound (presumably active) Ypt7 (pellet) by differential centrifugation (Brett et al., 2008). Compared to organelles isolated from wild type cells, MVBs and vacuolar lysosomes from *nhx1Δ* cells contained similar amounts of active Ypt7 on membranes, and this pool of Ypt7 was equally susceptible to inactivation by GAP activity (by addition of rGyp1-46 protein) or activation by addition of GTPγS a non-hydrolyzible analog of GTP (Figure 16A and B), suggesting that deleting NHX1 has no effect on Ypt7 activity. To further test this hypothesis, we treated isolated organelles from WT or *nhx1Δ* cells with GTPγS to activate Ypt7 and measured MVB-vacuole fusion (Figure 16C). We found that GTPγS treatment was unable to rescue the MVB-vacuole fusion defect caused by *nhx1Δ*. Finally, disrupting Rab-activation has been shown to affect targeting of Ypt7 to MVB and vacuolar lysosome membranes (Cabrera and Ungermann, 2013). Thus, we also assessed the effect of knocking out NHX1 on the distribution of Ypt7-GFP within cells using fluorescent microscopy. Consistent with our other findings, deleting NHX1 had no discernable effect on Ypt7-GFP targeting to MVBs and vacuolar lysosome membranes within live cells (Figure 16D). Together, these results suggest that Nhx1 does not target Ypt7 function to regulate organelle fusion.

Given that loss of NHX1 activity does not target Ypt7, we next performed a preliminary screen to determine if deleting NHX1 affected the cellular distribution of other GFP-tagged

proteins responsible for MVB-vacuolar lysosome fusion to better understand how Nhx1 contributes to the MVB-vacuolar lysosome fusion reaction. However, no discernable differences in cellular targeting of GFP-tagged components of the HOPS complex (Vps41) or other proteins implicated in membrane fusion were observed (data not shown). However, when studying GFP-tagged Vph1 (the stalk domain of the V-type H^+-ATPase complex that is exclusively found on vacuolar lysosome membranes in wild type cells), we found that Vph1-GFP abnormally accumulated on enlarged MVBs in *nhx1Δ* cells (Figure 16D). This observation made two important implications: (1) it is consistent with the hyper-acidification of the MVB lumen in *nhx1Δ* cells and may account for this observation, and (2) it suggests that deleting NHX1 may target a stage of the membrane fusion reaction proposed to be dependent on Vph1, which is after Ypt7 and HOPS function, but prior to complete bilayer merger by *trans*-SNARE complex zippering (Strasser et al., 2011). To test the latter hypothesis, we stimulated fusion *in vitro* with the soluble Qc-SNARE rVam7 in place of ATP, which would bypass any affects *nhx1Δ* may have on *trans*-SNARE complex assembly (Figure 16E). Indeed, rVam7 rescued fusion of organelles isolated from *nhx1Δ* cells to levels similar to wild type fusion under standard conditions. Pretreating reactions with anti-Sec17 antibody to promote entry of rVam7 into SNARE complexes further improved fusion, confirming that the SNARE machinery was intact on organelles isolated from *nhx1Δ* cells. Together, these results suggest that Nhx1 activity targets a component of the fusion machinery that functions upstream of *trans*-SNARE pairing and downstream of Ypt7 activation.

Figure 16. Loss of Nhx1 activity does not affect Ypt7 signaling

(A) Rab-GTPase activity assessed using membrane extraction by rGdi1. Organelles isolated from wild type (WT) or *nhx1Δ* cells were incubated with ATP for 40 minutes in the presence or absence of 5 μM rGdi1 or 3.6 μM rGyp1-46 during the last 10 minutes of incubation. As a control, reactions indicated were pretreated with 0.2 mM GTPγS to prevent membrane extraction of Ypt7 by rGdi1. Organelle membranes (pellet, P) were separated from soluble factors (supernatant, S) by centrifugation and Ypt7 was detected in both fractions by immunoblotting. (B) Evaluation of Ypt7 extraction by densitometric analysis of Western blots shown in A. (C) MVB-vacuole fusion values acquired 90 minutes after addition of ATP to reactions containing organelles isolated from WT or *nhx1Δ* cells that were pretreated with increasing concentrations of GTPγS for 10 minutes. (D) Fluorescence micrographs of live WT or *nhx1Δ* cells expressing either Vph1-GFP or Ypt7-GFP. Vacuole membranes and aberrant MVBs were stained with FM4-64. Scale bar, 2 μm. (E) Membrane fusion values from reactions containing organelles isolated from WT or *nhx1Δ* cells incubated for 90 minutes in the presence or absence of ATP or rVam7 (100 nM) to stimulate fusion. Fusion reactions indicated were pre-treated with 1.8 μM anti-Sec17 for 10 minutes to reveal more SNARE proteins (Thorngren et al., 2004). Mean ± S.E.M. values are plotted and $n \geq 3$ for each experiment shown. Note that panel A and E also appeared in the M.Sc. thesis of Mahmoud Karim, 2013.

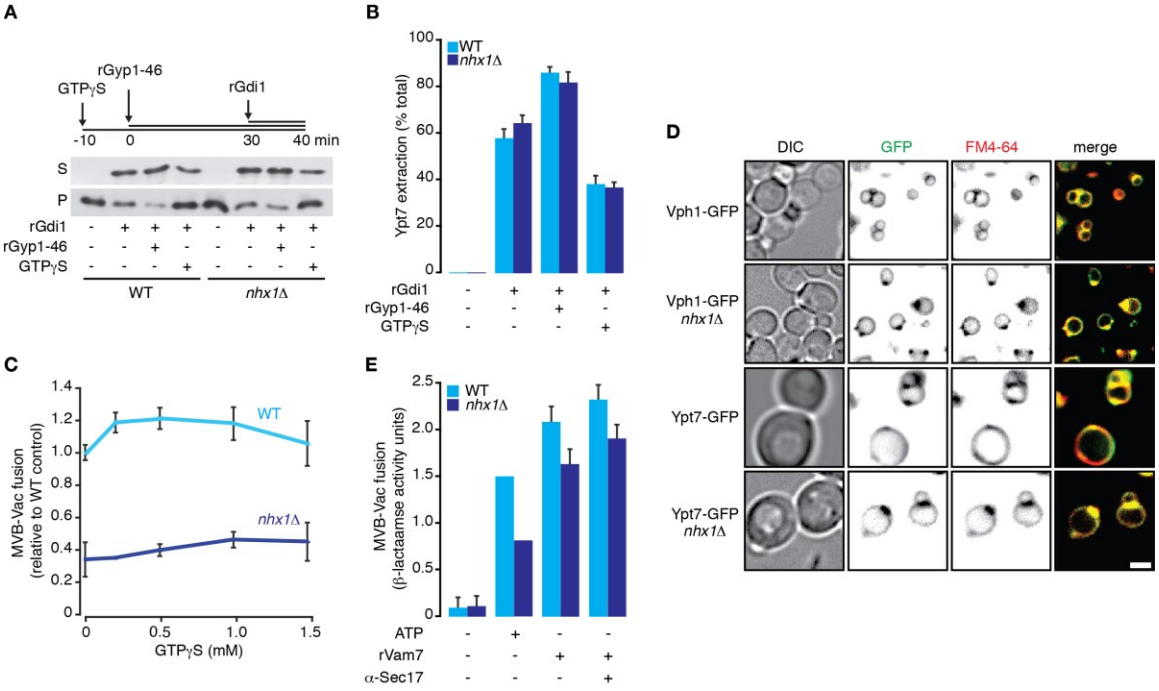
A
rGyp1-46
GTPγS
rGdi1
-10
0
30
40 min
S
P
rGdi1
rGyp1-46
GTPγS
WT
nhx1Δ
B
WT
nhx1Δ
Ypt7 extraction (% total)
rGdi1
rGyp1-46
GTPγS
C
WT
nhx1Δ
MVB-Vac fusion (relative to WT control)
GTPγS (mM)
E
WT
nhx1Δ
MVB-Vac fusion (β-lactaamse activity units)
ATP
rVam7
α-Sec17
D
DIC
GFP
FM4-64
merge
Vph1-GFP
Vph1-GFP nhx1Δ
Ypt7-GFP
Ypt7-GFP nhx1Δ

3.3.7 The ESCRT machinery activates Ypt7 to promote MVB-lysosome fusion

The ESCRT machinery mediates sorting and packaging of internalized surface proteins into intralumenal vesicles at the MVB (Henne et al., 2011). Many rounds of intralumenal vesicle formation occur to form a mature MVB that then fuses with the vacuolar lysosome to expose proteins to lumenal hydrolases for degradation. Deleting components of the ESCRT machinery causes internalized surface proteins to accumulate on enlarged endocytic compartments devoid of intralumenal vesicles within cells (Odorizzi et al., 1998a; Katzmann et al., 2001). Based on these observations, it has been hypothesized that proper protein sorting and intralumenal vesicle formation are needed to trigger the terminal step of this pathway, MVB-vacuolar lysosome fusion (Russell et al., 2012). To test this hypothesis, we used our new cell-free MVB-vacuolar lysosome fusion assay whereby we isolated organelles containing only the MVB fusion probe (Pep12-Fos-Gs-ω) from cells devoid of either VPS23, VPS36 or SNF7 (components of the ESCRT-I, ESCRT-II or ESCRT-III, respectively) and mixed them with organelles expressing only the lysosomal fusion probe (CPY50-Jun-Gs-α) isolated from wild type cells (Figure 17A). This approach ensures that the fusion machinery is properly delivered to vacuolar lysosome membranes, as knocking out components of the ESCRT machinery is known to block the CPY and CPS biosynthetic pathways to the vacuolar lysosome (Odorizzi et al., 1998a; Katzmann et al., 2001). Furthermore, ESCRTs only function on MVB membranes, not vacuolar lysosomes, so we reasoned that any defects in ESCRT-mediated signaling required to trigger MVB-vacuolar lysosome fusion should occur on MVBs isolated from cells devoid of ESCRT components. Using fluorescence microscopy, we first confirmed that the targeting domain of the MVB fusion probe (Pep12-GFP) was properly localized to aberrant, enlarged MVBs proximal to vacuolar lysosomes within mutant cells (Figure 17B; see Coonrod and Stevens 2010; Russell et al. 2012). Next, we measured mutant MVB fusion with wild type vacuolar lysosomes *in vitro* and found that deleting components of the ESCRT machinery blocked heterotypic fusion (Figure 17C), suggesting that ESCRT function is needed to trigger MVB-vacuolar lysosome fusion.

So how does the ESCRT machinery signal the fusion machinery to trigger mature MVB vacuolar lysosome fusion? According to a recent report by Odorizzi and colleagues, deletion of VPS4, a AAA-ATPase that catalyzes disassembly of ESCRT-III, prevents Rab-GTPase conversion at the MVB membrane whereby inactivation of Vps21 after an endosome-MVB fusion event for protein delivery triggers activation of Ypt7 to initiate the next trafficking step,

MVB-vacuolar lysosome fusion en route to the lysosome (Russell et al., 2012). Deleting VPS4 causes active Vps21 to accumulate on enlarged MVBs devoid of intralumenal vesicles, which disrupts Ypt7 activation, and presumably blocks MVB-vacuolar lysosome fusion. To validate this model, we treated isolated organelles with 0.2 mM GTPγS to constitutively activate GTPases including Ypt7 on membranes and measured heterotypic fusion to determine if it rescued MVB-vacuolar lysosome fusion defects caused by knocking out ESCRT subunits. As predicted, GTPγS treatment partially restores fusion defects caused by deleting ESCRT (Figure 17C). In addition, stimulating fusion with rVam7 instead of ATP to bypass the Ypt7 function also rescued fusion defects caused by deleting ESCRT components (Figure 17C). This result confirms that the SNAREs are functional on MVB membranes, and confirms that ESCRT function ultimately targets Rab-GTPase activation to trigger MVB-vacuolar lysosome fusion. To confirm that Ypt7 is the target of signaling triggered by ESCRT function, we introduced a Q68L mutation into Ypt7 to render it constitutively active (see Brett et al., 2008) in cells lacking VPS23, a subunit of the ESCRT-I complex, to overcome the MVB-vacuolar lysosome fusion defects caused by this mutation. After confirming that the targeting domain of the MVB fusion probe was properly localized in *vps23Δ* cells expressing Ypt7 Q68L (Figure 17D), we measured fusion between mutant MVBs and wild type vacuolar lysosomes *in vitro* and found that introduction of Ypt7 Q68L completely suppressed the defect in heterotypic fusion caused by deleting VPS23 (Figure 17E). Unlike fusion between wild type organelles, addition of GTPγS had no effect on heterotypic fusion in the presence of Ypt7 Q68L, suggesting that Ypt7 Q68L was indeed constitutively active and conferred sensitivity to GTPγS in our organelle fusion reactions. In all, these findings offer critical evidence in support of the hypothesis that the ESCRT machinery triggers MVB-vacuolar lysosome fusion by activation of Ypt7 through a Rab cascade mechanism.

3.3.8 Nhx1 and the ESCRT machinery use independent mechanisms to trigger heterotypic fusion

Although their contributions to MVB maturation are unique, knocking out either ESCRT subunits or Nhx1 disrupt MVB-vacuolar lysosome fusion. Unlike ESCRTs, Nhx1 does not target Ypt7 activity. However fusion defects caused by all knockout mutations can be rescued by addition of rVam7. Furthermore, intralumenal vesicles form in *nhx1Δ* cells suggesting that Nhx1 may function downstream of ESCRTs. Thus, it is possible that that ESCRT function may

stimulate Nhx1 to promote fusion. If so, given that chloroquine rescues MVB-vacuolar lysosome fusion when NHX1 is absent, we hypothesized that chloroquine should also rescue heterotypic fusion defects caused by deleting ESCRT subunits. Upon measuring MVB-vacuolar lysosome fusion *in vitro*, we found that chloroquine did not rescue defects caused by these mutations (Figure 17F), eliminating this possibility and suggesting that ESCRTs and Nhx1 use independent mechanisms to trigger MVB-vacuolar lysosome fusion.

Figure 17. Deletion of ESCRT components prevents Ypt7 activation necessary for MVB-vacuole fusion

(A) Cartoon illustrating the method used to study effects of deleting components of the ESCRT machinery on MVB-vacuolar lysosome fusion. Organelles isolated from wild type (WT) or mutant cells expressing the MVB fusion probe were mixed with organelles isolated from WT cells expressing the lysosomal fusion probe. (B) Micrographs of live WT, *vps23Δ*, *vps36Δ* or s*nf7Δ* cells expressing Pep12-GFP. Vacuoles membranes were stained with FM4-64. (C, F) MVB-vacuole fusion values from reactions containing organelles isolated from WT, *vps23Δ*, *vps36Δ* or *snf7Δ* cells. Reactions were conducted in the absence or presence of ATP, 0.2 mM GTPγS, or 100 nM rVam7 (C) or in the presence of increasing concentrations of chloroquine (F). (D) Micrographs of live WT or *vps23Δ*, or *vps23Δ* Ypt7-Q68L cells expressing Pep12-GFP. Vacuoles membranes were stained with FM4-64. (E) MVB-vacuole fusion values from reactions containing organelles isolated from WT, *vps23Δ* or *vps23Δ* Ypt7-Q68L cells in the absence or presence of ATP or 0.2 mM GTPγS. All fusion reactions were incubated for 90 min at 27°C. Fusion values shown are means ± S.E.M. normalized to fusion values from reactions containing WT organelles in the presence of ATP. $n \geq 3$ for all conditions shown. All scale bars, 2 μm.

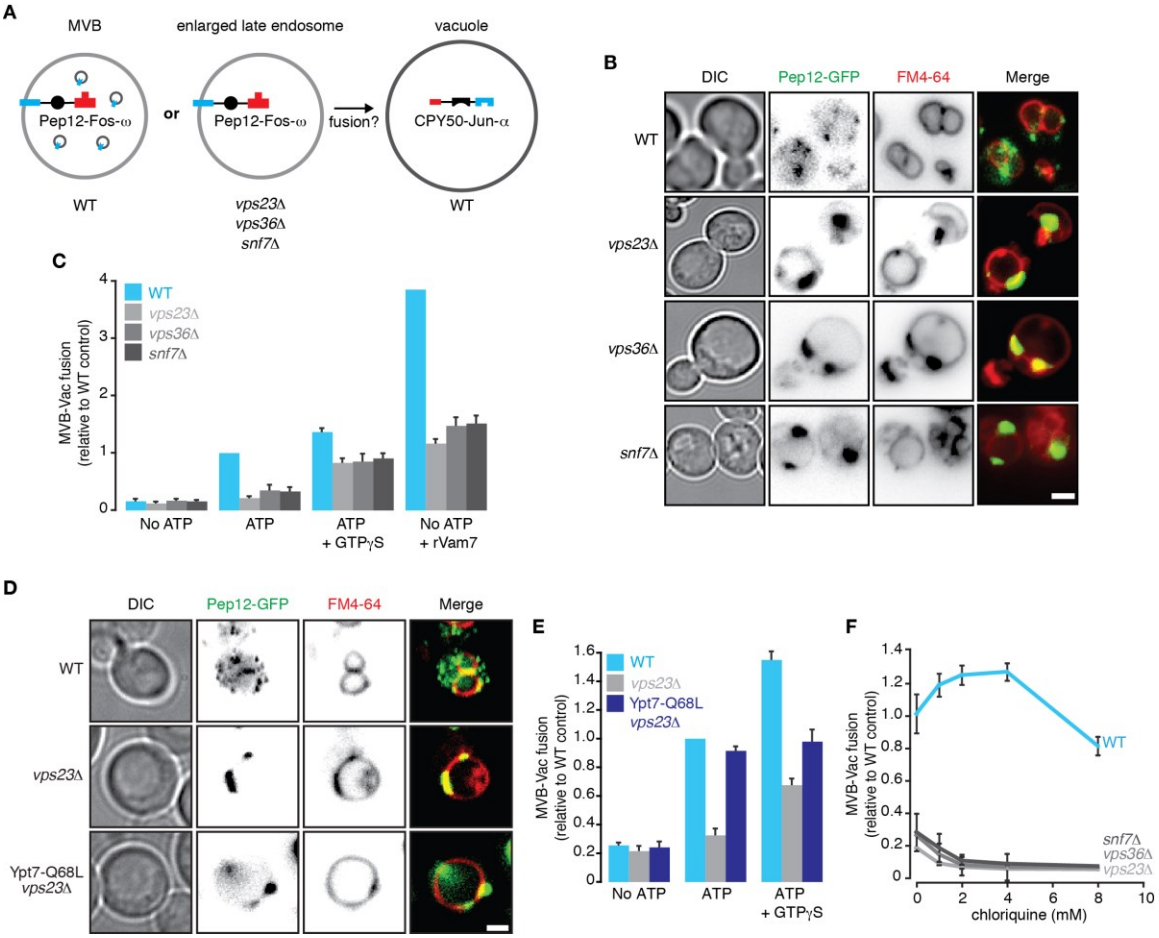
A
MVB
enlarged late endosome
vacuole
Pep12-Fos-ω
or
Pep12-Fos-ω
fusion?
CPY50-Jun-α
WT
vps23Δ
vps36Δ
snf7Δ
WT
B
DIC
Pep12-GFP
FM4-64
Merge
WT
vps23Δ
vps36Δ
snf7Δ
C
MVB-Vac fusion
(relative to WT control)
WT
vps23Δ
vps36Δ
snf7Δ
No ATP
ATP
ATP
+ GTPγS
No ATP
+ rVam7
D
DIC
Pep12-GFP
FM4-64
Merge
WT
vps23Δ
Ypt7-Q68L
vps23Δ
E
MVB-Vac fusion
(relative to WT control)
WT
vps23Δ
Ypt7-Q68L
vps23Δ
No ATP
ATP
ATP
+ GTPγS
F
MVB-Vac fusion
(relative to WT control)
WT
snf7Δ
vps36Δ
vps23Δ
chloriquine (mM)

3.4 Discussion

3.4.1 A new cell-free assay for MVB-lysosome fusion

Here we describe a new cell-free assay to measure MVB-vacuolar lysosome membrane fusion based on reconstitution of lumenal β-lactamase (Figure 11). Two additional lines of evidence confirmed that MVB-vacuolar lysosome fusion occurred within our fusion reaction *in vitro*: (1) We observed the accumulation of Nhx1-GFP, a polytopic protein that resides on the MVB, on vacuole membranes within the heterotypic fusion reaction over time, which is a predicted outcome of MVB-vacuolar lysosome fusion (Figure 15C), and (2) flattened organelle membrane interfaces reminiscent of docking sites that occur during other organelle fusion events were observed between MVBs and vacuolar lysosomes by TEM at 30 minutes into the reaction when the docking subreaction was predicted to occur (Figure 11G). The method of organelle isolation was crucial for success, and although MVBs are not separated from vacuolar lysosomes in these preparations, targeting the fusion probes to each organelle in separate yeast strains and mixing them later ensures that reconstituted β-lactamase activity represents only fusion that occurs *in vitro* under controlled conditions. We show that this new assay offers many experimental advantages that facilitate study of the MVB-vacuolar lysosome membrane fusion reaction in detail: (1) It is quantitative, and with maximum values observed at 10 times over background, this assay offers a robust, colorimetric alternative to fluorescence based techniques that rely on fluorescence colocalization (3X over background; Cao et al. 2015) or radiolabeled techniques that rely on interactions between Avidin-asialofetuin and I^{125}-labeled biotinylated polymeric IgA (4X over background; Pryor et al. 2000). (2) By mixing MVBs expressing one fusion probe isolated from mutant cells with vacuolar lysosomes containing the complementary fusion probe from wild type cells (or vice versa), it allowed us to identify the organelle with defective fusion machinery and eliminate possible effects of impaired delivery of biosynthetic cargo (such as fusogenic proteins) to vacuole membranes caused by deleting ESCRT or NHX1 genes (Robinson et al., 1988; Raymond et al., 1992; Bowers et al., 2000). (3) It permits kinetic analysis of the heterotypic membrane fusion reaction, as it can be initiated *in vitro* with the addition of either ATP or rVam7 protein. (4) It offers the convenience of using protein reagents to study subreactions of the process, or of changing the reaction buffer conditions to simulate changes in the "cytoplasm" to better understand how heterotypic fusion is regulated. Herein, we demonstrate the utility of this assay by characterizing the molecular mechanisms that contribute

to this process and reveal how it may be triggered after MVB maturation. Thus, we speculate that this powerful experimental tool will be of great utility to others interested in further studying mechanisms that contribute to this important step in endocytosis.

One noteworthy aspect of our design, however, is the over-expression the Qa-SNARE Pep12, which is used to target the fusion probe to MVBs, raising concerns of whether increased Pep12 levels could affect the fusion reaction. We believe that it has minimal effects on heterotypic fusion because (1) endosomal morphology looks normal in micrographs of cells expressing the probe, and (2) many groups have shown that over-expression of all SNAREs within the complex (three Q-SNAREs and an R-SNARE) is required to alter fusion of organelles (sometimes leading to lysis; e.g. Starai et al. 2007) or synthetic liposomes (e.g. Mima et al. 2008). It is also worth noting that we used the same probes and assay to measure MVB-MVB fusion *in vitro* without success (data not shown). We suspect that this outcome is likely a result of co-purification with vacuolar lysosomes, whereby MVBs seem to be more likely to encounter a vacuolar lysosome than a MVB *in vitro* (micrographs presented offer examples), decreasing the relative number of possible MVB-MVB fusion events that occur in the reaction. However, in theory, the same approach can be used to study other organelle membrane fusion events by swapping the targeting sequence and purifying the organelles using a method that ensures sufficient purification has occurred to permit organelle interactions *in vitro*, that isolates organelles in buffer that permits fusion (e.g. low osmolarity; Brett and Merz 2008), and that does not damage membranes (e.g. isolation by floatation; Conradt et al. 1992).

3.4.2 Unique features of the MVB-lysosome fusion reaction

Using this new cell-free assay, we generated evidence (see Figure 12) that complements results from studies relying on genetic approaches, trafficking assays and microscopy (e.g. Arlt et al. 2015) to validate the prevailing model of MVB-vacuolar lysosome membrane fusion (Bröcker et al. 2010; Epp et al. 2011; see figure 8). Specifically, we demonstrated that: (1) Heterotypic fusion does not require cytosolic components and is activated by addition of ATP to fusion reactions, suggesting ATP hydrolysis is necessary for membrane fusion. (2) Sec17, a SNARE chaperone and the only α-SNAP ortholog in *S. cerevisiae*, is required for heterotypic fusion, and likely functions during the priming stage of the reaction as it does for membrane fusion at other sites within cells (Clary et al., 1990; Mayer et al., 1996). (3) The Rab-GTPase Ypt7, not Vps21, is required for this fusion event. (4) The Ypt7-effector complex HOPS, and not

CORVET (the other MTC found on MVBs important for homotypic endosome fusion; Balderhaar and Ungermann 2013) is required for MVB-vacuolar lysosome fusion *in vitro*. We hypothesize that both Ypt7 and HOPS mediate the tethering and docking stages of this reaction, as they are critical for these stages of the homotypic vacuole fusion reaction (Ungermann et al., 2000; Price et al., 2000). (5) Pep12, the resident Qa-SNARE on MVBs, replaces Vam3, the vacuolar Qa-SNARE, in *trans*-SNARE complexes responsible for heterotypic lipid bilayer merger, the last stage of the reaction. Thus, it seems that the composition of the SNARE protein complex, rather than Rab-GTPases or MTCs, encode specificity between two distinct membrane fusion events. Because Q-SNAREs are thought to preassemble on a single membrane (Schwartz and Merz, 2009) and Vti1 is found on MVBs as well as vacuolar lysosomes (Gossing et al., 2013), we propose that MVB membranes donate Pep12 and Vti1 to the complex that assembles with the soluble Qc SANRE Vam7 and Nyv1 donated from vacuolar lysosome membranes. This finding is consistent with results from synthetic systems showing that recombinant Pep12, Nyv1, Vti1 and Vam7 protein complexes form, are stable and drive liposome fusion (Furukawa and Mima, 2014). Overexpression of VAM3 suppresses cellular trafficking defects in *pep12Δ* cells (Götte and Gallwitz, 1997), suggesting that they can replace each other in SNARE complexes as has been reported in other organisms (e.g. Arabidopsis thaliana; Uemura et al. 2010). Furthermore, Vps33, the Sec1/Munc18 family-protein within the HOPS complex responsible for *trans*-SNARE templating required for homotypic vacuole fusion (Baker et al., 2015), can substitute Vam3 with Pep12 with equal affinity (Lobingier and Merz, 2012), suggesting that there is a conserved mechanism of how *trans*-SNARE complexes form and zipper to mediate lipid bilayer merger in response to upstream signaling by active Ypt7 and HOPS.

During homotypic vacuolar lysosome fusion, Ypt7, HOPS and SNAREs assemble as a ring at the vertex between apposed membranes, creating a flat circular boundary area at the site of contact between organelles (Wang et al., 2003; Mattie et al., 2017; McNally et al., 2017). We observed similar flattened interfaces between MVBs and vacuoles by TEM (Figure 11G), suggesting that this machinery creates the same topological arrangement to mediate MVB-vacuolar lysosome fusion. Paralogs of these fusion proteins are found on all endocytic organelles within *S. cerevisiae* cells (Nickerson et al., 2009; Kümmel and Ungermann, 2014; Numrich and Ungermann, 2014). Thus we speculate that the vertex ring may be a topological requirement for these families of proteins to function in assemblies necessary for organelle membrane fusion in

the endocytic pathway. It is also noteworthy that the boundary membrane is internalized within the lumen as a byproduct of lipid bilayer merger at the vertex ring (Wang et al., 2002). Recently, we demonstrated that lysosomal polytopic proteins are selectively sorted into this boundary and upon membrane fusion are internalized and degraded by lumenal hydrolases (Mattie et al., 2017). Called the intralumenal fragment pathway, this process is important for lysosomal protein quality control, and is thought to remodel vacuolar lysosome membranes in response to cellular cues. Importantly, Ypt7 and possibly HOPS, but not ESCRTs, contribute to protein sorting in this pathway. Given that a similar boundary membrane forms during MVB vacuolar lysosome fusion and that Ypt7 and HOPS contribute to this event, it is tempting to speculate a similar mechanism may be used to degrade polytopic proteins on MVB membranes, or to remodel the membrane of the MVB-vacuolar lysosome fusion product to control organelle identity. Furthermore, it would explain the presence of large ILVs within MVBs that form in the absence of the ESCRT machinery (Stuffers et al., 2009).

At multiple sites within cells, Ca^{2+} fluxes are known to promote SNARE-zippering required for lipid bilayer merger (Pang and Südhof, 2010). Although we planned to use published methods to measure Ca^{2+} transients during MVB-vacuolar lysosome fusion events *in vitro* (e.g. Merz and Wickner 2004; Sasser et al. 2012), Ca^{2+} indicators (e.g. aequorin, Fluo-4) added to our cell-free heterotypic fusion reactions would not distinguish between Ca^{2+} released during homotypic fusion events or heterotypic events, as both occur in our samples. Instead we resorted to adding calcium chloride or divalent metal chelators to fusion reactions and found that the presence of cytoplasmic Ca^{2+} inhibits MVB-vacuolar lysosome fusion (Figure 13). This finding is in contrast to similar studies conducted using organelles isolated from mammalian cells whereby lumenal Ca^{2+} release by a purine receptor-type channel P2X4 is required for fusion (Cao et al., 2015). However, late endosomes (MVBs) were not distinguished from vacuolar lysosomes in these studies, making it difficult to compare results, and the *S. cerevisiae* genome does not include orthologous genes encoding purine receptor channel genes or other Ca^{2+} channels implicated in endosome-lysosome fusion (e.g. two pore channels; Tian et al., 2015), which may explain why our findings are different. Homotypic vacuolar lysosome fusion, on the other hand, requires lumenal Ca^{2+} efflux (although the channel responsible remains unknown; Merz and Wickner 2004). Thus, we speculate that Ca^{2+} release from vacuolar lysosomes may act as a switch to control trafficking at the vacuolar lysosome, whereby the release of lumenal Ca^{2+}

into the cytoplasm promotes homotypic fusion events whilst preventing heterotypic events, and vice versa.

3.4.3 ESCRT function triggers MVB-lysosome fusion by promoting Rab conversion

Prior to our study, correlational evidence was presented suggesting that ESCRTs contribute to MVB-vacuolar lysosome fusion (see Metcalf and Isaacs, 2010; Russell et al., 2012; Shideler et al., 2015). Herein, we show that knocking out a single component in any of the ESCRT complexes prevents MVB-vacuolar lysosome fusion *in vitro* (Figure 17C). Because these results were gleaned from reactions containing vacuolar lysosomes isolated from wild type cells mixed with aberrant MVBs from mutant cells, we are confident that the fusion defect is due to a defect present on the MVB, and eliminates the possibility that impaired delivery of biosynthetic cargo to vacuoles observed in mutant cells underlies observed heterotypic fusion defects (Robinson et al., 1988; Raymond et al., 1992). Because all mutations resulted in the same phenotype, we reason that the triggering mechanism for fusion must occur downstream from the component that functions latest in the pathway, Snf7 (ESCRT-III), consistent with it being activated after ILV formation has occurred (Russell et al., 2012). Although the precise molecular mechanism remains unknown, previous work suggested that blocking ESCRT function prevents activation of Ypt7 through disruption of a Rab-conversion mechanism through the accumulation of active Vps21 on aberrant MVB membranes (Russell et al., 2012; Shideler et al., 2015). Using our new cell-free assay, we were able to partially rescue defects in heterotypic fusion caused by ESCRT mutations by adding GTPγS to activate Ypt7, supporting this hypothesis (Figure 17C). We reason that partial recovery may result from GTPγS also activating Vps21, which would exacerbate the blockade in Rab conversion, thus counteracting the effect of GTPγS on Ypt7 activation (Shideler et al., 2015). Thus, as an alternative approach, we replaced wild type YPT7 with a constitutively active mutant (Ypt7-Q68L) to target only this Rab-GTPase and not Vps21. When expressed in cells lacking VPS23, a component of ESCRT-I, Ypt7-Q68L completely rescued heterotypic fusion *in vitro* (Figure 17E). Thus, we reason that ESCRT function during MVB maturation is required for activation of Ypt7 to trigger MVB-vacuolar lysosome fusion (Figure 18). Although the mechanism that couples ESCRT function with Ypt7 activation remains elusive, it likely involves stimulation of the GEF (guanine exchange factor) protein complex Mon1-Ccz1 responsible for Ypt7 activation (Nordmann et al., 2010) and the Rab-GAP Msb3 that inactivates Vps21 (Lachmann et al., 2012), possibly through coordination with the Rab-effectors

HOPS and BLOC 1 (Rana et al., 2015) on MVB membranes.

3.4.4 Nhx1 activity controls SNARE-mediated MVB-lysosome membrane fusion

Using our new cell-free heterotypic fusion assay, we were able to directly test the existing model of Nhx1 function and provide direct evidence for key aspects that were previously only implied: (1) We demonstrate that deleting NHX1 impairs MVB-vacuole fusion (Figure 15D) accounting for impaired delivery of internalized surface polytopic proteins to the vacuolar lumen for degradation (Bowers et al., 2000; Brett et al., 2005). (2) Although Nhx1 has not been reported to be present on vacuolar lysosome membranes *in vivo*, we demonstrate that Nhx1 can accumulate on these compartments after heterotypic fusion i*n vitro* (Figure 15C). This finding offers an explanation for the observed presence of Nhx1 on these isolated organelles reported by Fratti and colleagues (Qiu and Fratti, 2010), and offers an explanation as to why the vacuole lumen is hyperacidic in *nhx1Δ* cells in support of Nhx1 functioning as a H^+-leak pathway on both compartments (Nass and Rao, 1998; Ali et al., 2004). Although we did not pursue the basis of the discrepancy between observations made *in vitro* and *in vivo*, it is possible that Nhx1 proteins are recovered to the MVB after heterotypic fusion by the retromer pathway (Balderhaar et al., 2010; Arlt et al., 2015) and this mechanism is either impaired *in vitro* or occurs at a rate that was not accommodated by the 90 minute reaction. (3) We also demonstrate that MVBs, where Nhx1 is predominantly localized, are also hyperacidic within *nhx1Δ* cells (Figure 15H). We found that Vph1, the stalk domain of the vacuolar V-ATPase assembly, abnormally accumulated on MVBs within cells lacking NHX1 (Figure 16D). Given that MVB hyper-acidification *in vitro* requires ATP (Figure 15H), we hypothesize that Vph1 mislocalization to MVBs may underlie the phenotype; it could replace Stv1 in existing V-ATPase complexes or recruit more V-ATPase complexes to this compartment to increase H^+-pumping capacity (Kawasaki-Nishi et al., 2001). (4) Although the weak base chloroquine facilitated recovery of heterotypic fusion between organelles isolated from *nhx1Δ* cells, both homotypic and heterotypic fusion events were stimulated by chloroquine in the presence of NHX1, consistent with a recent report suggesting that luminal alkalinization promotes homotypic vacuolar lysosome membrane fusion (Desfougères et al., 2016). This result is consistent with the prevailing model of Nhx1 function whereby lumenal exchange activity drives MVB-vacuolar lysosome fusion. However, lumen-to-cytoplasm H^+ translocation by Nhx1 requires cytoplasm-to-lumen counter-transport of a monovalent cation, such as K^+ (Nass and Rao, 1998; Brett et al., 2005). In support of the model,

we found that cell-free heterotypic fusion is supported by Rb^+ in place of K^+ but only in the presence of NHX1 (Figure 15J). Nhx1 is the only known transporter on the MVB to accept Rb^+ as a substrate (Brett et al., 2005), albeit at a lower affinity than K^+, which possibly reflects the observed reduction in heterotypic fusion in the presence of NHX1 (Figure 15J). Furthermore, Nhx1 on MVBs may underlie the different pH and monovalent cationic profiles observed for MVB-vacuolar lysosome fusion as compared to vacuolar homotypic lysosome fusion (Figure 14). Thus, our results provide invaluable evidence to the prevailing model of Nhx1 function whereby lumenal H^+ export (resulting in alkalinization) coupled to monovalent cation import drives MVB-vacuolar lysosome fusion for degradation of internalized surface polytopic proteins.

But how does Nhx1 activity regulate heterotypic membrane fusion? Firstly, we confirmed that the defect is present on MVB membranes, as *in vitro* heterotypic fusion between *nhx1Δ* MVBs and wild type vacuoles was impaired whereas wild type MVB- *nhx1Δ* vacuole fusion was tolerated (Figure 15E). We originally hypothesized that Nhx1 activity alters the charge on MVB membranes by reducing protonation of negatively charged lipids on the outer leaflet promoting membrane association of cytoplasmic fusion proteins (e.g. HOPS; Stroupe et al., 2006b). However, we did not observe changes in the cellular distribution of GFP-tagged components of HOPS or Ypt7 within *nhx1Δ* cells (e.g. Figure 16D; data not shown). This result is consistent with a report demonstrating that fusion machinery proteins continue to co-purify with MVBs and vacuoles isolated from *nhx1Δ* cells at levels similar to wild type organelles (Qiu and Fratti, 2010), suggesting that deleting NHX1 does not affect the membrane association of soluble fusogenic proteins on MVBs or vacuolar lysosomes. Because the Rab-GAP Gyp6 was shown to bind and inhibit Nhx1 (Ali et al., 2004), we hypothesized that loss of NHX1 may inactivate Ypt7 accounting for impaired fusion. But deleting NHX1 had no effect on Ypt7 activation (Figure 16A and B), and addition of GTPγS to activate Ypt7 did not overcome fusion defects (Figure 16C), eliminating this possibility and suggesting that Nhx1 and ESCRT machinery target different components of the machinery underlying MVB-vacuolar lysosome fusion. Rather, heterotypic fusion defects caused by deleting NHX1 were overcome by adding rVam7 (Figure 16E), a soluble SNARE protein known to drive vacuole membrane fusion without a requirement for Ypt7 or HOPS (Thorngren et al., 2004). Thus, because MVBs within *nhx1Δ* cells contain ILVs (Kallay et al., 2011), we propose that $Na^+(K^+)/H^+$ exchange by Nhx1 is activated downstream of ESCRTs to promote MVB-vacuole fusion after maturation whereby lumenal

alkalinization by Nhx1 triggers an unknown target upstream of *trans*-SNARE complex formation independent of Ypt7 activation or HOPS function (Figure 18).

Orthologous machinery in metazoans has been implicated in both MVB maturation and MVB-vacuolar lysosome membrane fusion (e.g. Solinger and Spang, 2013; Pols et al., 2013; Wartosch et al., 2015) and this machinery is thought to drive these processes using mechanisms similar to those observed in *S. cerevisiae* (Luzio et al., 2010). Mutations in components of the ESCRT machinery are linked to human disorders including cancers and neurodegenerative disorders, whereby defects in endocytosis are observed (Saksena and Emr, 2009). Similarly, loss-of-function mutations in NHE6, a human ortholog of NHX1, are linked to Christianson syndrome, a devastating neurodevelopmental disorder (Gilfillan et al., 2008). Compelling work by the Morrow, Walkley and Strømme groups demonstrates a strikingly similar role for NHE6 in endocytosis within neurons where, for example, it is important for TrkB/Brain Derived Neurotropic Factor signaling for proper development of neural circuitry (Strømme et al., 2011; Ouyang et al., 2013). Mutations in NHE6 or its paralog NHE9 are also thought to impair endocytosis in astrocytes possibly underlying cellular defects that contribute to Alzheimer's disease (Prasad and Rao, 2015) or glioblastoma (Kondapalli et al., 2015). Regardless, our final model describing the molecular basis of MVB-vacuolar lysosome membrane fusion could explain observed cellular defects that underlie these diverse human diseases and offers strategies to overcome impairments in MVB-vacuolar lysosome fusion as potential therapies.

Figure 18. Working model of MVB-vacuole membrane fusion

Cartoon illustrating the fusion protein machinery underlying MVB-vacuolar lysosome membrane fusion and the ESCRT machinery or Nhx1 targets this process.

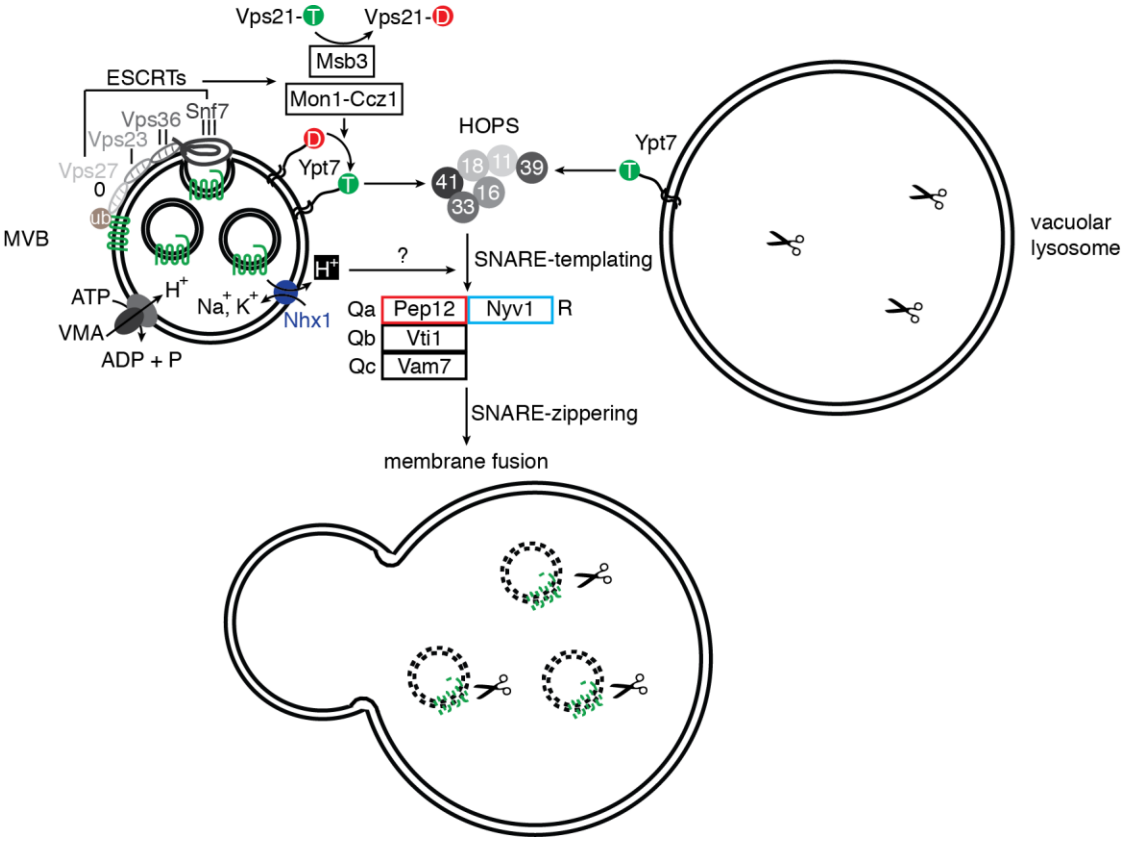

3.5 Materials and Methods

3.5.1 Yeast strains and reagents

All strains and plasmids used in this study are listed in Table 2. For cell-free organelle fusion assays, we used the *Saccharomyces cerevisiae* strain BJ3505 [*MATα pep4::HIS3 prbΔ1-1.6R his3–Δ200 lys2-801 trp1-Δ101 (gal3) ura3–52 gal2 can1*] because it is devoid of vacuolar lumenal proteases that would otherwise degrade lumenal fusion probes. For MVB-vacuolar lysosome fusion, BJ3505 cells were transformed with complementary fusion probes: pCB002 (pRS406-Pep12-Fos-Gs-ω) and pCB003 (pRS404-Pep12-Fos-Gs-ω) to target the MVB lumen or pYJ406-Jun (pRS406-CPY50-Jun-Gs-α) and pCB011 (pRS404-CPY50-Jun-Gs-α) to target the vacuolar lysosome lumen. For homotypic vacuolar lysosome fusion, BJ3505 cells were transformed with complementary fusion probes targeting the vacuolar lysosome lumen: pYJ406-Fos (pRS406-CPY50-Fos-Gs-ω) and pCB008 (pRS404-CPY50-Fos-Gs-ω) or pYJ406-Jun (pRS406-CPY50-Jun-Gs-α) and pCB011 (pRS404-CPY50-Jun-Gs-α). NHX1::GFP was knocked in or NHX1, VPS23, VPS36, and SNF7 were knocked out of BJ3505 cells using the Longtine method (Longtine et al., 1998). To assess localization of fusion probes, we transformed wild type or mutant BJ3505 cells with pCB035 (pRS406-Pep12-GFP) to target the MVB lumen or pCB044 (pRS406-CPY50-GFP) to target the vacuole lumen, and imaged live cells by fluorescence microscopy. All biochemical and yeast growth reagents were purchased from Sigma-Aldrich, Invitrogen or BioShop Canada Inc. All restriction enzymes, Ni-Sepharose 6FF, and glutathione Sepharose 4B, polymerases, and ligases were purchased from New England Biolabs (County Rd, Ipswich, MA, USA). Purified rabbit polyclonal antibody against Sec17 was a gift from William Wickner (Dartmouth College Hanover, NH, USA), whereas those against Vam3, Ypt7, Vps21, Vps33, Vps41, Vps10 and CPY were gifts from Alexey Merz (University of Washington, Seattle, WA, USA). Recombinant mouse antibody against Pep12 was purchased from Invitrogen (Mainway, Burlington, ON). Recombinant rabbit IgG against GFP was purchased from Abcam (Toronto, ON). Proteins used include recombinant Gdi1 purified from bacterial cells using a calmodulin-binding peptide intein fusion system (Brett et al., 2008), recombinant Gyp1-46 (the catalytic domain of the Rab-GTPase activating protein Gyp1) purified as previously described (Eitzen et al., 2000), and recombinant soluble Qc-SNARE Vam7 purified as previously described (Schwartz and Merz, 2009). Reagents used in fusion reactions were prepared in 10 mM Pipes-KOH, pH 6.8, and 200 mM sorbitol (Pipes-sorbitol buffer, PS).

3.5.2 Membrane fractionation by sucrose gradient

Yeast cells were grown in YPD overnight to OD_{600nm}= 1.6/ml, harvested, and spheroplasted with lyticase for 30 minutes at 30^{o}C. Spheroplasts then were sedimented and resuspended in 10 ml of TEA buffer (10 mM triethanolamine, pH 7.5, 100 mg/ml phenylmethylsulfonyl fluoride, 10 mM NaF, 10 mM NaN_3, 1 mM EDTA, and 0.8 M sorbitol) and homogenized on ice by Dounce homogenization (20 strokes). Cell lysates were centrifuged at 15000 g for 20 minutes, and the resulting supernatant then was centrifuged at 100000 g for 12 hours to sediment cellular membranes. Pellets were resuspended in 1 ml of TEA buffer and loaded onto a stepwise (20–70%) sucrose density gradient, and then centrifuged at 100000 g for 16 hours at 4°C to separate different cellular membranes by density. Samples were collected from the top, and each fraction was precipitated using 10% trichloroacetic acid, washed and resuspended in 100 µl of SDS-PAGE buffer. Fractions then were loaded into SDS-polyacrylamide gels and subjected to electrophoresis to separate proteins by size. Western blot analysis was performed to determine fractions that contain proteins of interest.

3.5.3 Organelle isolation and cell-free fusion assay

Organelles were isolated from yeast cells by a Ficoll floatation method as previously described (Haas et al., 1994). Organelle membrane fusion was assessed using a modified version of a published assay that relies on split β-lactamase complementation upon content mixing (Jun and Wickner, 2007). In brief, organelles were isolated from two separate strains that each express a single complementary fusion probe, and 6 µg of organelles from each strain were added to 60 µl fusion reactions in standard fusion buffer supplemented with 11 µM recombinant GST-Fos protein to reduce background caused by lysis. Reactions were incubated up to 90 minutes at 27°C and then stopped by placing them on ice. Content mixing was quantified by measuring the rate of nitrocefin hydrolysis by reconstituted β-lactamase. Then, 58 µl of the fusion reactions were transferred into a clear-bottom 96-well plate and mixed with 142 µl of nitrocefin developing buffer (100 mM NaPi pH 7.0, 150 µM nitrocefin, 0.2% Triton X-100). To measure nitrocefin hydrolysis, absorbance at 492 nm was monitored at 15 seconds intervals for 15 minutes at 30°C with a Synergy H1 multimode plate reading spectrophotometer (Biotek, Winooski, VT, USA). Slopes were calculated and one fusion unit is defined as 1 nmol of

hydrolyzed nitrocefin per minute from 12 µg of organelle proteins. Standard fusion buffer contains 125 mM KCl, 5 mM $MgCl_2$, ATP regenerating system (1 mM ATP, 40 mM creatine phosphate, 0.5 mg/ml creatine kinase), and 10 µM CoA in PS buffer. To block fusion, either antibodies raised against Sec17, Ypt7, Vps21, Vps33, Vps41, Vam3, Pep12, or purified recombinant Gdi1 (4 µM) or Gyp1-46 (5 µM) proteins were added to fusion reactions. Where indicated, vacuoles were pretreated with 0.2 mM GTPγS for 10 minutes at 27°C prior to addition to fusion reactions, or reactions were supplemented with 100 nM rVam7 and 10 µg/ml bovine serum albumin.

3.5.4 *Trans*-SNARE paring assay

Analysis of *trans*-SNARE complex formation was assayed as described (Jun and Wickner, 2007), whereby the levels of Nyv1 that co-immunoprecipitate with CBP::Pep12 or CBP::Vam3 were determined. Briefly, 45 µg of organelles each from CBY224 or DKY6281-CBP::Vam3 *nyv1Δ* and BJ3505 were incubated under fusion conditions for 60 minutes. Reactions were then placed on ice for 5 minutes, and samples were centrifuged (11000 g, 15 minutes, 4°C). Supernatants were decanted, and membrane fractions were resuspended in 180 µl solubilization buffer (20 mM Tris-Cl pH 7.5, 150 mM NaCl, 1 mM $MgCl_2$, 0.5% Nonidet P-40 alternative, 10% glycerol) with protease inhibitors (0.46 µg/ml leupeptin, 3.5 µg/ml pepstatin, 2.4 µg/ml pefabloc, 1 mM PMSF). Reactions were topped up to a final volume of 560 µl and nutated for 20 minutes at 4°C. Reactions were centrifuged again (16000 g, 20 minutes, 4°C) and supernatants collected. Next, 10% of the extracts were collected as input samples, and the remaining extracts were brought to 2 mM $CaCl_2$. The CBP::Pep12/Nyv1 or CBP::Vam3/Nyv1 complexes were recovered with calmodulin Sepharose beads 4B (GE Healthcare) by nutating overnight at 4°C, collected by brief centrifugation (4000 g, 2 minutes, 4°C), washed five times with sample buffer, and followed by bead sedimentation. Bound proteins were eluted by boiling beads (95°C, 10 minutes) in SDS sample buffer containing 5 mM EGTA for SDS-PAGE analysis and immunoblotting.

3.5.5 Ypt7 extraction assay

The Rab-GTPase extraction assay was performed as previously described (Brett et al., 2008). Briefly, 5X reactions containing 30 µg organelles from wild type or *nhx1Δ* BJ3505 cells were incubated under fusion condition for 30 minutes at 27°C. Then, 5 µM of rGdi1 was added,

and the reactions were further incubated for 10 more minutes. Samples (then immediately) were centrifuged (5000 g, 5 minutes, 4°C) to separate membrane bound proteins from those in the supernatant. Supernatant (100 µl) was transferred into fresh tubes and mixed with 25 µl 5X Laemmli SDS sample buffer while the pellets were resuspended in 100 µl 1X of the same sample buffer and boiled at 95°C for 10 minutes. One tenth of the total isolated supernatant or pellet was analyzed by Western blot.

3.5.6 Measurement of MVB lumenal pH

Wild type or *nhx1Δ* BJ3505 cells were transformed with pCB046 to express pHluorin (pH sensitive) fused to mCherry (pH-insensitive) at the C-terminus of Pep12. Organelles were isolated as previously described (Haas et al., 1994). Reactions (60 µl) containing 12 µg of isolated organelles were incubated at 27°C for 10 minutes with 50 µM nigericin in PS buffer titrated to pH values between 5.80 and 7.80. Fluorescence intensities for pHluorin (excitation at 485 nm, emission at 520 nm) and mCherry (excitation at 584 nm, emission at 610 nm) were then measured with a Synergy H1 multimode plate reading fluorometer (Bioteck, Winooski, VT, USA). A blank reference well containing 60 µl PS buffer was used to detect background fluorescence. Background subtracted pHluorin:mCherry ratio values were then plotted against pH values to generate a calibration curve. Sample fluorescence was then compared to the calibration curve to calculate MVB lumenal pH.

3.5.7 Western blot analysis

Sodium dodecyl sulfate-polyacrylamide gel electrophoresis (SDS-PAGE) was performed using a Bio-Rad mini protein system (Bio-Rad Laboratories, Hercules, CA, USA). After separation, proteins were transferred onto a nitrocellulose membrane by the wet transfer method at 12 V for 8 hours using a Royal Genie Blotter apparatus (Idea Scientific, Minneapolis, MN, USA). Membranes were blocked with 3% BSA in PBST buffer (137 mM NaCl, 2.7 mM KCl, 10 mM Na_2HPO_4, 2 mM KH_2PO_4, 0.1% Tween-20) and then washed twice with PBST and incubated with primary antibody diluted to 1:1000 in PBST for 1 hour at room temperature. Membranes were washed with PBST five times, and then incubated with HRP or FITC labeled goat anti-rabbit IgG diluted 1:10000 in PBST for 1 hour at room temperature. After an additional 5 washes with PBST, the membranes were probed to detect bound secondary antibody using GE Amersham Imager 600 for chemiluminescence or a Typhoon scanner for fluorescence (GE

Healthcare, Piscataway, NJ, USA).

3.5.8 Fluorescence microscopy

Live yeast cells stained with FM4-64 to label vacuole membranes were prepared for imaging using a pulse-chase method as previously described (Brett et al., 2008). For *in vitro* imaging, organelles isolated from strains expressing Nhx1-GFP, Pep12-GFP, or CPY50-GFP were stained with FM4-64 by treating organelles with 3 μM FM4-64 for 10 minutes at 27°C. Standard fusion reaction buffer was then added and organelles were incubated up to 90 minutes at 27°C and placed on ice prior to visualization. We used a Nikon Eclipse TiE inverted microscope equipped with a motorized laser TIRF illumination unit, Photometrics Evolve 512 EM-CCD camera, an ApoTIRF 1.49 NA 100x objective lens, and bright (50 mW) blue and green solid-state lasers operated with Nikon Elements software (housed in the Centre for Microscopy and Cellular Imaging at Concordia University). Micrographs were processed using ImageJ software (National Institutes of Health) and Adobe Photoshop CC. Images shown were adjusted for brightness and contrast, inverted and sharpened with an unsharp masking filter.

3.5.9 Transmission Electron Microscopy

Isolated organelles were processed for transmission electron microscopy (TEM) using a custom protocol (Mattie et al., 2017). Fusion reactions were centrifuged at 4^{o}C for 5 minutes, the supernatant was removed, 0.5 ml fixative (2.5% glutaraldehyde) was added to pellets and they were incubated overnight at 4^{o}C. Pellets then were washed with washing buffer (0.1M sodium cacodylate) three times for 10 minutes and incubated in 0.5 ml freshly prepared osmium tetroxide solution (1% OsO_4 in 1.5% KFeCN) for two hours at 4^{o}C. Pellets were then washed with water three times for 5 minutes prior to dehydration by adding increasing concentration of ethanol (30%, 50%, 70%, 80%, 90%, for 10 minutes each, and then in 100% ethanol, 3 times for 10 min) and treatment with 100% propylene oxide twice for 5 minutes. For sample infiltration, pellets were incubated in 1:1 volume ratio of propylene oxide:Epon for 1 hour at room temperature. The supernatant then was replaced with 100% Epon, and samples were placed under vacuum for 1 hour to remove bubbles and remaining traces of propylene oxide. The samples were incubated overnight at room temperature followed by the addition of 0.5 ml fresh 100% Epon for polymerization by incubation at 4^{o}C for 48 hours. Epon-embedded samples were cut into 90-100 nm sections using a Ultracut microtome and DiATOME Ultra diamond knife,

and each section then was placed on a copper mesh grid. Sections on grids were stained with 4% uranyl acetate for 8 min, then with 6% lead for 5 min, and followed by three washes with water. The final samples were imaged using FEI Tecnai 120 kV electron microscope outfitted with an AMT XR80C CCD camera system at the Facility for Electron Microscopy Research (McGill University, Montreal, QC). Digital images were processed using Adobe Photoshop CC software (Adobe Systems, San Jose, CA, USA). Brightness and contrast levels were adjusted and unsharpened filter was applied to images shown.

3.5.10 Data analysis and presentation

All quantitative data were processed using Microsoft Excel v.14.0.2 software (Microsoft Cooperation, Redmond, WA, USA), including calculation of mean and S.E.M. Data were plotted using Kaleida Graph v.4.0 software (Synergy Software, Reading, PA, USA). All figures were prepared using Adobe Illustrator CC software (Adobe Systems, San Jose, CA, USA). References were prepared using Mendeley software (Mendeley, New York, NY, USA).

Table 2: Yeast strains and plasmids used in this study.

Strain	Genotype	Source
BJ3505	*MATα pep4::HIS3 prb1-Δ1.6R his3–200 lys2–801 trp1Δ101 (gal3) ura3–52 gal2 can1*	Jones et al., 1982
CBY042	BJ3505; *NHX1-GFP::URA3*	This study
CBY044	BJ3505; *pCB002.ADHIpr-PEP12-FOS-GS-ω*, *pCB003.ADHIpr-PEP12-FOS-GS-ω*	This study
CBY046	BJ3505; *pYJ406.ADHIpr-CPY50-FOS-GS-ω*, *pCB008.ADHIpr-CPY50-FOS-GS-ω*	This study
CBY048	BJ3505; *pYJ406.ADHIpr-CPY50-JUN-GS-α*, *pCB011.ADHIpr-CPY50-JUN-GS-α*	This study
CBY049	CBY044; *nhx1Δ::KANMX*	This study
CBY050	CBY046; *nhx1Δ::KANMX*	This study
CBY051	CBY048; *nhx1Δ::KANMX*	This study
CBY058	BJ3505; *pCB035.ADHIpr-PEP12-GFP*	This study
CBY060	BJ3505; *pCB046.ADHIpr-PEP12-pHluorin-mCherry*	This study
CBY067	CBY058; *nhx1Δ::KANMX*	This study
CBY117	BJ3505; *pCB044.ADHIpr-CPY50-GFP*	This study
CBY118	CBY117; *nhx1Δ::KANMX*	This study
CBY130	CBY044; *nyv1Δ::KANMX*	This study
CBY131	CBY046; *nyv1Δ::KANMX*	This study
CBY132	CBY048; *nyv1Δ::KANMX*	This study
CBY134	CBY044; *vps8Δ::KANMX*	This study
CBY135	CBY046; *vps8Δ::KANMX*	This study
CBY136	CBY048; *vps8Δ::KANMX*	This study
CBY137	CBY058; *vps8Δ::KANMX*	This study
CBY138	CBY117; *vps8Δ::KANMX*	This study
CBY155	CBY058; *nyv1Δ::KANMX*	This study
CBY156	CBY117; *nyv1Δ::KANMX*	This study
CBY179	CBY058; *snf7Δ::KANMX*	This study
CBY199	CBY058; *vps23Δ::KANMX*	This study
CBY217	CBY058; *vps36Δ::KANMX*	This study
CBY196	CBY044; *vps23Δ::KANMX*	This study
CBY222	CBY044; *vps36Δ::KANMX*	This study
CBY223	CBY044; *snf7Δ::KANMX*	This study
CBY224	BJ3505 *nyv1Δ::TRP*1; *pCB045.ADHIpr-CBP-PEP12*	This study
CBY232	CBY044 *YPT7-Q68L::NATMX; vps23Δ::KANMX*	This study
CBY236	CBY058 *YPT7-Q68L::NATMX; vps23Δ::KANMX*	This study
Plasmid	**Description**	**Source**
pCB002	pRS406 *URA3*; *ADHIpr-PEP12-FOS-GS-ω*	This study
pCB003	pRS404 *TRP1*; *ADHIpr-PEP12-FOS-GS-ω*	This study

pYJ406-Fos-ω	pRS406 *URA3*; *ADHIpr-CPY50-FOS-GS-ω*	Jun and Wickner,2007
pCB008	pRS404 *TRP1*; *ADHIpr-CPY50-FOS-GS-ω*	This study
pYJ406-Jun-α	pRS406 *URA3*; *ADHIpr-CPY50-JUN-GS-α*	Jun and Wickner,2007
pCB011	pRS404 *TRP1*; *ADHIpr-CPY50-JUN-GS-α*	This study
pCB035	pRS406 *URA3*; *ADHIpr-PEP12-GFP*	This study
pCB044	pRS406 *URA3*; *ADHIpr-CPY50-GFP*	This study
pCB045	pRS406 *URA3*; *ADHIpr-CBP-PEP12*	This study
pCB046	pRS406 *URA3*; *ADHIpr-PEP12-pHluorin-mCherry*	This study

Chapter 4. Conclusions and future directions

4.1 Overview

Lysosomes are the recycling compartments of all eukaryotic cells. They receive biomaterials through both homotypic (lysosome-lysosome) and heterotypic (MVB- or autophagosome-lysosome) fusion events, which exposes them to the degradative environment of the lumen where they are broken down by acid hydrolases into small building blocks and returned to the cytoplasm by nutrient transporters for reuse (Russnak et al. 2001; Luzio et al. 2007; Li and Kane 2009). Thus, lysosomal function is crucial for cellular metabolism and clearance of toxic biomaterials that would otherwise cause cell death. Disruption of this function by targeting the molecular mechanisms underlying fusion, degradation, or recycling contributes to diverse human disorders, including lysosomal storage disorders, neurodegenerative disorders, and cancers (Parkinson-Lawrence et al. 2010; Ballabio and Gieselmann 2009; Lutgens et al. 2007).

Although critical for lysosome function, biogenesis, inheritance, homeostasis and remodeling, many mechanistic details underlying lysosomal membrane fusion are still unclear. In this thesis, I elucidated a role for HOPS in coordinating the interplay between Rab, protein kinase, and SNARE cycles to orchestrate homotypic lysosome fusion and regulate the amount of lysosome membrane internalized and degraded upon fusion. I also show that HOPS recognizes two distinct *trans*-SNARE complexes: One composed of exclusively lysosomal Q-SNAREs Vam3, Vti1 and Vam7, and the R-SNARE Nyv1 for homotypic fusion, and another composed of a non-cognate endosomal Q-SNARE bundle including Pep12, Vti1 and Vam7, and the lysosomal R-SNARE Nyv1, required for heterotypic MVB-vacuole membrane fusion. Therefore, my work fine-tunes our understanding of the molecular mechanisms underlying membrane fusion events at the lysosome membrane.

4.2 Rab-Kinase-SNARE cycles are regulated by HOPS to orchestrate vacuolar lysosome fusion and control ILF formation

In Chapter 2, I described a point mutation in Ypt7 (D44N) that uncouples Rab activation from effector (Vps41) binding (Figure 7B and C). I found that Ypt7-D44N impairs pore formation (inner leaflet merger), but has no effect on lipid mixing (outer leaflet merger; Figure

6A and B), causing fewer ILFs to form during fusion events in live cells and *in vitro* (Figures 5C and 6G; video 1). The abnormally high lipid to content mixing ratio (Figure 6E), suggests that the transition from lipid stalk to pore formation is stalled and causes hemifusion diaphragms to accumulate (Figure 6F, H, I, J, K). Although it cannot bind Vps41, Ypt7-D44N continues to support tethering and docking (Figure 8A and B) but HOPS is not stabilized on membranes (Figure 7E and F), compromising the formation and stability of *trans*-SNARE complexes (Figure 8C and D). These observations suggest that the Ypt7-Vps41 interaction is dispensable for membrane tethering and docking during HVF but is required for *trans*-SNARE complex zippering that mediates pore formation. The addition of exogenous rVam7 to drive *trans*-SNARE complex assembly and promote stability rescued fusion defects caused by Ypt7-D44N (Figure 8E), confirming that the Ypt7-Vps41 interaction likely contributes to SNARE complex proofreading and protection by HOPS required for full SNARE-pin zippering (Starai et al. 2008; Lobingier et al. 2014).

Importantly, the D44N mutation in Ypt7 did not interfere with its cellular distribution or the ability to activate the Rab. In fact, the entire pool of Ypt7-D44N that co-purified with isolated organelles was GDI resistant (Figure 7C and D) and caused extensive vacuolar lysosome tethering, similar to the addition of GTPγS to organelles harboring the wild type Ypt7 (Figure 8A), suggesting that Ypt7-D44N was hyperactive, consistent with it being resistant to inactivation by GAPs (Vollmer et al., 1999). As previously reported, active Ypt7 binds Vps41 to shield it from Yck3 (Hickey et al., 2009), which otherwise phosphorylates Vps41 causing it to dissociate from membranes (Brett et al., 2008). Consistent with these reports, Ypt7-D44N causes hyper-phosphorylation of Vps41 (Figure 7G) and its dissociation from membranes during the fusion reaction (Figure 7E). Stabilizing HOPS on membranes by deleting YCK3 overcomes fusion defects caused by Ypt7-D44N and restores ILF formation (Figure 9). Thus, I conclude that phosphorylation of Vps41 by Yck3 targets pore formation to reduce ILF production (Figure 10).

Altogether, these results further refine our knowledge of how multisubunit tethering complexs like HOPS coordinate the functions of Rabs (Ypt7), protein kinases (Yck3), and SNAREs to drive membrane fusion and fine-tune ILF formation: (1) Ypt7-Vps39 and the ALPS motif within Vps41 play a direct role in membrane tethering, while Ypt7-effector interaction is exclusively needed for *trans*-SNARE complex stabilization by HOPS, and (2) phosphorylation

of HOPS by Yck3 targets and stalls pore formation, causing expansion of hemifusion diaphragms to reduce ILF production.

Several MTCs have been identified in eukaryotes and are categorized into two groups: (1) the CATCHR (complex associated with tethering containing helical rods) family of MTCs functioning in the secretory pathway like Golgi-associated retrograde protein (GARP) complex required for transport between the endosome and the trans-Golgi network, the dependence on SLY1–20 (Dsl) complex required for transport from Golgi to endoplasmic reticulum, the conserved oligomeric Golgi (COG) complex required for intra-Golgi trafficking, and the exocyst, which drives tethering of post-Golgi vesicles to the plasma membrane (Yu and Hughson, 2010), and (2) MTCs that act in the endolysosomal pathway HOPS and CORVET (Solinger and Spang, 2013). The fact that all MTCs bind small GTPases, most commonly Rabs, and interact with SNARE proteins to recognize, tether, and orchestrate SNARE mediated membrane fusion (Solinger and Spang, 2013; Kuhlee et al., 2015; Spang, 2016) suggests that MTCs function in similar ways and raises the following question. Do all multisubunit tethering complexes-mediated fusion events produce ILFs? Based on my results with HVF, I speculate that ILF formation is a conserved feature of all membrane fusion events that are driven by coordinated interactions between GTPases, MTCs, and SNARE proteins, and soon new technologies in super-resolution fluorescence microscopy (e.g., lattice light-sheet microscopy; Chen et al., 2014) will reveal the answer to this question.

4.3 Ypt7, HOPS and a non-cognate SNARE complex underlie MVB-vacuolar lysosome fusion

In Chapter 3, I developed a new cell-free content mixing assay to measure MVB-vacuole fusion kinetics. It is based on the reconstitution of β-lactamase activity from its two subunits (ω and α) that I initially targeted to the MVB and the vacuolar lysosome, respectively. Expressing the fusion probes in separate yeast strain and then mixing the isolated organelles ensured that the fusion reaction is controlled and the resulting β-lactamase activity is indicative of authentic MVB-vacuole fusion events (Figure 11A). Using this assay, I was able to confirm previous reports, mainly by the Ungermann group, suggesting that Ypt7 and its cognate tethering complex HOPS are required for both HVF and heterotypic MVB-vacuole fusion (Figure 12A and B). Consistent with it being the only α-SNAP in *S. cerevisiae*, I found that Sec17, which is required for cis-SNARE complex disassembly during the priming stage of HVF is also needed for MVB-

vacuole fusion (Figure 12B). In addition to that, I was able to dissect the *trans*-SNARE complex required to drive MVB-vacuole fusion, and found that it is composed of the endosomal SNAREs Pep12 (Qa) and Vti1 (Qb) in complex with the vacuolar R-SNARE Nyv1 and the soluble Qc-SNARE Vam7. This unique *trans*-SNARE complex is what ensures specificity between HVF (Vam3, Vti1, Vam7, and Nyv1) and MVB-vacuole fusion as the remaining machinery is shared by both fusion events (Figure 12B, D, E, F, and G).

But how could homotypic and heterotypic fusion events be balanced? Yck3 phosphorylates Vam3 when the HVF reaction is blocked (Brett et al., 2008). However, it is not yet known whether Yck3 or any other kinase phosphorylates its ortholog Pep12 on endosomes. Hence, I speculate that Vam3 phosphorylation by Yck3 could function as a switch mechanism to free the vacuolar R-SNARE Nyv1 and the Qc-SNARE Vam7 for endosomal Pep12 and Vti1 SNAREs to engage in this non-cognate complex unique to MVB-vacuolar lysosome fusion. It is noteworthy that at the site of contact between the MVB and the vacuole a flat circular boundary area similar to that observed at contact sites between docked vacuolar membranes is observed. This boundary membrane is internalized within the lumen as a byproduct of lipid bilayer merger at the vertex ring during HVF to recycle vacuolar lysosome polytopic proteins (Wang et al., 2002; Mattie et al., 2017; McNally et al., 2017). Therefore, based on the similarity in the underlying fusion machinery and the shared topological arrangement between docked vacuolar membranes and MVB-vacuole membranes, I speculate that the same mechanism also exists to recycle MVB polytopic proteins. Thus, I propose that Yck3 phosphorylates the vacuolar Qa-SNARE Vam3 to balance homotypic and heterotypic fusion events and regulate the endocytic and ILF degradation pathways important for lysosomal and MVB membrane remodeling and biogenesis.

4.4 MVB maturation triggers fusion with vacuolar lysosomes

ESCRT proteins are crucial for MVB maturation and biogenesis. In Chapter 3, I also show that deleting any of the components of the ESCRT machinery blocks MVB-vacuole fusion *in vitro* (Figure 7C). Elegant work by the Odorizzi group revealed that when ESCRT protein Vps4 was inactivated, MVBs accumulated hyperactive Vps21 and inactive Ypt7, suggesting that the Vps21 to Ypt7 Rab conversion cascade was impaired. After establishing that heterotypic fusion *in vitro* requires active Ypt7 (Figure 12B), I introduced a point mutation into Ypt7 (Q68L) to render it constitutively active (Brett et al. 2008). As expected, Ypt7-Q68L rescued MVB-

vacuolar lysosome fusion in the absence of VPS23 (a component of ESCRT-I; Figure 17C and E). Thus, my results provide direct evidence in support of the hypothesis that ESCRT-mediated MVB maturation activates Ypt7 to trigger fusion with vacuolar lysosomes.

Nhx1 is an MVB resident protein (Nass and Rao 1998). Herein, we show that Nhx1-GFP decorates the limiting membranes of vacuolar lysosomes upon MVB-vacuole fusion (Figure 15C). Nhx1 ion exchange activity is what contributes to the distinct ionic profile of MVB-vacuole fusion. It can tolerate K^+ replacement with Rb^+ and regulates luminal pH of MVBs (Figure 15F, G, H, I, and J). Deleting NHX1 impairs MVB-vacuole fusion (Figure 15D and C) and impairs the cellular distribution of the proton pump (Vph1) from the vacuole to the MVB membrane (Figure 16D), which would count for the hyper-acidification of the MVB lumen in the absence of NHX1. I also show that Nhx1 does not regulate Ypt7 activity through its interaction with Gyp6, a Rab GAP protein (Ali et al. 2004; Figure 16A, B, and C). However, addition of rVam7 rescued fusion defects observed in *nhx1Δ* (Figure 16E) suggesting that *trans*-SNARE assembly is intact and functions downstream of Nhx1 activity, hence I hypothesize that ion exchange activity after ESCRT mediated MVB maturation targets an unknown factor upstream the *trans*-SNARE complex to mediate MVB-vacuole membrane fusion (Figure 18).

Although both ESCRTs and Nhx1 functions are required for MVB biogenesis and fusion with the vacuolar lysosome, the mechanisms by which they contribute to MVB-vacuolar lysosome fusion are different. Nhx1 ion exchange activity seems to target *trans*-SNARE complexes, whereas ESCRTs appear to be required for Ypt7 activation. But what is the link between ESCRT function and Ypt7 activation? When ESCRTs function is impaired, ubiquitylated cargoes destined for degradation at the vacuolar lysosome accumulate at the limiting membrane of the late endosome and cannot be sorted into ILVs (Rieder et al., 1996; Russell et al., 2012). I speculate that this defect in membrane remodeling, causes an increase in surface tension at the endosome membrane, and in response, endosomes tend to flatten their membranes to diffuse this tension by forming aberrant stacks of flattened cisternae, which could interfere with Mon1-Ccz1 (Ypt7-GEF) recruitment to membranes and ultimately disrupts Ypt7 activation. Unlike Mon1-Ccz1, Vps9 (Vps21-GEF) possess a CUE domain capable of recognizing ubiquitylated cargos at the endosome (Prag et al., 2003; Shideler et al., 2015), hence Vps9 is enriched at these aberrant structures in response to ESCRT dysfunction causing Vps21 to become hyperactive (see Russell et al., 2012). This is consistent with the proposed Rab

conversion cascade theory, which states that activation of a Rab recruits the GAP for the proceeding Rab. Mon1-Ccz1 is not recruited to the membranes upon ESCRT dysfunction, and hence it cannot recruit Msb3 (Vps21-cognate GAP) to inactivate Vps21 (Rana et al., 2015).

4.5 Future directions

4.5.1 Yck3 activation coordinates completion of Rab cycle

My working model of HVF shown in Figure 10 of Chapter 2, suggests that Yck3 activation might occur after *trans*-SNARE pairing whereby it phosphorylates Mon1 (a component of the Ypt7 GEF complex) causing it to dissociate from organelle membranes (Lawrence et al., 2014). Thus, I speculate that Yck3 activation may promote Ypt7 inactivation by its cognate GAP protein (Gyp7; Brett et al., 2008), which together with Vam3-phosphorylation, may release SNAREs from HOPS and synchronize disassembly of the fusion machinery (Alpadi et al., 2012). To test this hypothesis, we could conduct a Rab-extraction assay using Gdi1 to assess the proportion of active Ypt7 protein present on organelles isolated from WT or *yck3Δ* cells (Eitzen et al., 2000; Brett et al., 2008; Figures 7C and 16A). In a similar approach, we could also incubate isolated organelles with or without purified recombinant Yck3 in the presence or absence of ATP and then subject them to extraction by rGdi1. As a positive control, we can pretreat isolated organelles with GTPγS to prevent activation and extraction of Ypt7 by rGdi1. If my hypothesis is correct, I predict that more Ypt7 will be extracted in reactions incubated with rYck3 in an ATP-dependent manner.

4.5.2 Autophagosome-lysosome fusion

The second major pathway that delivers biomaterials to lysosomes via a heterotypic fusion event is the autophagic pathway. Although crucial for cell survival, the molecular mechanism regulating the fusion of autophagosomes with lysosomes has not been fully established. However, like HVF and MVB-lysosome fusion, autophagosome-lysosome fusion requires the NSF ortholog Sec18 (Ishihara et al., 2001), the Rab-GTPase Ypt7 (Kirisako et al., 1999), the HOPS complex (Liang et al., 2008; Rieder and Emr, 1997), and SNARE proteins (Jiang et al., 2014). However, most of these studies were based on fluorescence co-localization techniques and Western blot analysis (Darsow et al., 1997; Jiang et al., 2014; Diao et al., 2015), which do not permit the dissection of the fusion subreactions with molecular precision. Recognizing the

impact of cell-free fusion assays on our understanding of homotypic vacuolar lysosome and heterotypic MVB-vacuolar lysosome fusion, it is very appealing to fuse the ω-subunit of β-lactamase followed by the proto oncogene c-Fos to the C-terminus of the autophagosome marker protein Atg8 (LC3 ortholog) to target this fusion probe to the autophagosome lumen, then isolate these compartments by a flotation gradient that does not damage organelles (e.g. opti-prep) and mix them with vacuolar lysosomes carrying the complementary fusion probe CPY50-Jun-α (see Figure 11A) in a buffer that permits fusion to quantify this heterotypic fusion event. Based on my results in Chapter 3, I predict that a unique *trans*-SNARE complex would confer specificity to this fusion event as Ypt7 and HOPS are shared with HVF and MVB-vacuole fusion.

4.5.3 Nhx1 targets *trans*-SNARE complex assembly

How does NHX1 work? In my targeted screen to identify components of the fusion machinery that show altered cellular distribution upon NHX1 deletion, I made two important observations: (1) None of the GFP-tagged fusion machinery proteins (e.g., Ypt7, HOPS, SNAREs) showed noticeable change in their cellular distribution in WT versus NHX1 knockout cells, and (2) Vac1 and Vps45 which are exclusively found on the MVB (Peterson et al. 1999) were diffused in the cytoplasm upon NHX1 deletion (data not shown). Vac1 contains a FYVE zinc finger domain that binds [PI(3)P], critical for its association with the MVB membrane (Tall et al. 1999). It also has been shown that lowering the pH enhances the interaction of the EEA1 complex and Vps27, both containing similar FYVE domains, with [PI(3)P]-containing membranes *in vitro* and *in vivo*, while increasing the pH impedes their affinity to [PI(3)P], indicating that pH-dependency is a general function of the FYVE finger family (He et al. 2009; Kutateladze 2006).

Thus, I propose that deleting NHX1 abolishes the capacity of the MVB to counterbalance the V-ATPase (Vph1) activity, resulting in an accumulation of protons in the MVB lumen (see Figures 15H and 16D). As a consequence, the MVB lumen will become hyper-acidic and that the local environment surrounding the MVB becomes alkaline, disrupting Vac1 association with the MVB membrane. Vac1 binds Vps45, which is an SM protein orthologous to Vps33 (Hashizume et al. 2009; Koumandou et al. 2007), that mediates the interaction between endosomal Qa-SNARE Pep12 on the MVB and Qb-SNARE Vti1 on Golgi-derived vesicles to drive membrane trafficking to the MVB (Tall et al. 1999). Because Vps33 physically interacts with Pep12, and

both are required for MVB-vacuole fusion (Figure 12B; Subramanian 2004; Lobingier and Merz 2012), it would be very interesting to assay for a direct interaction between Vac1 and Vps33 and determine whether Vac1 is required for Vps33 mediated *trans*-SNARE complex templating of endosomal Pep12 with vacuolar Nyv1 necessary for MVB-vacuole fusion. I predict that *trans*-SNARE pairing between endosomal Pep12 and vacuolar Nyv1 to be defective such that Vac1 cannot bind Pep12 in the absence of NHX1.

If our prediction appears to be true, then Vac1 could be the unknown factor that functions downstream of Nhx1 ion exchange activity to orchestrate *trans*-SNARE complex assembly between the MVB and the vacuolar lysosome similar to its function in orchestrating *trans*-SNARE assembly between Golgi-derived vesicles and the MVB (Peterson et al., 1999). Therefore, pretreating isolated organelles from NHX1 knockout with the weak base chloroquine, which accumulates in the MVB lumen and rescues MVB-vacuole content mixing in the absence of NHX1 (Figure 15I) also would recover the Vac1-Pep12 interaction and *trans*-SNARE complex assembly required for MVB-vacuole lipid bilayer merger. This strategy could be used for the treatment of patients with loss-of-function mutations in NHE6 and NHE9; as such a treatment could rescue endocytosis defects causing impaired degradation of neurotransmitter receptors at the synapse of neuron cells, underlying Autism Spectrum Disorders (ASDs).

References

Ali, R., C.L. Brett, S. Mukherjee, and R. Rao. 2004. **Inhibition of Sodium/Proton Exchange by a Rab-GTPase-activating Protein Regulates Endosomal Traffic in Yeast**. *J. Biol. Chem.* 279:4498–4506.

Alpadi, K., A. Kulkarni, V. Comte, M. Reinhardt, A. Schmidt, S. Namjoshi, A. Mayer, and C. Peters. 2012. **Sequential analysis of *trans*-SNARE formation in intracellular membrane fusion**. *PLoS Biol.* 10.

Angers, C.G., and A.J. Merz. 2009. **HOPS interacts with Apl5 at the vacuole membrane and is required for consumption of AP-3 transport vesicles**. *Mol. Biol. Cell*. 20:4563–4574.

Arlt, H., K. Auffarth, R. Kurre, D. Lisse, J. Piehler, and C. Ungermann. 2015. **Spatiotemporal dynamics of membrane remodeling and fusion proteins during endocytic transport**. *Mol. Biol. Cell*. 26:1357–70.

Baker, R.W., P.D. Jeffrey, M. Zick, B.P. Phillips, W.T. Wickner, and F.M. Hughson. 2015. **A direct role for the Sec1/Munc18-family protein Vps33 as a template for SNARE assembly**. *Science (80-.).* 349:1111–1114.

Balch, W.E., B.S. Glick, and J.E. Rothman. 1984. **Sequential intermediates in the pathway of intercompartmental transport in a cell-free system**. *Cell*. 39:525–536.

Balderhaar, H.J. kleine, and C. Ungermann. 2013. **CORVET and HOPS tethering complexes - coordinators of endosome and lysosome fusion**. *J. Cell Sci.* 126:1307–16.

Balderhaar, H.J.K., H. Arlt, C. Ostrowicz, C. Bröcker, F. Sündermann, R. Brandt, M. Babst, and C. Ungermann. 2010. **The Rab GTPase Ypt7 is linked to retromer-mediated receptor recycling and fusion at the yeast late endosome**. *J. Cell Sci.* 123:4085–4094.

Balderhaar, H.J.K., J. Lachmann, E. Yavavli, C. Bröcker, A. Lürick, and C. Ungermann. 2013. **The CORVET complex promotes tethering and fusion of Rab5/Vps21-positive membranes**. *Proc. Natl. Acad. Sci. U. S. A.* 110:3823–8.

Barr, F., and D.G. Lambright. 2010. **Rab GEFs and GAPs**. *Curr. Opin. Cell Biol.* 22:461–470.

Becherer, K.A., S.E. Rieder, S.D. Emr, and E.W. Jones. 1996. **Novel syntaxin homologue, Pep12p, required for the sorting of lumenal hydrolases to the lysosome-like vacuole in yeast.** *Mol. Biol. Cell*. 7:579–94.

Boeddinghaus, C., A.J. Merz, R. Laage, and C. Ungermann. 2002. **A cycle of Vam7p release from and PtdIns 3-P-dependent rebinding to the yeast vacuole is required for homotypic vacuole fusion**. *J. Cell Biol.* 157:79–89.

Bourne, H.R., D.A. Sanders, and F. McCormick. 1991. **The GTPase superfamily: conserved structure and molecular mechanism**. *Nature*. 349:117–127.

Bowers, K., B.P. Levi, F.I. Patel, and T.H. Stevens. 2000. **The sodium/proton exchanger Nhx1p is required for endosomal protein trafficking in the yeast *Saccharomyces cerevisiae***. *Mol. Biol. Cell*. 11:4277–4294.

Boysen, J.H., and A.P. Mitchell. 2006. **Control of Bro1-domain protein Rim20 localization by external pH, ESCRT machinery, and the *Saccharomyces cerevisiae* Rim101 pathway**. *Mol. Biol. Cell*. 17:1344–1353.

Brett, C.L., and A.J. Merz. 2008. **Osmotic Regulation of Rab-Mediated Organelle Docking**. *Curr. Biol.* 18:1072–1077.

Brett, C.L., R.L. Plemel, B.T. Lobinger, M. Vignali, S. Fields, and A.J. Merz. 2008. **Efficient termination of vacuolar Rab GTPase signaling requires coordinated action by a GAP and a protein kinase**. *J. Cell Biol.* 182:1141–1151.

Brett, C.L., D.N. Tukaye, S. Mukherjee, and R. Rao. 2005. **The yeast endosomal Na^+K^+/H^+ exchanger Nhx1 regulates cellular pH to control vesicle trafficking**. *Mol. Biol. Cell*. 16:1396–1405.

Bröcker, C., S. Engelbrecht-Vandré, and C. Ungermann. 2010. **Multisubunit tethering complexes and their role in membrane fusion**. *Curr. Biol.* 20.

Bröcker, C., A. Kuhlee, C. Gatsogiannis, H.J. kleine Balderhaar, C. Hönscher, S. Engelbrecht-Vandré, C. Ungermann, and S. Raunser. 2012. **Molecular architecture of the multisubunit homotypic fusion and vacuole protein sorting (HOPS) tethering complex**. *Proc. Natl. Acad. Sci. U. S. A.* 109:1991–6.

Bugnicourt, A., M. Froissard, K. Sereti, H.D. Ulrich, R. Haguenauer-Tsapis, and J.-M. Galan. 2004. **Antagonistic roles of ESCRT and Vps class C/HOPS complexes in the recycling of yeast membrane proteins**. *Mol. Biol. Cell*. 15:4203–14.

Cabrera, M., L. Langemeyer, M. Mari, R. Rethmeier, I. Orban, A. Perz, C. Bröcker, J. Griffith, D. Klose, H.J. Steinhoff, F. Reggiori, S. Engelbrecht-Vandré, and C. Ungermann. 2010. **Phosphorylation of a membrane curvature-sensing motif switches function of the HOPS subunit Vps41 in membrane tethering**. *J. Cell Biol.* 191:845–859.

Cabrera, M., M. Nordmann, A. Perz, D. Schmedt, A. Gerondopoulos, F. Barr, J. Piehler, S. Engelbrecht-Vandré, and C. Ungermann. 2014. **The Mon1-Ccz1 GEF activates the Rab7 GTPase Ypt7 via a longin-fold-Rab interface and association with PI3P-positive membranes**. *J. Cell Sci.* 127:1043–1051.

Cabrera, M., C.W. Ostrowicz, M. Mari, T.J. LaGrassa, F. Reggiori, and C. Ungermann. 2009. **Vps41 Phosphorylation and the Rab Ypt7 Control the Targeting of the HOPS Complex to Endosome-Vacuole Fusion Sites**. *Mol. Biol. Cell*. 20:1937–1948.

Cabrera, M., and C. Ungermann. 2013. **Guanine nucleotide exchange factors (GEFs) have a**

critical but not exclusive role in organelle localization of rab GTPases. *J. Biol. Chem.* 288:28704–28712.

Cang, C., K. Aranda, Y.J. Seo, B. Gasnier, and D. Ren. 2015. T**MEM175 Is an Organelle K^+ Channel Regulating Lysosomal Function**. *Cell*. 162:1101–1112.

Cao, Q., X.Z. Zhong, Y. Zou, R. Murrell-Lagnado, M.X. Zhu, and X.-P. Dong. 2015. **Calcium release through P2X4 activates calmodulin to promote endolysosomal membrane fusion**. *J. Cell Biol.* 209:879–894.

Cheever, M.L., T.K. Sato, T. de Beer, T.G. Kutateladze, S.D. Emr, and M. Overduin. 2001. **Phox domain interaction with PtdIns(3)P targets the Vam7 t-SNARE to vacuole membranes**. *Nat. Cell Biol.* 3:613–618.

Chen, B.-C., W.R. Legant, K. Wang, L. Shao, D.E. Milkie, M.W. Davidson, C. Janetopoulos, X.S. Wu, J.A. Hammer, Z. Liu, B.P. English, Y. Mimori-Kiyosue, D.P. Romero, A.T. Ritter, J. Lippincott-Schwartz, L. Fritz-Laylin, R.D. Mullins, D.M. Mitchell, J.N. Bembenek, A.-C. Reymann, R. Bohme, S.W. Grill, J.T. Wang, G. Seydoux, U.S. Tulu, D.P. Kiehart, and E. Betzig. 2014. **Lattice light-sheet microscopy: Imaging molecules to embryos at high spatiotemporal resolution**. *Science (80).* 346:1257998–1257998.

Clary, D.O., I.C. Griff, and J.E. Rothman. 1990. **SNAPs, a family of NSF attachment proteins involved in intracellular membrane fusion in animals and yeast**. *Cell*. 61:709–721.

Collins, K.M., and W.T. Wickner. 2007. ***Trans*-SNARE complex assembly and yeast vacuole membrane fusion**. *Proc. Natl. Acad. Sci. U. S. A.* 104:8755–8760.

Conradt, B., A. Haas, and W. Wickner. 1994. **Determination of four biochemically distinct, sequential stages during vacuole inheritance *in vitro***. *J. Cell Biol.* 126:99–110.

Conradt, B., J. Shaw, T. Vida, S. Emr, and W. Wickner. 1992. ***In vitro* reactions of vacuole**

inheritance in *Saccharomyces cerevisiae*. *J. Cell Biol.* 119:1469–1479.

Coonrod, E.M., L.A. Graham, L.N. Carpp, T.M. Carr, L. Stirrat, K. Bowers, N.J. Bryant, and T.H. Stevens. 2013. **Homotypic Vacuole Fusion in Yeast Requires Organelle Acidification and Not the V-ATPase Membrane Domain**. *Dev. Cell*. 27:462–468.

Coonrod, E.M., and T.H. Stevens. 2010. **The Yeast vps Class E Mutants: The Beginning of the Molecular Genetic Analysis of Multivesicular Body Biogenesis**. *Mol. Biol. Cell*. 21:4042–4056.

D'Agostino, M., H.J. Risselada, and A. Mayer. 2016. **Steric hindrance of SNARE transmembrane domain organization impairs the hemifusion-to-fusion transition**. *EMBO Rep.* 364:1048–1060.

Darsow, T., S.E. Rieder, and S.D. Emr. 1997. **A multispecificity syntaxin homologue, Vam3p, essential for autophagic and biosynthetic protein transport to the vacuole**. *J. Cell Biol.* 138:517–529.

Davenport, N.R., K.J. Sonnemann, K.W. Eliceiri, and W.M. Bement. 2016. **Membrane dynamics during cellular wound repair**. *Mol. Biol. Cell*. 1–10.

Denis, V., and M.S. Cyert. 2002. **Internal Ca^{2+} release in yeast is triggered by hypertonic shock and mediated by a TRP channel homologue**. *J. Cell Biol.* 156:29–34.

Desfougères, Y., S. Vavassori, M. Rompf, R. Gerasimaite, and A. Mayer. 2016. **Organelle acidification negatively regulates vacuole membrane fusion *in vivo***. *Sci. Rep.* 6:29045.

Diao, J., R. Liu, Y. Rong, M. Zhao, J. Zhang, Y. Lai, Q. Zhou, L.M. Wilz, J. Li, S. Vivona, R.A. Pfuetzner, A.T. Brunger, and Q. Zhong. 2015. **ATG14 promotes membrane tethering and fusion of autophagosomes to endolysosomes**. *Nature*. 520:563–566.

Dubuke, M.L., and M. Munson. 2016. **The Secret Life of Tethers: The Role of Tethering Factors in SNARE Complex Regulation**. *Front. cell Dev. Biol.* 4:42.

de Duve, C. 2005. **The lysosome turns fifty**. *Nat. Cell Biol.* 7:847–9.

Edgar, J.R., E.R. Eden, and C.E. Futter. 2014. **Hrs- and CD63-Dependent Competing Mechanisms Make Different Sized Endosomal Intraluminal Vesicles**. *Traffic*. 15:197–211.

Eitzen, G., E. Will, D. Gallwitz, A. Haas, and W. Wickner. 2000. **Sequential action of two GTPases to promote vacuole docking and fusion**. *EMBO J.* 19:6713–6720.

Epp, N., R. Rethmeier, L. Krämer, and C. Ungermann. 2011. **Membrane dynamics and fusion at late endosomes and vacuoles - Rab regulation, multisubunit tethering complexes and SNAREs**. *Eur. J. Cell Biol.* 90:779–785.

Eskelinen, E.-L., and P. Saftig. 2009. **Autophagy: a lysosomal degradation pathway with a central role in health and disease**. *Biochim. Biophys. Acta*. 1793:664–73.

Fasshauer, D., R.B. Sutton, A.T. Brunger, and R. Jahn. 1998. **Conserved structural features of the synaptic fusion complex: SNARE proteins reclassified as Q- and R-SNAREs**. *Proc. Natl. Acad. Sci. U. S. A.* 95:15781–6.

Franke, B., B.M. Neale, and S. V. Faraone. 2009. **Genome-wide association studies in ADHD**. *Hum. Genet.* 126:13–50.

Fratti, R.A., Y. Jun, A.J. Merz, N. Margolis, W. Wickner, and B. Wickner. 2004. **Interdependent assembly of specific regulatory lipids and membrane fusion proteins into the vertex ring domain of docked vacuoles**. *J. Cell Biol.* 167:1087–1098.

Friend, D.S. 1969. **Cytochemical staining of multivesicular body and golgi vesicles**. *J. Cell*

Biol. 41:269–279.

Furukawa, N., and J. Mima. 2014. **Multiple and distinct strategies of yeast SNAREs to confer the specificity of membrane fusion**. *Sci. Rep.* 4:4277.

Garrett, M.D., J.E. Zahner, C.M. Cheney, and P.J. Novick. 1994. **GDI1 encodes a GDP dissociation inhibitor that plays an essential role in the yeast secretory pathway**. *EMBO J.* 13:1718–28.

Gilfillan, G.D., K.K. Selmer, I. Roxrud, R. Smith, M. Kyllerman, K. Eiklid, M. Kroken, M. Mattingsdal, T. Egeland, H. Stenmark, H. Sjuholm, A. Server, L. Samuelsson, A. Christianson, P. Tarpey, A. Whibley, M.R. Stratton, P.A. Futreal, J. Teague, S. Edkins, J. Gecz, G. Turner, F.L. Raymond, C. Schwartz, R.E. Stevenson, D.E. Undlien, and P. Stromme. 2008. **SLC9A6 Mutations Cause X-Linked Mental Retardation, Microcephaly, Epilepsy, and Ataxia, a Phenotype Mimicking Angelman Syndrome**. *Am. J. Hum. Genet.* 82:1003–1010.

Goody, R.S., A. Rak, and K. Alexandrov. 2005. **The structural and mechanistic basis for recycling of Rab proteins between membrane compartments**. *Cell. Mol. Life Sci.* 62:1657–1670.

Gossing, M., S. Chidambaram, and G. Fischer von Mollard. 2013. **Importance of the N-Terminal Domain of the Qb-SNARE Vti1p for Different Membrane Transport Steps in the Yeast Endosomal System**. *PLoS One*. 8.

Götte, M., and D. Gallwitz. 1997. **High expression of the yeast syntaxin-related Vam3 protein suppresses the protein transport defects of a pep12 null mutant**. *FEBS Lett.* 411:48–52.

Griff, I.C., R. Schekman, J.E. Rothman, and C.A. Kaiser. 1992. **The yeast SEC17 gene product is functionally equivalent to mammalian α-SNAP protein**. *J. Biol. Chem.* 267:12106–

12115.

Grosshans, B.L., D. Ortiz, and P. Novick. 2006. **Rabs and their effectors: achieving specificity in membrane traffic**. *Proc. Natl. Acad. Sci. U. S. A.* 103:11821–7.

Haas, A. 1995. **A quantitative assay to measure homotypic vacuole fusion *in vitro***. *Methods Cell Sci.* 17:283–294.

Henderson, K.A., A.L. Hughes, and D.E. Gottschling. 2014. **Mother-daughter asymmetry of pH underlies aging and rejuvenation in yeast**. *Elife*. 3:e03504.

Henne, W.M., N.J. Buchkovich, and S.D. Emr. 2011. **The ESCRT Pathway**. *Dev. Cell*. 21:77–91.

Heuser, J. 1989. **Changes in lysosome shape and distribution correlated with changes in cytoplasmic pH**. *J. Cell Biol.* 108:855–864.

Hickey, C.M., C. Stroupe, and W. Wickner. 2009. **The major role of the Rab Ypt7p in vacuole fusion is supporting HOPS membrane association**. *J. Biol. Chem.* 284:16118–16125.

Hickey, C.M., and W. Wickner. 2010. **HOPS initiates vacuole docking by tethering membranes before *trans*-SNARE complex assembly**. *Mol. Biol. Cell*. 21:2297–2305.

Ho, R., and C. Stroupe. 2015. **The HOPS/class C Vps complex tethers membranes by binding to one Rab GTPase in each apposed membrane**. *Mol. Biol. Cell*. 26:2655–63.

Ho, R., and C. Stroupe. 2016. **The HOPS/Class C Vps Complex Tethers High-Curvature Membranes via a Direct Protein Membrane Interaction**. *Traffic*. 17:1078–1090.

Hofmann, M.W., K. Peplowska, J. Rohde, B.C. Poschner, C. Ungermann, and D. Langosch. 2006. **Self-interaction of a SNARE Transmembrane Domain Promotes the**

Hemifusion-to-fusion Transition. *J. Mol. Biol.* 364:1048–1060.

Hönscher, C., M. Mari, K. Auffarth, M. Bohnert, J. Griffith, W. Geerts, M. van der Laan, M. Cabrera, F. Reggiori, and C. Ungermann. 2014. **Cellular metabolism regulates contact sites between vacuoles and mitochondria**. *Dev. Cell*. 30:86–94.

Huber, L.A., and D. Teis. 2016. **Lysosomal signaling in control of degradation pathways**. *Curr. Opin. Cell Biol.* 39:8–14.

Huotari, J., and A. Helenius. 2011. **Endosome maturation**. *EMBO J.* 30:3481–3500.

Hutagalung, A.H., and P.J. Novick. 2011. **Role of Rab GTPases in membrane traffic and cell physiology**. *Physiol. Rev.* 91:119–49.

Ishihara, N., M. Hamasaki, S. Yokota, K. Suzuki, Y. Kamada, A. Kihara, T. Yoshimori, T. Noda, and Y. Ohsumi. 2001. **Autophagosome requires specific early Sec proteins for its formation and NSF/SNARE for vacuolar fusion**. *Mol. Biol. Cell*. 12:3690–702.

Izawa, R., T. Onoue, N. Furukawa, and J. Mima. 2012. **Distinct contributions of vacuolar Qabc- and R-SNARE proteins to membrane fusion specificity**. *J. Biol. Chem.* 287:3445–3453.

Jiang, P., T. Nishimura, Y. Sakamaki, E. Itakura, T. Hatta, T. Natsume, and N. Mizushima. 2014. **The HOPS complex mediates autophagosome-lysosome fusion through interaction with syntaxin 17**. *Mol. Biol. Cell*. 25:1327–1337.

Jun, Y., and W. Wickner. 2007. **Assays of vacuole fusion resolve the stages of docking, lipid mixing, and content mixing**. *Proc. Natl. Acad. Sci. U. S. A.* 104:13010–13015.

Jun, Y., H. Xu, N. Thorngren, and W. Wickner. 2007. **Sec18p and Vam7p remodel *trans*-**

SNARE complexes to permit a lipid-anchored R-SNARE to support yeast vacuole fusion. *EMBO J.* 26:4935–4945.

Kallay, L.M., C.L. Brett, D.N. Tukaye, M.A. Wemmer, A. Chyou, G. Odorizzi, and R. Rao. 2011. **Endosomal $Na^+(K^+)/H^+$ exchanger Nhx1/Vps44 functions independently and downstream of multivesicular body formation**. *J. Biol. Chem.* 286:44067–44077.

Kato, M., and W. Wickner. 2001. **Ergosterol is required for the Sec18/ATP-dependent priming step of homotypic vacuole fusion**. *EMBO J.* 20:4035–4040.

Katzmann, D.J., M. Babst, and S.D. Emr. 2001. **Ubiquitin-dependent sorting into the multivesicular body pathway requires the function of a conserved endosomal protein sorting complex, ESCRT-I**. *Cell*. 106:145–155.

Kawasaki-Nishi, S., T. Nishi, and M. Forgac. 2001. **Yeast V-ATPase Complexes Containing Different Isoforms of the 100-kDa a-subunit Differ in Coupling Efficiency and *in vivo* Dissociation**. *J. Biol. Chem.* 276:17941–17948.

Kirisako, T., M. Baba, N. Ishihara, K. Miyazawa, M. Ohsumi, T. Yoshimori, T. Noda, and Y. Ohsumi. 1999. **Formation process of autophagosome is traced with Apg8/Aut7p in yeast**. *J. Cell Biol.* 147:435–446.

Klionsky, D.J., P.K. Herman, and S.D. Emr. 1990. **The fungal vacuole: composition, function, and biogenesis**. *Microbiol. Rev.* 54:266–292.

Klionsky, D.J., and Y. Ohsumi. 1999. **Vacuolar import of proteins and organelles from the cytoplasm**. *Annu. Rev. Cell Dev. Biol.* 15:1–32.

Klumperman, J., and G. Raposo. 2014. **The complex ultrastructure of the endolysosomal system**. *Cold Spring Harb. Perspect. Biol.* 6.

Knippschild, U., A. Gocht, S. Wolff, N. Huber, J. Löhler, and M. Stöter. 2005. **The casein kinase 1 family: Participation in multiple cellular processes in eukaryotes**. *Cell. Signal.* 17:675–689.

Kojima, A., J.Y. Toshima, C. Kanno, C. Kawata, and J. Toshima. 2012. **Localization and functional requirement of yeast Na^+/H^+ exchanger, Nhx1p, in the endocytic and protein recycling pathway**. *Biochim. Biophys. Acta - Mol. Cell Res.* 1823:534–543.

Kondapalli, K.C., J.P. Llongueras, V. Capilla-Gonzalez, H. Prasad, A. Hack, C. Smith, H. Guerrero-Cazares, A. Quinones-Hinojosa, and R. Rao. 2015. **A leak pathway for luminal protons in endosomes drives oncogenic signalling in glioblastoma**. *Nat Commun*. 6:6289.

Krishnakumar, S.S., D.T. Radoff, D. Kümmel, C.G. Giraudo, F. Li, L. Khandan, S.W. Baguley, J. Coleman, K.M. Reinisch, F. Pincet, and J.E. Rothman. 2011. **A conformational switch in complexin is required for synaptotagmin to trigger synaptic fusion**. *Nat. Struct. Mol. Biol.* 18:934–940.

Kucharczyk, R., a M. Kierzek, P.P. Slonimski, and J. Rytka. 2001. **The Ccz1 protein interacts with Ypt7 GTPase during fusion of multiple transport intermediates with the vacuole in S. cerevisiae**. *J. Cell Sci.* 114:3137–3145.

Kuhlee, A., S. Raunser, and C. Ungermann. 2015. **Functional homologies in vesicle tethering**. *FEBS Lett.* 589:2487–2497.

Kümmel, D., and C. Ungermann. 2014. **Principles of membrane tethering and fusion in endosome and lysosome biogenesis**. *Curr. Opin. Cell Biol.* 29:61–66.

Kweon, Y., A. Rothe, E. Conibear, and T.H. Stevens. 2003. **Ykt6p is a multifunctional yeast R-SNARE that is required for multiple membrane transport pathways to the vacuole**. *Mol. Biol. Cell*. 14:1868–81.

Lurick, A., A. Kuhlee, C. Brocker, D. Kummel, S. Raunser, and C. Ungermann. 2015. **The Habc domain of the SNARE Vam3 interacts with the HOPS tethering complex to facilitate vacuole fusion**. *J. Biol. Chem.* 290:5405–5413.

Lachmann, J., F.A. Barr, and C. Ungermann. 2012. **The Msb3/Gyp3 GAP controls the activity of the Rab GTPases Vps21 and Ypt7 at endosomes and vacuoles**. *Mol. Biol. Cell*. 23:2516–26.

Lachmann, J., C. Ungermann, and S. Engelbrecht-Vandré. 2011. **Rab GTPases and tethering in the yeast endocytic pathway**. *Small GTPases*. 2:182–186.

LaGrassa, T.J., and C. Ungermann. 2005. **The vacuolar kinase Yck3 maintains organelle fragmentation by regulating the HOPS tethering complex**. *J. Cell Biol.* 168:401–414.

Lawrence, G., C.C. Brown, B.A. Flood, S. Karunakaran, M. Cabrera, M. Nordmann, C. Ungermann, and R.A. Fratti. 2014. **Dynamic association of the PI3P-interacting Mon1-Ccz1 GEF with vacuoles is controlled through its phosphorylation by the type 1 casein kinase Yck3**. *Mol. Biol. Cell*. 25:1608–19.

Liang, C., J. Lee, K. Inn, M.U. Gack, Q. Li, E.A. Roberts, I. Vergne, V. Deretic, P. Feng, C. Akazawa, and J.U. Jung. 2008. **Beclin1-binding UVRAG targets the class C Vps complex to coordinate autophagosome maturation and endocytic trafficking**. *Nat. Cell Biol.* 10:776–87.

Li, S.C., and P.M. Kane. 2009. **The yeast lysosome-like vacuole: Endpoint and crossroads**. *Biochim. Biophys. Acta - Mol. Cell Res.* 1793:650–663.

.

Liu, T.-T., T.S. Gomez, B.K. Sackey, D.D. Billadeau, and C.G. Burd. 2012a. **Rab GTPase regulation of retromer-mediated cargo export during endosome maturation**. *Mol. Biol. Cell*. 23:2505–2515.

Liu, T.-T.T., T.S. Gomez, B.K. Sackey, D.D. Billadeau, and C.G. Burd. 2012b. **Rab-GTPase**

regulation of retromer-mediated cargo export during endosome maturation. *Mol. Biol. Cell*. 23:2505–2515.

Lobingier, B.T., and A.J. Merz. 2012. **Sec1/Munc18 protein Vps33 binds to SNARE domains and the quaternary SNARE complex**. *Mol. Biol. Cell*. 23:4611–22.

Lobingier, B.T., D.P. Nickerson, S.Y. Lo, and A.J. Merz. 2014. **SM proteins Sly1 and Vps33 co-assemble with Sec17 and SNARE complexes to oppose SNARE disassembly by Sec18**. *Elife*. 2014:1–3.

Lürick, A., J. Gao, A. Kuhlee, E. Yavavli, L. Langemeyer, A. Perz, S. Raunser, and C. Ungermann. 2016. **Multivalent Rab interactions determine tether-mediated membrane fusion**. *Mol. Biol. Cell*. 11.

Luzio, J.P., S.R. Gray, and N. a Bright. 2010. **Endosome-lysosome fusion**. *Biochem. Soc. Trans.* 38:1413–1416.

Luzio, J.P., Y. Hackmann, N.M.G. Dieckmann, and G.M. Griffiths. 2014. **The biogenesis of lysosomes and lysosome-related organelles**. *Cold Spring Harb. Perspect. Biol.* 6.

Luzio, J.P., V. Poupon, M.R. Lindsay, B.M. Mullock, R.C. Piper, and P.R. Pryor. 2003. **Membrane dynamics and the biogenesis of lysosomes**. *Mol Membr Biol*. 20:141–154.

Marcusson, E.G., B.F. Horazdovsky, J.L. Cereghino, E. Gharakhanian, and S.D. Emr. 1994. **The sorting receptor for yeast vacuolar carboxypeptidase Y is encoded by the VPS10 gene**. *Cell*. 77:579–586.

Markgraf, D.F., F. Ahnert, H. Arlt, M. Mari, K. Peplowska, N. Epp, J. Griffith, F. Reggiori, and C. Ungermann. 2009. **The CORVET subunit Vps8 cooperates with the Rab5 homolog Vps21 to induce clustering of late endosomal compartments**. *Mol. Biol. Cell*. 20:5276–5289.

Mattie, S., E.K. McNally, M.A. Karim, H. Vali, and C.L. Brett. 2017. **How and why intralumenal membrane fragments form during vacuolar lysosome fusion**. *Mol. Biol. Cell*. 28:309–321.

Mayer, A., and W. Wickner. 1997. **Docking of yeast vacuoles is catalyzed by the ras-like GTPase Ypt7p after symmetric priming by Sec18p (NSF)**. *J. Cell Biol.* 136:307–317.

Mayer, A., W. Wickner, and A. Haas. 1996. **Sec18p (NSF)-driven release of Sec17p (α-SNAP) can precede docking and fusion of yeast vacuoles**. *Cell*. 85:83–94.

McNally, E.K., M.A. Karim, and C.L. Brett. 2017. **Selective Lysosomal Transporter Degradation by Organelle Membrane Fusion**. *Dev. Cell*. 40:151–167.

Merz, A.J., and W.T. Wickner. 2004. ***Trans*-SNARE interactions elicit Ca^{2+} efflux from the yeast vacuole lumen**. *J. Cell Biol.* 164:195–206.

Metcalf, D., and A.M. Isaacs. 2010. **The role of ESCRT proteins in fusion events involving lysosomes, endosomes and autophagosomes**. *Biochem. Soc. Trans.* 38:1469–1473.

Mima, J., C. Hickey, H. Xu, Y. Jun, and W. Wickner. 2008. **Reconstituted membrane fusion requires regulatory lipids, SNAREs and synergistic SNARE chaperones**. *EMBO J.* 27:2031–2042.

Von Mollard, G.F., S.F. Nothwehr, and T.H. Stevens. 1997. **The yeast V-SNARE Vti1p mediates two vesicle transport pathways through interactions with the t-SNAREs Sed5p and Pep12p**. *J. Cell Biol.*

Morrow, E.M., S.-Y. Yoo, S.W. Flavell, T.-K. Kim, Y. Lin, R.S. Hill, N.M. Mukaddes, S. Balkhy, G. Gascon, A. Hashmi, S. Al-Saad, J. Ware, R.M. Joseph, R. Greenblatt, D. Gleason, J.A. Ertelt, K.A. Apse, A. Bodell, J.N. Partlow, B. Barry, H. Yao, K. Markianos,

R.J. Ferland, M.E. Greenberg, and C.A. Walsh. 2008. **Identifying autism loci and genes by tracing recent shared ancestry**. *Science*. 321:218–23.

Nass, R., and R. Rao. 1998. **Novel localization of a Na^+/H^+ exchanger in a late endosomal compartment of yeast: Implications for vacuole biogenesis**. *J. Biol. Chem.* 273:21054–21060.

Nass, R., and R. Rao. 1999. **The yeast endosomal $Na^{+/}H^+$ exchanger, Nhx1, confers osmotolerance following acute hypertonic shock**. *Microbiology*. 145:3221–3228.

Nichols, B.J., C. Ungermann, H.R. Pelham, W.T. Wickner, and A. Haas. 1997. **Homotypic vacuolar fusion mediated by t- and v-SNAREs**. *Nature*. 387:199–202.

Nickerson, D.P., C.L. Brett, and A.J. Merz. 2009. **Vps-C complexes: gatekeepers of endolysosomal traffic**. *Curr. Opin. Cell Biol.* 21:543–551.

Nikolaus, J., M. Stöckl, D. Langosch, R. Volkmer, and A. Herrmann. 2010. **Direct visualization of large and protein-free hemifusion diaphragms**. *Biophys. J.* 98:1192–1199.

Nordmann, M., M. Cabrera, A. Perz, C. Bröcker, C. Ostrowicz, S. Engelbrecht-Vandré, and C. Ungermann. 2010. **The Mon1-Ccz1 complex is the GEF of the late endosomal Rab7 homolog Ypt7**. *Curr. Biol.* 20:1654–1659.

Numrich, J., and C. Ungermann. 2014. **Endocytic Rabs in membrane trafficking and signaling**. *Biol. Chem.* 395:327–333.

Odorizzi, G., M. Babst, and S.D. Emr. 1998a. **Fab1p PtdIns(3)P 5-kinase function essential for protein sorting in the multivesicular body**. *Cell*. 95:847–858.

Odorizzi, G., C.R. Cowles, and S.D. Emr. 1998b. **The AP-3 complex: A coat of many colours**. *Trends Cell Biol.* 8:282–288.

Orr, A., W. Wickner, S.F. Rusin, A.N. Kettenbach, and M. Zick. 2015. **Yeast vacuolar HOPS, regulated by its kinase, exploits affinities for acidic lipids and Rab:GTP for membrane binding and to catalyze tethering and fusion**. *Mol. Biol. Cell*. 26:305–315.

Ostrowicz, C.W., C. Bröcker, F. Ahnert, M. Nordmann, J. Lachmann, K. Peplowska, A. Perz, K. Auffarth, S. Engelbrecht-Vandré, and C. Ungermann. 2010. **Defined Subunit Arrangement and Rab Interactions Are Required for Functionality of the HOPS Tethering Complex**. *Traffic*. 11:1334–1346.

Ouyang, Q., S.B. Lizarraga, M. Schmidt, U. Yang, J. Gong, D. Ellisor, J.A. Kauer, and E.M. Morrow. 2013. **Christianson Syndrome Protein NHE6 Modulates TrkB Endosomal Signaling Required for Neuronal Circuit Development**. *Neuron*. 80:97–112.

Overmeyer, J.H., and W.A. Maltese. 1992. **Isoprenoid requirement for intracellular transport and processing of murine leukemia virus envelope protein**. *J. Biol. Chem.* 267:22686–22692.

Pang, Z.P., and T.C. Südhof. 2010. **Cell biology of Ca^{2+}-triggered exocytosis**. *Curr. Opin. Cell Biol.* 22:496–505.

Parkinson, K., A.E. Baines, T. Keller, N. Gruenheit, L. Bragg, R.A. North, and C.R.L. Thompson. 2014. **Calcium-dependent regulation of Rab activation and vesicle fusion by an intracellular P2X ion channel**. *Nat. Cell Biol.* 16:87–98.

Pearce, D. a, C.J. Carr, B. Das, and F. Sherman. 1999. **Phenotypic reversal of the btn1 defects in yeast by chloroquine: a yeast model for Batten disease**. *Proc. Natl. Acad. Sci. U. S. A.* 96:11341–11345.

Peng, H., N. Kang, J. Xu, P.K. Stanton, and J. Kang. 2013. **Two distinct modes of exocytotic fusion pore expansion in large astrocytic vesicles**. *J. Biol. Chem.* 288:16872–16881.

Peplowska, K., D.F. Markgraf, C.W. Ostrowicz, G. Bange, and C. Ungermann. 2007. **The CORVET Tethering Complex Interacts with the Yeast Rab5 Homolog Vps21 and Is Involved in Endo-Lysosomal Biogenesis**. *Dev. Cell*. 12:739–750.

Perera, R.M., and R. Zoncu. 2016. **The Lysosome as a Regulatory Hub**. *Annu. Rev. Cell Dev. Biol.* 32:annurev-cellbio-111315-125125.

Peters, C., P.D. Andrews, M.J. Stark, S. Cesaro-Tadic, a Glatz, a Podtelejnikov, M. Mann, and a Mayer. 1999. **Control of the terminal step of intracellular membrane fusion by protein phosphatase 1**. *Science*. 285:1084–1087.

Peters, C., and A. Mayer. 1998. **Ca^{2+}/calmodulin signals the completion of docking and triggers a late step of vacuole fusion**. *Nature*. 396:575–580.

Peterson, M.R., C.G. Burd, and S.D. Emr. 1999. **Vac1p coordinates Rab and phosphatidylinositol 3-kinase signaling in Vps45p-dependent vesicle docking/fusion at the endosome**. *Curr. Biol.* 9:159–162.

Peterson, M.R., and S.D. Emr. 2001. **The class C Vps complex functions at multiple stages of the vacuolar transport pathway**. *Traffic*. 2:476–486.

Pieren, M., A. Schmidt, and A. Mayer. 2010. **The SM protein Vps33 and the t-SNARE H(abc) domain promote fusion pore opening**. *Nat. Struct. Mol. Biol.* 17:710–717.

Piper, R.C., and D.J. Katzmann. 2007. **Biogenesis and function of multivesicular bodies**. *Annu. Rev. Cell Dev. Biol.* 23:519–47.

Plemel, R.L., B.T. Lobingier, C.L. Brett, C.G. Angers, D.P. Nickerson, A. Paulsel, D. Sprague, and A.J. Merz. 2011. S**ubunit organization and Rab interactions of Vps-C protein complexes that control endolysosomal membrane traffic**. *Mol. Biol. Cell*. 22:1353–63.

Pols, M.S., C. Ten Brink, P. Gosavi, V. Oorschot, and J. Klumperman. 2013. **The HOPS Proteins hVps41 and hVps39 Are Required for Homotypic and Heterotypic Late Endosome Fusion**. *Traffic*. 14:219–232.

Prag, G., S. Misra, E.A. Jones, R. Ghirlando, B.A. Davies, B.F. Horazdovsky, and J.H. Hurley. 2003. **Mechanism of ubiquitin recognition by the CUE domain of Vps9p**. *Cell*. 113:609–620.

Prasad, H., and R. Rao. 2015. **The Na^+/H^+ exchanger NHE6 modulates endosomal pH to control processing of amyloid precursor protein in a cell culture model of alzheimer disease**. *J. Biol. Chem.* 290:5311–5327.

Price, A., D. Seals, W. Wickner, C. Ungermann, and B. Wickner. 2000. **The docking stage of yeast vacuole fusion requires the transfer of proteins from a cis-SNARE complex to a Rab/Ypt protein**. *J. Cell Biol.* 148:1231–1238.

Pryor, P.R., B.M. Mullock, N.A. Bright, S.R. Gray, and J.P. Luzio. 2000. **The role of intraorganellar Ca^{2+} in late endosome-lysosome heterotypic fusion and in the reformation of lysosomes from hybrid organelles**. *J. Cell Biol.* 149:1053–1062.

Qiu, Q.-S., and R. a Fratti. 2010. **The Na^+/H^+ exchanger Nhx1p regulates the initiation of *Saccharomyces cerevisiae* vacuole fusion**. *J. Cell Sci.* 123:3266–3275.

Rana, M., J. Lachmann, and C. Ungermann. 2015. **Identification of a Rab GAP cascade that controls recycling of the Rab5 GTPase Vps21 from the vacuole**. *Mol. Biol. Cell*. 26:2535–49.

Raymond, C.K., I. Howald-Stevenson, C.A. Vater, and T.H. Stevens. 1992. **Morphological classification of the yeast vacuolar protein sorting mutants: evidence for a prevacuolar compartment in class E vps mutants**. *Mol. Biol. Cell*. 3:1389–402.

Reese, C., F. Heise, and A. Mayer. 2005. ***Trans*-SNARE pairing can precede a hemifusion intermediate in intracellular membrane fusion**. *Nature*. 436:410–414.

Reese, C., and A. Mayer. 2005. **Transition from hemifusion to pore opening is rate limiting for vacuole membrane fusion**. *J. Cell Biol.* 171:981–990.

Ricci, a J., Y.C. Wu, and R. Fettiplace. 1998. **The endogenous calcium buffer and the time course of transducer adaptation in auditory hair cells**. *J. Neurosci.* 18:8261–77.

Rieder, S.E., L.M. Banta, K. Köhrer, J.M. McCaffery, and S.D. Emr. 1996. **Multilamellar endosome-like compartment accumulates in the yeast vps28 vacuolar protein sorting mutant**. *Mol. Biol. Cell*. 7:985–99.

Robinson, J.S., D.J. Klionsky, L.M. Banta, and S.D. Emr. 1988. **Protein sorting in *Saccharomyces cerevisiae*: isolation of mutants defective in the delivery and processing of multiple vacuolar hydrolases**. *Mol. Cell. Biol.* 8:4936–4948.

Russell, M.R.G., T. Shideler, D.P. Nickerson, M. West, and G. Odorizzi. 2012. **Class E compartments form in response to ESCRT dysfunction in yeast due to hyperactivity of the Vps21 Rab GTPase**. *J. Cell Sci.* 125:5208–20.

Russnak, R., D. Konczal, and S.L. McIntire. 2001. **A Family of Yeast Proteins Mediating Bidirectional Vacuolar Amino Acid Transport**. *J. Biol. Chem.* 276:23849–23857.

Saksena, S., and S.D. Emr. 2009. **ESCRTs and human disease**. *Biochem. Soc. Trans.* 37:167–72.

Sasser, T.L., and R.A. Fratti. 2014. **Class C ABC transporters and *Saccharomyces cerevisiae* vacuole fusion**. *Cell. Logist.* 4:e943588.

Sasser, T.L., M. Padolina, and R.A. Fratti. 2012. **The yeast vacuolar ABC transporter Ybt1p**

regulates membrane fusion through Ca^{2+} transport modulation. *Biochem. J.* 448:365–72.

Schmidt, O., and D. Teis. 2012. **The ESCRT machinery**. *Curr. Biol.* 22.

Schwartz, M.L., and A.J. Merz. 2009. **Capture and release of partially zipped *trans*-SNARE complexes on intact organelles**. *J. Cell Biol.* 185:535–49.

Seals, D., G. Eitzen, N. Margolis, W. Wickner, and A. Price. 2000a. **A Ypt/Rab effector complex containing the Sec1 homolog Vps33p is required for homotypic vacuole fusion**. *Proc. Natl. Acad. Sci. U. S. A.* 97:9402–9407.

Seaman, M.N.J., J.M. McCaffery, and S.D. Emr. 1998. **A membrane coat complex essential for endosome-to-Golgi retrograde transport in yeast**. *J. Cell Biol.* 142:665–681.

Shideler, T., D.P. Nickerson, A.J. Merz, and G. Odorizzi. 2015. **Ubiquitin binding by the CUE domain promotes endosomal localization of the Rab5 GEF Vps9**. *Mol. Biol. Cell*. 26:1345–56.

Solinger, J.A., and A. Spang. 2013. **Tethering complexes in the endocytic pathway: CORVET and HOPS**. *FEBS J.* 280:2743–2757.

Spang, A. 2016. **Membrane Tethering Complexes in the Endosomal System**. *Front. Cell Dev. Biol.* 4:35.

Starai, V.J., C.M. HIckey, and W. Wickner. 2008. **HOPS proofreads the trans-SNARE complex for yeast vacuole fusion**. *Mol. Biol. Cell*. 19:2500–2508.

Starai, V.J., Y. Jun, and W. Wickner. 2007. **Excess vacuolar SNAREs drive lysis and Rab bypass fusion**. *Proc. Natl. Acad. Sci. U. S. A.* 104:13551–13558.

Starai, V.J., N. Thorngren, R.A. Fratti, and W. Wickner. 2005. **Ion regulation of homotypic vacuole fusion in *Saccharomyces cerevisiae***. *J. Biol. Chem.* 280:16754–16762.

Stenmark, H. 2009. **Rab GTPases as coordinators of vesicle traffic**. *Nat. Rev. Mol. Cell Biol.* 10:513–25.

Strasser, B., J. Iwaszkiewicz, O. Michielin, and A. Mayer. 2011. **The V-ATPase proteolipid cylinder promotes the lipid-mixing stage of SNARE-dependent fusion of yeast vacuoles**. *EMBO J.* 30:4126–4141.

Strømme, P., K. Dobrenis, R. V. Sillitoe, M. Gulinello, N.F. Ali, C. Davidson, M.C. Micsenyi, G. Stephney, L. Ellevog, A. Klungland, and S.U. Walkley. 2011. **X-linked Angelman-like syndrome caused by Slc9a6 knockout in mice exhibits evidence of endosomal-lysosomal dysfunction**. *Brain*. 134:3369–3383.

Stroupe, C., K.M. Collins, R.A. Fratti, and W. Wickner. 2006a. **Purification of active HOPS complex reveals its affinities for phosphoinositides and the SNARE Vam7p**. *EMBO J.* 25:1579–89.

Stroupe, C., K.M. Collins, R.A. Fratti, and W. Wickner. 2006b. **Purification of active HOPS complex reveals its affinities for phosphoinositides and the SNARE Vam7p**. *EMBO J.* 25:1579–1589.

Stuffers, S., C. Sem Wegner, H. Stenmark, and A. Brech. 2009. **Multivesicular endosome biogenesis in the absence of ESCRTs**. *Traffic*. 10:925–937.

Subramanian, S. 2004. **The Sec1/Munc18 Protein, Vps33p, Functions at the Endosome and the Vacuole of *Saccharomyces cerevisiae***. *Mol. Biol. Cell*. 15:2593–2605.

Teter, S. a, and D.J. Klionsky. 2000. **Transport of proteins to the yeast vacuole: autophagy, cytoplasm-to-vacuole targeting, and role of the vacuole in degradation**. *Semin. Cell*

Dev. Biol. 11:173–179.

Thorngren, N., K.M. Collins, R. a Fratti, W. Wickner, and A.J. Merz. 2004. **A soluble SNARE drives rapid docking, bypassing ATP and Sec17/18p for vacuole fusion**. *EMBO J.* 23:2765–2776.

Tian, X., U. Gala, Y. Zhang, W. Shang, S. Nagarkar Jaiswal, A. di Ronza, M. Jaiswal, S. Yamamoto, H. Sandoval, L. Duraine, M. Sardiello, R. V. Sillitoe, K. Venkatachalam, H. Fan, H.J. Bellen, and C. Tong. 2015. **A Voltage-Gated Calcium Channel Regulates Lysosomal Fusion with Endosomes and Autophagosomes and Is Required for Neuronal Homeostasis**. *PLoS Biol.* 13.

Tokunaga, M., N. Imamoto, and K. Sakata-Sogawa. 2008. **Highly inclined thin illumination enables clear single-molecule imaging in cells**. *Nat. Methods*. 5:159–61.

Uemura, T., M.T. Morita, K. Ebine, Y. Okatani, D. Yano, C. Saito, T. Ueda, and A. Nakano. 2010. **Vacuolar/pre-vacuolar compartment Qa-SNAREs VAM3/SYP22 and PEP12/SYP21 have interchangeable functions in *Arabidopsis***. *Plant J.* 64:864–873.

Ungermann, C., A. Price, and W. Wickner. 2000. **A new role for a SNARE protein as a regulator of the Ypt7/Rab-dependent stage of docking**. *Proc. Natl. Acad. Sci. U. S. A.* 97:8889–8891.

Ungermann, C., K. Sato, and W. Wickner. 1998. **Defining the functions of *trans*-SNARE pairs**. *Nature*. 396:543–548.

Ungermann, C., and W. Wickner. 1998. **Vam7p, a vacuolar SNAP-25 homolog, is required for SNARE complex integrity and vacuole docking and fusion**. *EMBO J.* 17:3269–3276.

Vollmer, P., E. Will, D. Scheglmann, M. Strom, and D. Gallwitz. 1999. **Primary structure and biochemical characterization of yeast GTPase- activating proteins with substrate**

preference for the transport GTPase Ypt7p. *Eur. J. Biochem.* 260:284–290.

Wang, C.-W. 2003. **Yeast homotypic vacuole fusion requires the Ccz1-Mon1 complex during the tethering/docking stage**. *J. Cell Biol.* 163:973–985.

Wang, L., A.J. Merz, K.M. Collins, and W. Wickner. 2003. **Hierarchy of protein assembly at the vertex ring domain for yeast vacuole docking and fusion**. *J. Cell Biol.* 160:365–374.

Wang, L., E.S. Seeley, W. Wickner, and A.J. Merz. 2002. **Vacuole Fusion at a Ring of Vertex Docking Sites Leaves Membrane Fragments within the Organelle**. *Cell*. 108:357–369.

Wartosch, L., U. Gunesdogan, S.C. Graham, and J.P. Luzio. 2015. **Recruitment of VPS33A to HOPS by VPS16 Is Required for Lysosome Fusion with Endosomes and Autophagosomes**. *Traffic*. 727–742.

Weisman, L.S. 2003. **Yeast vacuole inheritance and dynamics**. *Annu. Rev. Genet.* 37:435–460.

Wen, W., L. Chen, H. Wu, X. Sun, M. Zhang, and D.K. Banfield. 2006. **Identification of the yeast R-SNARE Nyv1p as a novel longin domain-containing protein**. *Mol. Biol. Cell*. 17:4282–4299.

Wichmann, H., L. Hengst, and D. Gallwitz. 1992. **Endocytosis in yeast: Evidence for the involvement of a small GTP-binding protein (Ypt7p)**. *Cell*. 71:1131–1142.

Wickner, W. 2010. **Membrane fusion: five lipids, four SNAREs, three chaperones, two nucleotides, and a Rab, all dancing in a ring on yeast vacuoles**. *Annu. Rev. Cell Dev. Biol.* 26:115–136.

Wiedelhold, K., and D. Fasshauer. 2009. **Is assembly of the SNARE complex enough to fuel membrane fusion?** *J. Biol. Chem.* 284:13143–13152.

Will, E., and D. Gallwitz. 2001. **Biochemical Characterization of Gyp6p, a Ypt/Rab-specific GTPase-activating Protein from Yeast**. *J. Biol. Chem.* 276:12135–12139.

Wilschut, J., N. Duzgunes, R. Fraley, and D. Papahadjopoulos. 1980. **Studies on the mechanism of membrane fusion: kinetics of calcium ion induced fusion of phosphatidylserine vesicles followed by a new assay for mixing of aqueous vesicle contents**. *Biochemistry*. 19:6011–6021.

Wurmser, A.E., T.K. Sato, and S.D. Emr. 2000. **New component of the vacuolar class C-Vps complex couples nucleotide exchange on the Ypt7 GTPase to SNARE-dependent docking and fusion**. *J. Cell Biol.* 151:551–62.

Xu, H., Y. Jun, J. Thompson, J. Yates, and W. Wickner. 2010. **HOPS prevents the disassembly of *trans*-SNARE complexes by Sec17p/Sec18p during membrane fusion**. *EMBO J.* 29:1948–1960.

Xu, H., and D. Ren. 2015. **Lysosomal physiology**. *Annu Rev Physiol*. 77:57–80.

Xu, W., F.J. Smith, R. Subaran, and A.P. Mitchell. 2004. **Multivesicular body-ESCRT components function in pH response regulation in *Saccharomyces cerevisiae* and *Candida albicans***. *Mol. Biol. Cell*. 15:5528–37.

Yu, I.-M., and F.M. Hughson. 2010. **Tethering factors as organizers of intracellular vesicular traffic**. *Annu. Rev. Cell Dev. Biol.* 26:137–156.

Zick, M., and W. Wickner. 2012. **Phosphorylation of the effector complex HOPS by the vacuolar kinase Yck3p confers Rab nucleotide specificity for vacuole docking and fusion**. *Mol. Biol. Cell*. 23:3429–37.

Zick, M., and W. Wickner. 2013. **The tethering complex HOPS catalyzes assembly of the soluble SNARE Vam7 into fusogenic *trans*-SNARE complexes**. *Mol. Biol. Cell*.

24:3746–3753.

Zick, M., and W. Wickner. 2016. **Improved reconstitution of yeast vacuole fusion with physiological SNARE concentrations reveals an asymmetric Rab(GTP) requirement**. *Mol. Biol. Cell*. 27:2590–2597.